University of Pennsylvania
ScholarlyCommons

Publicly Accessible Penn Dissertations

2021

Aspects Of Deregulated Glucose Metabolism In Liver And Kidney Cancer

Jason Godfrey
University of Pennsylvania

Aspects Of Deregulated Glucose Metabolism In Liver And Kidney Cancer

Abstract

Deregulated glucose metabolism is a critical component of cancer growth and survival, as is clinically evident by FDG-PET imaging of enhanced glucose uptake in tumors. However, the efficacy of direct pharmacological intervention of glycolysis, a critical biochemical pathway that catabolizes glucose, has yet to be realized. As an alternative approach, we explored the potential therapeutic value of two physiological pathways that oppose glucose catabolism in either liver or kidney cancer: gluconeogenesis and glycogen synthesis, respectively. In liver cancer, I hypothesized that gluconeogenesis could be stimulated by glucagon signaling to antagonize glycolysis and reduce tumor cell growth. Upon supraphysiologic overexpression of the glucagon receptor, GCGR, glucagon treatment of the liver cancer cell line, SNU398, reproducibly decreased cell viability, but without transcriptionally inducing gluconeogenic gene expression, regardless of the epigenetic landscape. In kidney cancer, we hypothesized that disrupting glycogen breakdown could prevent release of glucose under stress conditions and inhibit tumor cell proliferation. Through genetic knockout of key enzymes and carbon-13 labeling, we observed that glycogen metabolism does not affect tumor growth, despite metabolic utilization of glycogen-derived glucose in culture conditions without glucose. In conclusion, we describe context-specific approaches to targeting glucose metabolism in cancer that warrant further investigation.

Degree Type
Dissertation

Degree Name
Doctor of Philosophy (PhD)

Graduate Group
Cell & Molecular Biology

First Advisor
Celeste Simon

Subject Categories
Biochemistry | Cell Biology | Molecular Biology

ASPECTS OF DEREGULATED GLUCOSE METABOLISM IN LIVER AND KIDNEY CANCER

Jason T. Godfrey

A DISSERTATION

in

Cell and Molecular Biology

Presented to the Faculties of the University of Pennsylvania

in

Partial Fulfillment of the Requirements for the

Degree of Doctor of Philosophy

2021

Supervisor of Dissertation

_____

M. Celeste Simon, Ph.D.
Arthur H. Rubenstein, MBBCh Professor

Graduate Group Chairperson

_____

Daniel S. Kessler, Ph.D.
Associate Professor of Cell and Developmental Biology

Dissertation Committee

Marisa S. Bartolomei, Ph.D., Perelman Professor of Cell and Developmental Biology
Sandra W. Ryeom, Ph.D., Associate Professor of Cancer Biology
Donita C. Brady, Ph.D., Harrison McCrea Dickson, M.D. and Clifford C. Baker, M.D. Presidential Associate Professor
Terence P. Gade, M.D., Ph.D., Assistant Professor of Radiology and Cancer Biology

ACKNOWLEDGMENTS

I'd like to express my gratitude to the following people for all their support:

- My thesis mentor, Dr. Celeste Simon, and Dr. Brian Keith for their teaching, encouragement, patience, and generosity
- Current and previous members of the Simon lab, with a special thanks to the following people:
    o Our lab manager, Michelle Burrows, for her technical guidance and substantial support
    o Former research technicians, Jennifer Finan and Vivek Nimgaonkar, for our philosophical discussions and being fun to be around
    o Senior scientist, Dr. Nicolas Skuli, for his effort and willingness to help with experiments, analyze data, and brainstorm next steps
    o Former graduate student, Dr. Danielle Sanchez, for her advice on the graduate program and experiments
    o Former medical student, Dr. Jun Song, for his unique perspective and friendship
    o Former postdoctoral fellow, Dr. Pearl Lee, for giving me feedback and our chats while walking home
- Thesis committee member, Dr. Sandra Ryeom, who really helped clarify and put in motion the graduation process
- Fellow graduate students, Aoi Wakabayashi and Ian Folkert, for being great to talk with
- My friend and former neighbor, Dana Lee, who was easy to talk to and got dinner with me every so often
- My longtime friend, Jeff Narewski, for all our great conversations
- And lastly, my family: Mom, Dad, Jenna, Kyle, Chris, and our pets, Korra, Luna, Comet, Cookie, and Chip

The journey to a PhD is a solitary one. The research is your own. The effort is your own. And the knowledge and skills gained are your own. However, despite these undeniable truths, without the support of my colleagues, friends, and family, I may very well have not been able to tough it out. As sincerely as words can convey, thank you all.

ABSTRACT

ASPECTS OF DEREGULATED GLUCOSE METABOLISM IN LIVER AND KIDNEY

CANCER

Jason T. Godfrey

M. Celeste Simon

Deregulated glucose metabolism is a critical component of cancer growth and survival, as is clinically evident by FDG-PET imaging of enhanced glucose uptake in tumors. However, the efficacy of direct pharmacological intervention of glycolysis, a critical biochemical pathway that catabolizes glucose, has yet to be realized. As an alternative approach, we explored the potential therapeutic value of two physiological pathways that oppose glucose catabolism in either liver or kidney cancer: gluconeogenesis and glycogen synthesis, respectively. In liver cancer, I hypothesized that gluconeogenesis could be stimulated by glucagon signaling to antagonize glycolysis and reduce tumor cell growth. Upon supraphysiologic overexpression of the glucagon receptor, GCGR, glucagon treatment of the liver cancer cell line, SNU398, reproducibly decreased cell viability, but without transcriptionally inducing gluconeogenic gene expression, regardless of the epigenetic landscape. In kidney cancer, we hypothesized that disrupting glycogen breakdown could prevent release of glucose under stress conditions and inhibit tumor cell proliferation. Through genetic knockout of key enzymes and carbon-13 labeling, we observed that glycogen metabolism does not affect tumor growth, despite metabolic utilization of glycogen-derived glucose in culture conditions without glucose. In conclusion, we describe context-specific approaches to targeting glucose metabolism in cancer that warrant further investigation.

TABLE OF CONTENTS

LIST OF TABLES

LIST OF FIGURES

Extended Data 3.3 (related to 3.2)	Glycogen is dispensable for ccRCC cell growth *in vitro*	94
3.3	ccRCC tumor cells do not rely on glycogen breakdown for growth *in vitro* despite glycolytic entry of glycogen-derived glucose	95
Extended Data 3.4 (related to 3.3)	PYGL is not required for glycogen breakdown and *in vitro* ccRCC cell growth	96
Extended Data 3.5 (related to 3.3)	ccRCC tumor cells do not rely on glycogen breakdown for growth	97
Extended Data 3.6 (related to 3.3)	Glycogen-derived glucose broadly enters the central carbon pathway during glucose starvation	98
Extended Data 3.7 (related to 3.3)	Glycogen availability does not alter cell migration	99
3.4	Genetic perturbation in glycogen metabolism does not alter ccRCC xenograft progression *in vivo*	100

Chapter 1: Introduction to Glucose Metabolism in Cancer

1.1 Glucose Metabolism and its Role in Cancer

Glucose Metabolism in Normal Physiology

Carbohydrates are one of the major macromolecule nutrients that support life on Earth, along with fat and protein. In humans, although different cell and tissue types are differentially adapted to a particular nutrient, for example the neuronal dependency on sugars due to the exclusion of albumin-bound fat by the blood brain barrier, glucose can be utilized by all cells (Berg et al, 2002. Biochemistry)[1]. Glucose is metabolically derived from the catalytic digestion of complex carbohydrates obtained from the diet, like starch, and absorbed into the body through the small intestine and passed through the liver before entering the circulation. Upon pancreatic release of insulin, cells begin expressing glucose transporters at the plasma membrane to import the acquired glucose and ultimately fuel many aspects of cell biology and function (Chang et al, 2004)[2].

Glucose is trapped within the cytosol of cells via phosphorylation and then is processed further by different enzymes spanning a multitude of reactions, broadly referred to as the central carbon pathway, to meet the metabolic demands of a given cell under an existing set of conditions. Within the central carbon pathway, glucose catabolism occurs via multiple metabolic machineries that are critical to cell function (**Fig. 1.1; pg. 30**). Cytosolic glycolysis and mitochondrial tricarboxylic acid (TCA) cycle generate energy in the form of adenosine triphosphate (ATP), as well as intermediate metabolites important for other cellular processes. The pentose phosphate pathway maintains redox homeostasis, through the regeneration of NAPDH, and produces the ribose backbone necessary for nucleic acids. The hexosamine biosynthesis pathway facilitates protein glycosylation, via the conversion of glucose to UDP-GlcNAc, crucial for cell-to-cell signaling (Zhu and Thompson 2019)[3]. Glucose can also be used for *de novo*

2

triglyceride and fatty acid synthesis from glycolytic and TCA intermediates, respectively. Amino acid synthesis, such as serine, which itself can be incorporated into folate recycling and one-carbon metabolism, is catalyzed from the catabolism of glucose. Components of these metabolic pathways may also be present outside of the cytosol and mitochondria, as studies have shown nuclear localization of enzymes involved in glycolysis and the tricarboxylic acid cycle (Boukouris et al, 2016; Huangyang and Simon, 2018)[4,5].

Due to the ubiquitous nature of glucose in underpinning virtually all aspects of cellular biochemistry, stress responses and programmed cell death are common fates during glucose deprivation. Previous work has shown that diminished glucose uptake in the absence of growth factor stimulation induces mitochondrial-based apoptosis, which can be ameliorated by increasing the expression of glucose transporters (Vander Heiden et al, 2001)[6]. In renal epithelial models of ischemia, glucose removal reduces the expression of chaperone proteins and increases mRNA levels of unfolded protein response factors (Bouvier et al, 2012)[7]. Similar results have been observed in the context of cerebral and myocardial ischemia, whereby an elevation in glucose transporters may provide a protective effect (Espinoza-Rojo et al, 2010; Sun et al, 1994)[8,9]. Due to these vast requirements of glucose, and the lethal consequences of its deficiencies, strict regulation of blood sugar is critical in maintaining normal cell function.

Systemically, serological glucose homeostasis is controlled by a number of hormones with complex interactions. Insulin and glucagon, small peptide hormones secreted by the pancreas, directly regulate circulating glucose by increasing cellular uptake or production of glucose, respectively. The steroidal family of adrenal gland-synthesized glucocorticoids acts on their nuclear receptors to promote glucose synthesis

3

in the liver (Kuo et al, 2015)[10]. Epinephrine, a critical neurotransmitter and hormone part of the fight or flight response, works together with glucagon and glucocorticoids to amplify their effects on glucose metabolism (Sherwin and Sacca, 1984)[11]. In fact, epinephrine binds a G-coupled protein receptor, β_2-adrenergic receptor, mechanistically similar to glucagon (discussed below), whose expression levels correlate with a gluconeogenic response to epinephrine (Kim et al, 2009)[12]. Pharmacologic administration of active thyroid hormone, triiodothyronine (T3), in human subjects resulted in an 18% increase in blood glucose levels, accompanied by a 30% increase in gluconeogenic conversion of labeled alanine to labeled glucose (Sandler et al, 1983)[13].

Other hormones, like somatostatin (Del Guercio et al, 1976)[14] and glucagon-like-peptide 1 (MacDonald et al, 2002)[15] produced in the gut, and adipocyte-derived leptin (Koch et al, 2010)[16] can induce glucose uptake, reduce hyperglycemia, and help overcome insulin resistance in models of diabetes. Inhibition of myostatin, which is secreted by myocytes to block skeletal muscle hypertrophy, was shown to increase mRNA levels of genes involved in glucose uptake, suggesting myostatin may also contribute to glucose homeostasis (Coleman et al, 2016)[17]. Intrinsically, cells also possess mechanisms to effectively sense glucose availability by activating proteins specifically in response to relative ratios of ATP:AMP, whereby higher amounts of AMP can stimulate AMP kinase to increase glucose uptake and thereby restore energy levels (Yuan et al, 2013)[18].

As an extension of glucose regulation at both an organismal and cellular level, glucose is also saved for future utilization in two ways when energy and nutrients are plentiful. The direct method of glucose storage comes in the form of glycogen (discussed later), which is comprised of a core protein, glycogenin, surrounded by a branching

4

network of covalently-bound glucose molecules. Glycogen constitutes a major component of skeletal muscle, where it is rapidly depleted to support muscle activity, and the liver, where it is broken down into glucose and released into the circulation during periods of fasting. Excess glucose can also be indirectly converted into fatty acids through hepatic lipogenesis, and stored in adipose tissue as triglycerides (Glimcher and Lee, 2009)[19].

Overall, glucose metabolism is central to human biology. The widely pleotropic purposes of glucose, in conjunction with multiple mechanisms to regulate its serological and intracellular concentrations, highlights the paramount role of glucose metabolism in normal physiology. Unsurprisingly, in pathological states, abnormal glucose utilization can also be critical in promoting disease onset and severity.

Examples of Glucose Metabolism in Diabetes and Hereditary Diseases

Aberrant glucose metabolism, either amplified or dampened, can result in or contribute to a number of pathologies. In the case where glucose uptake and/or catabolism is enhanced, this can sustain diseases characterized by abnormal cell growth, i.e. cancer (discussed later). In contrast, when cells lack adequate capability to import glucose from the circulation, usually a consequence of insulin resistance, this can effectuate hyperglycemia and diabetic symptoms. High blood sugar concentration can even lead to pathological osmolality gradients, whereby water and other solutes diffuse out of cells to maintain equilibrium. This chemical phenomenon alone can result in a wide range of deleterious effects, including hypertension, hypertonic cell states, and electrolyte imbalances due to elevated renal reabsorption of glucose and sodium (Liamis

et al, 2014)[20]. Therefore, understanding mechanisms driving deregulated glucose metabolism is critical to developing new therapeutics or preventing disease onset.

Notably, insulin resistance is a major mechanistic driver of both types of diabetes, which collectively accounts for as much as 10.5% of the population in the US (National Diabetes Statistics Report, 2020)[21]. Whereas type I diabetes involves an autoimmune response to insulin-secreting β-cells of the pancreas, which effectively depletes insulin, type II diabetes is generally characterized by poor long-term nutrition, such as high fat and/or sugar consumption, which is thought to induce states of insulin insensitivity through multiple mechanisms. One theory postulates that high carbohydrate intake forces continued overproduction of insulin that induces ER-dependent stress responses, resulting in the loss of β-cell integrity and insulin capacity (Muoio and Newgard, 2008)[22]. Moreover, this reduced insulin production can be exacerbated by the consequential relaxation of negative feedback on glucagon signaling, which is normally opposed and shut off by insulin secretion during food intake, leading to even greater circulating glucose and hyperglycemia (Kawamori et al, 2009; Gromada et al, 2009)[23,24]. In fact, drugs targeting effectors of glucagon signaling are in development for the treatment of type II diabetes (discussed later).

Insulin resistance, hyperglycemia, and the inability of cells to import glucose have numerous pathophysiological ramifications, including diabetic neuropathy (Said, 2007)[25] and ketoacidosis (Dhatariya et al, 2020)[26]. Tissues that express insulin-dependent glucose transporter 4 (GLUT4), such as skeletal muscle and adipose tissue, are particularly sensitive to insulin resistance (Yang et al, 2001)[27]. Impaired glucose uptake in myocytes can induce sarcopenia through stabilization of the transcription factor, Krüppel-like factor 15 (Hirata et al, 2019)[28], which itself can stimulate GLUT4 expression

6

(Gray et al, 2002)[29], suggesting mechanisms of defective negative feedback. Likewise, when insulin cannot suppress fat lipolysis, inflammatory conditions via M1 macrophage polarization can occur due to adipocyte-secreted factors (Odegaard and Chawla, 2013)[30]. Insulin resistance can also have glucose-independent effects, evident in the vasculature whereby deficient insulin signaling can disrupt angiogenesis, vasodilation, and pericyte integrity (Escudero et al, 2017)[31], potentially contributing to atherosclerosis (Rask-Madsen et al, 2010)[32] and ischemia (He et al, 2006)[33].

While significantly less common than adult onset type II diabetes, there are also a wide variety of hereditary disorders characterized by dysfunctional glucose metabolism, known as inborn errors of metabolism (El-Hattab, 2015)[34]. These pathologies are due to specific, often autosomal recessive, mutations in genes involved in carbohydrate processing. One example particularly relevant for the work described in this dissertation is the inactivating mutation of the gene, glucose-6-phosphatase catalytic subunit alpha (*G6PC*), which can result in the pathological accumulation of hepatic glycogen, contribute to liver inflammation, and increases the risk for liver cancer (Chou and Mansfield, 2008)[35].

Glucose Metabolism in Cancer

While diabetes and some genetic disorders of glucose metabolism are major risk factors for cancer development, the pathological nature of glucose metabolism is reverse in the context of cancer. Rather, tumor cells display increased uptake of glucose, which can be diagnostically distinguished from surrounding normal tissue via fluorodeoxyglucose PET imaging (Zhu et al, 2011)[36]. Oncogenic drivers and hyperactive mitogenic pathways, such as Ras, PI3K/Akt, c-Myc, and HIFs can induce the

transcription of glucose transporters and ultimately contribute to an elevated import of glucose (Ancey et al, 2018)[37]. Loss of tumor suppressor genes, such as TP53, can also increase the uptake and utilization of glucose in cancer cells (Levine and Puzio-Kuter, 2010)[38].

Although recent studies suggest intratumoral myeloid cells may be mostly responsible for the increased consumption of glucose (Reinfeld et al, 2021)[39], elevated catabolism of glucose is commonly measured in both human and murine tumors, such as in patients with lung cancers (Hensley et al, 2016)[40] and mouse models of liver cancer (Mendez-Lucas et al, 2017)[41]. In addition to providing the cell with energy, enhanced glycolysis, as well as oxidation of glucose, are thought to critically support processes necessary for continual anabolic growth in tumors (Lunt and Vander Heiden, 2011)[42]. Examples of such processes include the reinforcement of antioxidant recycling and mitigating reactive oxygen species which can be facilitated by increasing metabolic flux of glucose through the pentose phosphate pathway (Patra and Hay, 2014)[43]. Tumor vascularity is another process affected by glucose metabolism, as pyruvate dehydrogenase kinase, a glycolytic enzyme that increases the reduction of pyruvate to lactate, has been shown to increase tumor vessel density without inducing standard angiogenic factors, such as VEGF, in Wnt-driven models of colon cancer (Pate et al, 2014)[44].

In the context of invasiveness and metastasis, prostate cancer cells with greater migratory ability displayed enhanced glycolytic capacity (Shiraishi et al, 2015)[45]. Elevated glucose import and glycolysis can also contribute to epithelial-to-mesenchymal transition (EMT), which correlates with tumor aggressiveness (Masin et al, 2014)[46]. Conversely, transcription factors that repress EMT, such as Snail, have been reported to

redirect the increased uptake of glucose away from bioenergetics and towards the pentose phosphate pathway under stress conditions, thereby promoting tumor cell adaptability (Kim et al, 2017)[47]. In a similar vein, a single-cell metabolomics analysis of circulating tumor cells (CTCs), derived from an *in vivo* breast cancer model, suggested a subset of CTCs displayed greatly increased rates of glucose uptake relative to the parental cell line (Sasportas et al, 2014)[48].

In regards to the tumor microenvironment, transcriptomic studies in breast cancer identified a positive association between glycolytic gene expression and inflammation pathways, such as IL-17 signaling (Li et al, 2020)[49]. Interestingly, this study also revealed that high glycolytic gene expression associated with decreased cAMP signaling pathway genes, some of which regulate gluconeogenesis (discussed later). Additionally, upregulated tumor glycolysis is also thought to promote immune evasion via lowering extracellular pH due to increased lactic acid export, which favors the differentiation of tumor-associated macrophages and fibroblasts (Kareva and Hahnfeldt, 2013)[50]. Gastric tumor cells with high metastatic capacity have been shown to alter the glucose metabolism of adjacent fibroblasts themselves, inducing up to a 30% increase in rate of lactate production (Kogure et al, 2020)[51].

Therefore, not only does amplified glucose uptake and catabolism fuel cell growth, as one would expect, it also contributes to many other areas of tumor biology. Targeting glycolysis and disrupting glucose catabolism, specifically in tumor tissue, with pharmacological agents is a rational approach to overall treatment strategies for cancer patients (Hamanaka and Chandel, 2012)[52].

1.2 Inhibition of Glucose Metabolism in Cancer

Glycolysis

The clinical efficacy of direct glycolytic inhibitors remains unclear, as drugs targeting the enzymes that catalyze glucose catabolic reactions exist largely in the experimental phase (Akins et al, 2018)[53]. However, some compounds have been briefly evaluated in clinical trials. 2-deoxyglucose (2DG), a metabolically inert analog of glucose has been shown to reduce cancer cell viability through multiple mechanisms (Pelicano et al, 2006; Ralser et al, 2008)[54,55], especially in combination with oxidative phosphorylation inhibition (Sahra et al, 2010)[56] or under hypoxic conditions (Liu et al, 2001; Maher et al, 2007)[57,58]. However, as a monotherapy, 2DG did not offer any significant benefit to prostate cancer patients in a phase II clinical trial (NCT00633087). Another attractive class of anti-glycolytic compounds analyzed are inhibitors of lactate dehydrogenase (LDH). While many LDH inhibitors suffer from off-target effects, a recent study utilizing a LDHA/B isoform-specific molecule, NCI-006, showed significant *in vivo* efficacy in blocking pyruvate to lactate reduction, as well as decreasing tumor proliferation in a pancreatic adenocarcinoma xenograft model (Oshima et al, 2020)[59]. Additionally, an inhibitor of the lactate exporter, monocarboxylate transporter 1, is currently in a phase I clinical trial in lymphoma patients (NCT01791595).

Pentose Phosphate Pathway

The first and rate-limiting step of the pentose phosphate pathway is catalyzed by the enzyme, glucose-6-phosphate dehydrogenase (G6PDH). Importantly, this enzyme also produces NAPDH, a critical cofactor in antioxidant and lipid synthesis, thereby making it an ideal target for blocking the anabolic benefits of the pentose phosphate pathway. One

inhibitor of G6PDH, dehydroepiandrosterone (DHEA), has been shown to

noncompetitively block the reverse reaction mediated by G6PDH (Gordon et al, 1995)[60]

and increase cell death in cancer models (Fang et al, 2016)[61]. Additionally, DHEA has

been employed clinically for treatment of cancer, especially in breast cancer and the

mitigation of complications due to breast cancer (NCT04705883). However, it is unclear

whether DHEA can attentuate disease progression or promote survival. Moreover,

DHEA is a precursor molecule to the sex hormones, and as such it has a wide range of

effects, including anti-inflammatory and gender-specific fat composition (Morales et al,

1998)[62], which raise questions about its specificity for G6PDH. More recently identified

inhibitors, such as the plant-based polydactin (Mele et al, 2018)[63] and a chemically

modified aminoquinazolinone, G6PDi-1 (Ghergurovich et al, 2020)[64], have also shown

effectiveness at reducing G6PDH activity and disrupting the pentose phosphate pathway

in the context of cancer and the immune system. Further experimentation and more

clinical trials could incorporate these compounds, or their bioavailable derivatives, into

cancer therapy strategies.

Hexosamine Biosynthesis Pathway

The end product of the hexosamine pathway is the molecule uridine diphosphate *N*-

acetylglucosamine (UDP-GlcNAc), which is utilized by enzymes to modify proteins,

lipids, and amino sugars with GlcNAc groups. These glycosylations are critical for many

aspects of cell biology, such as the cytoskeletal and nuclear architecture, extracellular

matrix remodeling, intracellular signaling and enzyme activity, and the glycocalyx.

Perhaps unique to this pathway is that the synthesis of UDP-GlcNAc requires not only

glucose, but also glutamine, acetyl-CoA, and UTP, and therefore can theoretically be

regulated in complex ways. Nevertheless, the initial rate limiting step is catalyzed by

glutamine-fructose-6-phosphate amidotransferase 1 (GFAT1). An analysis in pancreatic cancer patients reveals that high expression of GFAT1 correlates with decreased overall survival rates and increased lymph node metastasis (Yang et al, 2016)[65]. Intriguingly, preclinical trials of an inhibitor to GFAT1, 6-diazo-5-oxo-L-norleucine (DON), may have synergize with the anti-PD1 immunotherapy to reduce tumor burden and enhance survival in pancreatic cancer models (Sharma et al, 2020)[66]. Additionally, inhibitors of the enzyme that functionally transfers GlcNAc to its target, O-linked N-acetylglucosamine transferase (OGT), are being developed and have shown efficacy in eliminating leukemia cells in both subcutaneous and circulating models (Asthana et al, 2018)[67]. While hexosamine blockade is a rationale therapeutic target, more efforts are needed to translate GFAT1 or OGT drugs into the clinic.

Glycerol-3-Phosphate Synthesis

Lipid droplets are organelles primarily composed of cholesterol esters and triacylglycerols encased by a phospholipid monolayer. Physiologically, lipid droplets serve as a source of fatty acids, and by extension energy, primarily in adipocytes. However, emerging data has revealed that lipid droplets are increased in a variety of cancers, such as glioblastoma (Wu e. al, 2020)[68], renal cell carcinoma (Du et al, 2017)[69] and metastatic pancreatic adenocarcinoma (Rozeveld et al, 2020)[70], and play a vital component to cancer cell progression through a multitude of mechanisms (Cruz et al, 2020)[71]. Breast tumor cells can even induce catabolism of lipid droplets in fatty liver cells, and possibly uptake the released fatty acids to facilitate metastasis (Li et al, 2020)[72]. Therefore, inhibiting *de novo* lipogenesis to reduce lipid droplet formation, and subsequent utilization, is a potential therapeutic strategy in cancer. Triacylglycerol and phospholipid synthesis requires the production of glycerol-3-phosphate, which forms the

basis of the polar head group. Glycerol-3-phosphate dehydrogenase (GPD) is the

enzyme that catalyzes glycerol-3-phosphate from the glycolytic metabolite,

dihydroxyacetone phosphate. Mixed data on GDP1 exists, whereby in glioblastoma it

may be involved in stem cell maintenance (Rusu et al, 2019)[73], but in other models, such

as lung and prostate, ectopic expression of GDP1 together with metformin inhibited

xenograft growth (Xie et al, 2020)[74]. However, enzymes that first esterifies glycerol-3-

phosphate with fatty acid groups, glycerol-3-phosphate acyltransferases (GPAT), have

been shown to promote tumor progression in ovarian (Marchan et al, 2017)[75] and liver

(Ellis et al, 2012)[76] cancer. While an inhibitor with broad activity against GPAT enzymes,

FSG67, has been demonstrated to decrease fat mass in preclinical murine models of

obesity (Kuhajda et al, 2011)[77], it remains unknown if this compound is effective in

cancer or whether it is translatable to human patients.

De Novo Serine Production

The epigenetic landscape is heavily studied field in tumor biology, particularly DNA

and histone methylation, and is widely accepted to be dysregulated in cancer. In the

context of metabolism, *S*-adenosylmethionine (SAM) is the substrate utilized to transfer

methyl groups to chromatin. SAM can be synthesized from methionine through the

reactions of multiple pathways, collectively referred to as one-carbon metabolism.

Specifically, serine is used as a substrate to generate methyl-tetrahydrofolate, which

then goes on to transfer its methyl group to homocysteine, thereby recycling methionine

and SAM. Previous studies have revealed serine auxotrophy in colorectal cancer

models, whereby specialized diets absent in serine or glycine reduced tumor burden

(Maddocks et al, 2017)[78]. Conversely, other cancers able to produce serine on their own

from glucose or gluconeogenic sources are sensitive to inhibition of enzymes involved in

de novo serine biosynthesis. The rate-limiting enzyme, phosphoglycerate

dehydrogenase (PHGDH), has been shown to increase glucose-derived serine in

tumors, as well as accelerate tumorigenesis in genetically engineered mouse models of

both triple negative breast cancer and BRAF^{V600E} melanoma (Sullivan et al, 2019)[79].

Additionally, the anti-p53 oncogene, MDM2, can stimulate gene expression of enzymes

involved in serine biosynthesis through direct chromatin interaction (Riscal et al, 2016)[80].

Moreover, serine-derived glutathione redox is perturbed upon MDM2 shRNA depletion in

non-small cell lung cancer cells, which correlates with enhanced sensitization to dietary

serine deprivation in xenograft models. Therefore, inhibitors targeting PHGDH are a

rational approach to attenuating serine metabolism in cancer patients. At this time,

PHGDH drugs remain under investigation in discovery and preclinical phases

(McNamee et al, 2021)[81].

TCA Cycle and Oxidative Phosphorylation

The TCA cycle comprises of a cyclic series of reactions canonically designed to burn

off glucose carbons, and thereby generate carbon dioxide, whilst transferring electrons

to molecular oxygen via coupling to 4 transmembrane protein complexes of oxidative

phosphorylation. Importantly, the electron transport chain generates a pH and proton

concentration gradient which ultimately drives the energetic production of ATP by ATP

synthase (also referred to as complex V). In terms of energy synthesis, production of key

secondary metabolites, and its cellular role as a hub for interconnected pathways and

processes, disrupting the TCA cycle and/or oxidative phosphorylation remains a highly

attractive target in cancer. Since the TCA cycle can be fed carbon from not only glucose

but amino acids, like glutamine, and fatty acids through β-oxidation, many potential

targets exist that could impair proper mitochondrial activity.

14

Perhaps the most widely used drug is metformin, which has traditionally been used to treat diabetes and experimental data has suggested numerous mechanisms to explain its ability to improve blood sugar via effects on the mitochondria. Specifically, metformin can disrupt oxidative phosphorylation (Madiraju et al, 2014)[82], induce calcium-dependent mitochondrial dysfunction (Loubiere et al, 2017)[83], activate AMPK to regulate mitochondrial fission (Wang et al, 2019)[84], and may alter the electron-coupling of complex I (Cameron et al, 2018)[85]. However, many of the precise mechanisms of metformin are still under investigation, despite its widespread use in diabetes. Metformin has been tested and is currently in clinical trials for cancer (NCT02028221) but its efficacy as a single agent or in combination with other drugs remains unclear.

Newer, more specific compounds that target individual mitochondrial enzymes are being developed. One such drug in phase I clinical trials for cancer, IACS-01079, blocks complex I activity and reduces experimental models of glioblastoma and leukemia (Molina et al, 2018)[86]. Inhibitors for another protein, mitochondrial pyruvate carrier (MPC), which is effectively the initial step in the TCA cycle, are also under development as an adjuvant therapy to radiation in cancer (Corbet et al, 2018)[87]. Lastly, an emerging cancer target is glutamine metabolism, which is an important component of sustaining the TCA cycle through α-ketoglutarate. CB-839 is an inhibitor of glutamine catabolism that has shown antitumor efficacy in sarcoma models (Lee et al, 2020)[88] and is currently being tested in phase II clinical trials (NCT04265534).

In summary, a variety of potent and specific compounds against enzymes involved in pathways of glucose metabolism are being considered for cancer treatment. With the discovery and clinical optimization of these drugs still ongoing, another potentially effective approach in antagonizing glucose catabolism as a whole process could be by

stimulating glucagon-dependent gluconeogenesis (Khan et al, 2015)[89] or disrupting

glycogen homeostasis (Khan et al, 2020)[90].

1.3 Glucagon, Gluconeogenesis, and Glycogen

Glucagon

Upon fasting conditions, the body maintains glucose homeostasis via two processes:

glycogenolysis and gluconeogenesis (**Fig. 1.2; pg. 31**). Glycogenolysis releases stored

glucose, whereas gluconeogenesis synthesizes glucose from non-carbohydrate sources,

such as lactate, alanine, and fatty acids. Both pathways mainly occur in the liver,

followed by the kidney, and are directly regulated by circulating hormones. Normally,

rates of hepatic glycogen breakdown and gluconeogenesis are elevated in response to

glucagon, a major regulator of blood glucose homeostasis (Ahren, 2015)[91]. The gene

encoding glucagon, *GCG*, is initially transcribed and translated into a pre-proglucagon

molecule that is catalytically cleaved in a tissue specific manner into at least 4 distinct

small peptides, whereby the glucagon isoform is secreted by exocrine α-cells of the

pancreas upon a complex network of metabolic, hormonal, and neurological stimuli

(Elliot et al, 2015)[92].

Canonically, falling blood sugar triggers glucagon-dependent metabolic rewiring in

the liver to promote glucose production and secretion (Gerich et al, 1976; Ramnanan et

al, 2011)[93,94]. Specifically, hepatic β-oxidation of hydrolyzed fatty acid stores, alanine

uptake and ALT-mediated conversion to pyruvate, and glutamine anaplerosis via GLS2

are all upregulated by glucagon signaling; all of which provides the carbon and energy

necessary for *de novo* glucose production (Habegger et al, 2010; Adeva-Andany et al,

2019; Miller et. al, 2018)[95-97]. Other encoded peptides are synthesized via tissue-specific alternative cleavage, such as glucagon-like-peptide 1 (GLP-1), which is produced in both α-cells and enteroendocrine cells of the gut (Ellingsgaard et al, 2011)[98]. Interestingly, GLP-1 has largely the opposite effects of glucagon, increasing insulin and regulating satiation (Shah and Vella, 2014)[99].

GCG-null mice develop normally, despite low blood glucose levels in 2 week old mice, which is largely normalized at 2-3 months of age (Hayashi et al, 2009)[100]. This suggests that other hormones and factors may compensate for a lack of glucagon, and its related peptides, over time. In humans, no mutations in *GCG* in any diseases have been identified. Glucagon is deployed therapeutically for restoring blood glucose during life-threatening instances hypoglycemia (Kedia, 2011)[101], but not as a routine treatment. Nevertheless, glucagon acts as a ligand that binds to the G-coupled glucagon receptor (GCGR), a class B G-coupled protein receptor that, upon ligand interaction, primarily leads to the dissociation of G_s alpha subunits that stimulate adenylyl cyclase activity and produces cyclic AMP (cAMP) (Qiao et al, 2020)[102].

Previous studies have demonstrated that *GCGR*-deficient mice are viable and display lower levels of circulating glucose levels similar to *GCG*-null mice (Gelling et al, 2003)[103]. However, loss of GCGR results in elevated glucagon secretion, most likely due to a lack of negative feedback, which can lead to a rare type of pancreatic neuroendocrine tumor characterized by α-cell hyperplasia, increased serum amino acid concentrations, and enhanced mammalian target of rapamycin activity (Solloway et al, 2015; Smith et al, 2020)[104,105]. A small percentage of *GCGR* missense mutations exist in humans that create variants with reduced glucagon binding affinity and correlate with insulin-independent diabetic symptoms (Hager et al, 1995)[106]. Conversely, in patients

17

with predominantly insulin-dependent diabetes (and therefore require insulin injections), antibody and antisense RNAi-based antagonists of GCGR are under clinical investigation in their capacity to combat hyperglycemia, either as single agents or in combination with other therapeutics, such as metformin (Scheen et al, 2017; Morgan et al, 2019; Wang et al, 2021)[107-109].

The functional result of glucagon-GCGR-$G_s\alpha$-adenylyl cyclase interaction is the generation of the secondary messenger: cyclic AMP (cAMP) (Miller et al, 2013)[110]. Canonically, cAMP binds to the regulatory subunits of protein kinase A (PKA), initiating the auto-phosphorylation of its catalytic domains (Smith et al, 2017)[111]. In the short term, active PKA can phosphorylate a number of targets, such as phosphorylase kinase (Brushia and Walsh, 1999)[112] to activate glycogen breakdown and release stored glucose (Magnusson et al, 1995)[113]. PKA has also been demonstrated to enhance lipolysis, particularly in adipocytes and hepatocytes; however, the mechanism remains unclear. Some evidence suggests PKA can directly phosphorylate and inactivate AMPK at Ser 173 (Djouder et al, 2010)[114], which may amplify its ability to activity hormone-sensitive lipase (HSL) (Duncan et al, 2007)[115]. Conversely, another study reported AMPK impeded lipogenesis through its phosphorylation and inhibition of acetyl-CoA carboxylase 1 (ACC1) (Peng et al, 2012)[116], a rate limiting enzyme in the early steps of fatty acid synthesis.

In addition to potential involvement of $G_q\alpha$-phospholipase C-mediated Ca^{+2} release downstream of GCGR (Xu and Xie, 2009)[117], PKA can also raise intracellular Ca^{+2} levels via phosphorylation of IP_3R calcium channels in the ER (Wang et al, 2012)[118]. Similar to cAMP, cytosolic calcium allosterically interacts with the inhibitory domains of many enzymes, including the phosphatase calcineurin and the kinase holoenzyme,

Ca+2/calmodulin-dependent protein kinase II (CAMKII) (Meyers et al, 2017)[119]. Indeed, knockouts of specific CAMKII targets, such as hepatic lipases (ATGL), significantly reduced plasma glucose concentrations following glucagon treatment in mice (Perry et al, 2020)[120].

In the long term, PKA and CAMKII function lead to activation of transcription factors that control gluconeogenic and lipolytic gene expression, such as cAMP response element-binding protein (CREB), forkhead box protein O1 (FoxO1), and peroxisome proliferator-activated receptor α (Herzig et al, 2001; Ozcan et al, 2012; Longuet et al, 2008)[121-123]. Increased gluconeogenic gene expression, integrated with enhanced fatty acid oxidation, rewires hepatic metabolism to synthesize and export glucose from non-carbohydrate sources (i.e. amino acids and lipids) in an energy-demanding process (Rui, 2014)[124]. Notably, muscle-secreted lactate and alanine are oxidized and deaminated into pyruvate in hepatocytes, respectively, followed by pyruvate carboxylase (PC)-mediated catalysis into oxaloacetate (OAA). OAA serves as a critical intermediate metabolite connecting the TCA cycle with gluconeogenesis (Cappel et al, 2019)[125]. In effect, glucagon signaling contributes to blood sugar homeostasis by raising systemic glucose concentration via liver-dependent glycogenolysis and gluconeogenesis.

Lastly, important to consider are the effects of other hormones on potentiating glucagon signaling and negative feedback mechanisms to maintain homeostasis. Glucocorticoids, thyroid hormone, and catecholamines can amplify the effects of glucagon, as previously mentioned. Conversely, cAMP and PKA signaling is diminished by activation of phosphodiesterases, which can be stimulated by insulin (Degerman et al, 1997)[126] and CAMKII (Mika et al, 2015)[127]. Surface expression of GCGR is regulated by endocytic internalization, which facilitates glucagon-mediated deubiquitination to

hypothetically stabilize downstream signaling (Kaur et al, 2020)[128]. Additionally, in immunoprecipitation experiments, GCGR may directly associate with a 14-3-3 protein (YWHAB) that slightly reduces its activity (Ji et al, 2021)[129]. Systemically, upon glucagon-induced hepatic glucose production, the pancreatic β cells begin to secrete insulin, which then blocks glucagon signaling as described above, and ultimately accounts for the physiological cycling of insulin and glucagon signaling in response to states of feeding or fasting, respectively.

Gluconeogenesis

Three irreversible gluconeogenic enzymes are required for full pathway engagement: phosphoenolpyruvate carboxykinase (PCK), fructose-1,6-bisphosphatase (FBP), and glucose-6-phosphate catalytic subunit C (G6PC). Physiologically, the pathway begins in oxygenated, periportal hepatocytes where glucagon signaling opposes Wnt/β-catenin transcriptional programs to stimulate gluconeogenic and lipolytic gene expression (Halpern et al, 2017; Cheng et al, 2018)[130,131]. These genes initiate a metabolic machinery that converts adipocyte-derived fat stores or anaerobic byproducts of muscle activity into precursors for glucose production, such as acetyl-CoA and pyruvate, respectively. Pyruvate in particular is then shuttled into the mitochondrial matrix via mitochondrial pyruvate carrier proteins, whereby it can enter the TCA cycle as acetyl-CoA or oxaloacetate (OAA) directly, by pyruvate dehydrogenase complex (PDC) or pyruvate carboxylase (PC), respectively.

Following metabolite shuttling via antiporters between the mitochondrial matrix and intermembrane space, cytosolic OAA is then decarboxylated and phosphorylated in a GTP-dependent reaction by PCK1 to produce phosphoenolpyruvate (PEP), the first rate

limiting step of gluconeogenesis. Important to note, based on the relative NADH redox state of the cell, PEP can also be generated directly in the mitochondria by PCK2. Nevertheless, PEP is a glycolytic metabolite that can now undergo a series of reversible, upward steps to synthesize fructose-1,6-bisphophate, by FBP1, and finally glucose, by G6PC. Notably, these last reactions of dephosphorylation do not generate ATP, but rather free inorganic phosphate, which can be utilized for the endergonic reaction of cellular respiration upon re-feeding. This resulting unmodified, *de novo* glucose diffuses out of the cell through facultative glucose transporters, namely GLUT2 in hepatocytes (Karim et al, 2012)[132], whereby it ultimately contributes to maintaining blood sugar homeostasis.

All of the gluconeogenic enzymes are under investigation for potential roles in tumor suppression, as many cancer cells favor high rates of glucose import and glycolysis, rather than glucose production and export (Wang and Dong, 2019)[133]. Previous studies have identified anti-tumorigenic roles of FBP1 in a variety of cancers (Jin et al, 2017; Lu et al, 2020; Li et al, 2016)[134-136], particularly in clear cell renal cell and hepatocellular carcinomas (Li et al, 2014; Li et al, 2020)[137,138]. Data on PCK1 has been mixed, whereby PCK1 overexpression accelerates colorectal xenograft growth (Montal et al, 2015)[139] but then may antagonize hepatoma proliferation (Xiang et al, 2021)[140], suggesting contextual roles of PCK1 for a given tumor type and metabolic stress. For G6PC, although some data has suggested it can protect glioblastoma cells from 2-deoxyglucose (Abbadi et al, 2014)[141], G6PC has mostly been characterized in glycogen storage disease type Ia, in which patients have dysfunctional, somatic mutations in GP6C (Lei et al, 1996)[142]. Interestingly, glycogen storage disease does predispose and correlate with patients developing liver cancer (Kishnani et al, 2009)[143], although this may be more due to

chronic inflammation from hepatomegaly and liver damage rather than strictly adverse metabolic effects (Kim et al, 2017)[144].

Glycogen

The biochemical function of glycogen is to store glucose when ATP levels are high and release glucose, in the form of glucose-1-phosphate, through a process known as glycogenolysis when ATP levels decline (Adeva-Andany et al, 2016)[145]. Briefly, glycogen is constructed via a core protein unit, glycogenin, from which glucose molecules are covalently linked together through linear α(1-4) and branched α(1-6) bonds by glycogen synthases (GYS), and reciprocally degraded via hydrolysis by glycogen phosphorylases (PYG) to yield both monosaccharides (glucose) and polysaccharides (maltose, etc.). This dynamic process is tightly regulated on multiple levels in mammals, both systemically by the insulin/glucagon axis and intracellularly through energy-sensing mechanisms, such as AMPK and HIF-1α. All of these factors converge on the regulation of GYS and PYG, pushing the equilibrium to either glycogen synthesis or breakdown. Specifically, the activities of GYS and PYG are both controlled posttranslational modifications, particularly phosphorylation.

In normal human physiology, the vast majority of glycogen resides in two tissue types: the liver, and high-energy consuming organs, including skeletal muscle and brain (Cali et al, 2019)[146]. Upon temporary drops in blood sugar levels, such as during sleep, hormonal cues immediately stimulate hepatic glycogenolysis, accounting for as much as 50% of the increase plasma glucose concentrations (Gerich, 2010)[147]. The kidney, while contributing mainly through gluconeogenesis, does not substantially contain glycogen, let alone provide glucose via glycogen breakdown (Stumvoll et al, 1997)[148].

Comparatively, tissues that require high energy levels, and therefore readily available glucose, lack the enzyme G6PC, which prevents glycogen-derived glucose from diffusing out of the cell. Other cell types have been reported to utilize glycogen as well, such as macrophages. In fact, a recent study in mice showed that LPS-stimulated inflammatory factors can be suppressed with an inhibitor of glycogenolysis (Ma et al, 2020)[149]. Cell non-autonomous cases of glycogen catabolism have also been described, such as co-culture experiments of cancer-associated fibroblasts inducing the breakdown of glycogen in ovarian cancer cells (Curtis et al, 2019)[150].

In tumors, increased glycogen abundance has been widely reported across a variety of subtypes, including kidney, suggesting that glycogen may confer some metabolic benefit within the tumor microenvironment (Rousset et al, 1981)[151]. However, another hypothesis could be that as tumor cells uptake more glucose, all metabolic processes downstream are relatively increased compared to adjacent normal tissue, but glycogen is simply a collateral metabolite. Another theory supported by previous studies proposes that intratumoral hypoxia can promote glycogen accumulation (Shen et al, 2010; Dauer and Lengyel, 2019)[152,153]. This oxygen-dependent effect may be more relevant for cancer cell viability, as coordinating glucose catabolism with tumor vascularization may then optimize production of ATP and TCA cycle intermediates, whilst maintaining mitochondrial integrity. Without adequate oxygen as the final electron acceptor, unregulated oxidative phosphorylation can become uncoupled with the electron transport chain, leading to potentially toxic levels of reactive oxygen species (Chiu et al, 2019)[154]. Therefore, glycogen metabolism in cancer may be both irrelevant and functionally necessary depending on the precise spatiotemporal nutrient conditions with a tumor microenvironment.

Glucagon signaling, gluconeogenesis, and glycogen processing are all interwoven components of glucose metabolism. In cancer, despite advances in our understanding of the role of individual genes, crosstalk between these pathways remains largely unexplored as a whole. Particularly in the cancers of gluconeogenic cell lineages, there are few published studies on the effects of glucagon, gluconeogenesis, and glycogen on glucose metabolism. For example, HIF-driven kidney cancers display greater levels of glycogen than normal renal epithelium, as do many tumors, but the metabolic purpose or consequences resulting from that increased tumor glycogen is as of yet, unknown. In liver cancer which mostly originates from hepatocytes, the dominant gluconeogenic cell type, it is similarly unknown if deregulated hepatic GCGR activity accounts for some of the correlations between gluconeogenic gene expression and liver cancer progression.

Furthermore, studies have not addressed if kidney or liver cancer cells are responsive to glucagon. Research into glucagon and GCGR has predominantly been focused on diabetes, whereby GCGR antagonists are being tested to therapeutically control hyperglycemia (Sharma et al, 2018)[155]. While inactivating mutations in GCGR can lead aberrant amino acid signaling and result in a rare type of pancreatic neuroendocrine tumor (Zhou et al, 2009; Yu et al, 2011)[155,157], as mentioned previously, the literature is very limited with regards to the general role of glucagon signaling in cancer (Yagi et al, 2018)[158]. With this in mind, this body of work aims to study the roles of glucagon, gluconeogenesis, and glycogen in the context of liver and kidney cancer.

1.4 Background on Liver and Kidney Cancer

Liver Cancer

Primary liver cancer, or hepatocellular carcinoma (HCC), is the 4th most common tumor type and is estimated to affect over 1 million people worldwide (Villanueva, 2019; Kim and Viatour, 2020)[159,160]. HCC also represents the second leading cause of cancer deaths globally, with mortality rates steadily increasing over the past 20 years (American Cancer Society, 2018)[161]. HCC is characterized as a progressive, often inflammatory, disease with the following risk factors: alcohol abuse, obesity-related non-alcoholic steatohepatitis, chronic hepatitis C or B infections, aflatoxin exposure, hereditary hemochromatosis, anabolic steroids, and tobacco use. Many of these pathological insults mechanistically lead to liver damage and ultimately cirrhosis, which reports estimate accounts for 80% of all HCC (Simonetti et al, 1991)[162]. While surgery remains the most effective treatment for early, single nodule HCC, current non-surgical treatment options, such as transarterial chemoembolization and radiofrequency ablation, have limited efficacy and reflect the poor five-year survival rates of 12%, averaged across all disease stages (Bedossa and Paradis, 2011)[163].

A major obstacle to effective treatment is due in large part to the genetic heterogeneity of hepatic tumors. For example, unlike melanomas which often harbor targetable mutations in the oncogene BRAF, HCCs display a diverse set of non-druggable mutations, specifically in the gene, *CTNNB1*, which encodes β-catenin and is present in approximately 30% of HCC patients. These driver mutations were found to be predictive of better overall survival (Wang et al, 2015)[164]. Promoter mutations in the gene encoding for telomerase, *TERT*, is thought to be a common early event in HCC initiation, that distinguishes regenerative nodules to neoplastic growths in a background of cirrhotic liver (Kim et al, 2019; Muller et al, 2020)[165,166]. Moreover, in HCCs developed from a non-cirrhotic liver, approximately half of tumors with *TERT* promoter mutations

also harbored activating mutations in *CTNNB1* (Nault et al, 2013)[167]. In contrast, mutually exclusive mutations in the tumor suppressor gene, *TP53*, account for another 30% of tumors, which generally correlate with enhanced cancer cell aggression and shorter overall survival (Villanueva and Hoshida, 2011)[168].

Patient response to targeted therapy has been disappointing, as Sorafenib, an FDA-approved kinase inhibitor for advanced HCC, only extends survival by a couple of months (Llovet et al, 2008; Bruix et al, 2015)[169,170]. Clinical trials incorporating immunotherapies are ongoing (Pinato et al, 2020)[171], but preliminary data comparing the efficacy of Nivolumab, targeting the anti-T cell modulator PD1, to Sorafenib has not yet shown any statistical benefit in median overall survival or progression-free survival as a monotherapy (NCT02576509). However, a recent phase 3 clinical trial in 501 patients with inoperable HCC demonstrated that treatment with a related immunotherapeutic, Atezolizumab, in tandem with an anti-angiogenic agent, Bevacizumab, provided an additional 2.5 months of median progression-free survival (Finn et al, 2020)[172]. This suggests that optimal drug interventions may require combination strategies against multiple aspects of tumor biology. Nevertheless, these clinical and molecular observations underscore HCC heterogeneity (Jeng et al, 2015; Ally et al, 2017)[173,174] and the necessity of new treatment strategies.

Targeting tumor metabolism, specifically disrupting glycolysis and promoting gluconeogenesis, may represent a therapeutic opportunity applicable across liver cancers. According to The Cancer Genome Atlas (TCGA), normalized RNA-seq reads of enzymes that directly catalyze gluconeogenesis are robustly decreased across liver cancer patients. Moreover, the response to glucagon, a master regulator of gluconeogenic gene expression, has not been evaluated in the context of liver cancer.

26

Therefore, a precise investigation into the potential tumor suppressive role of glucagon signaling in liver cancer was required.

Kidney Cancer

Kidney cancer ranks 8th in yearly incidence rates out of the nearly 200 distinct cancer classifications in the US (NCI SEER, 2018)[175]. In fact, clinical data up to 2017 indicates that kidney cancer incidence had among the greatest percent increase among males and females for all cancer types in this latest period analyzed, highlighting a need for deeper comprehension of the disease. Clear cell renal cell carcinoma (ccRCC) is the predominant disease subtype, accounting for more than 70% of patient cases, with a majority of tumors harboring loss-of-function mutations in the von Hippel Lindau (*VHL*) tumor suppressor (Sanchez et al, 2018)[176]. pVHL is an E3 ligase component that recognizes oxygen-dependent hydroxylation sites on hypoxia inducible factors (HIFs) to negatively regulate HIF protein levels through the ubiquitin-proteosome system. Only during acute hypoxia is pVHL unable to interact with HIFs and, by extension, are HIF proteins stabilized to initiate an adaptive response to low oxygen. The vast majority of ccRCC tumors lack pVHL expression or function and uniquely exhibit chronic HIF-α stabilization, regardless of tumor oxygenation. As such, these tumors categorically display transcriptomic profiles driven by either HIF-1α and HIF-2α together (H1H2) or HIF-2α solely (H2) (Gordan et al, 2008)[177]. Recent pharmacological advances in the development of small molecule inhibitors of HIF-2α, such as PT2385, have shown therapeutic promise in preclinical and clinical settings, supporting oncogenic addiction to HIFs in ccRCC (Wallace et al, 2016; Courtney et al, 2018)[178,179]. However, the scope of HIF-controlled downstream pathways that are clinically relevant for disease progression remains incompletely defined.

Perhaps the most striking phenotypic aftermath of pVHL deficiency in ccRCC tumors is a histologically clear cytoplasm. This is due to the removal of large intracellular lipid droplets, harboring cholesterol esters and triglycerides, and accumulated granules of glycogen during tissue processing for pathology (Zhang et al, 2017; Riscal et al, 2019)[180,181]. We previously reported that HIF-2α promotes lipid storage by regulating the expression of an essential lipid droplet coat protein, Perilipin-2 (*PLIN2*), in ccRCC (Qiu et al, 2015)[182]. *PLIN2* knockdown eradicates lipid droplets and strongly abrogates cell viability, illuminating the importance of lipid homeostasis in ccRCC (Ackerman et al, 2018)[183]. However, regulation or biological relevance of glycogen metabolism in ccRCC has not been investigated in careful detail, despite emerging data that support a pro-tumorigenic role for glycogen in other cancers, such as glioblastoma (GBM) and non-small cell lung cancer (NSCLC), under metabolic stress conditions (Favaro et al, 2012; Sun et al, 2019)[184,185]. Therefore, a thorough assessment of glycogen metabolism in ccRCC was warranted.

1.5 Study Rationale, Experimental Hypotheses, and Project Goals

Based on the aforementioned literature data and our current understanding of cancer metabolism, along with its therapeutic potential, we propose the following project questions (**Fig. 1.3; pg. 32**): (1) can glucagon signaling induce gluconeogenic gene expression to perturb liver cancer growth? The rationale for this investigation lies in the natural role of gluconeogenesis in directly opposing glycolysis. Since glucose catabolism is vital for tumor growth, we hypothesized that if glucagon signaling can activate gluconeogenesis in liver cancer cells, it would have a tumor suppressive effect. Therefore, the goals of this project are to describe the biological consequences of

glucagon/GCGR stimulation in liver cancer models, through ELISAs measuring cAMP production, western blots of downstream effector activity, qPCR assessment of target gluconeogenic gene expression, and cell viability assays.

(2) Can disruption of glycogen metabolism diminish tumor cell proliferation in kidney cancer? The rationale for this query originates from the uncharacterized role of elevated glycogen in kidney cancer, which could theoretically store glucose under hypoxic conditions for optimal catabolism. However, since the majority of clear cell renal cell carcinoma are driven by HIFs, regardless of oxygenation, the metabolic balance between glycogen synthesis and breakdown is unclear, and it may be that simply perturbing the equilibrium one way or the other results in reduced cancer cell viability. Thus, the goals of this project are to qualify the effects of blocking either GYS1-mediated glycogen synthesis or PYGL/B-regulated glycogenolysis by CRISPR/Cas9 technology, followed by quantification of glycogen levels, *in vitro* and *in vivo* proliferation rates, and metabolic tracing of glycogen-derived glucose during nutrient deprivation.
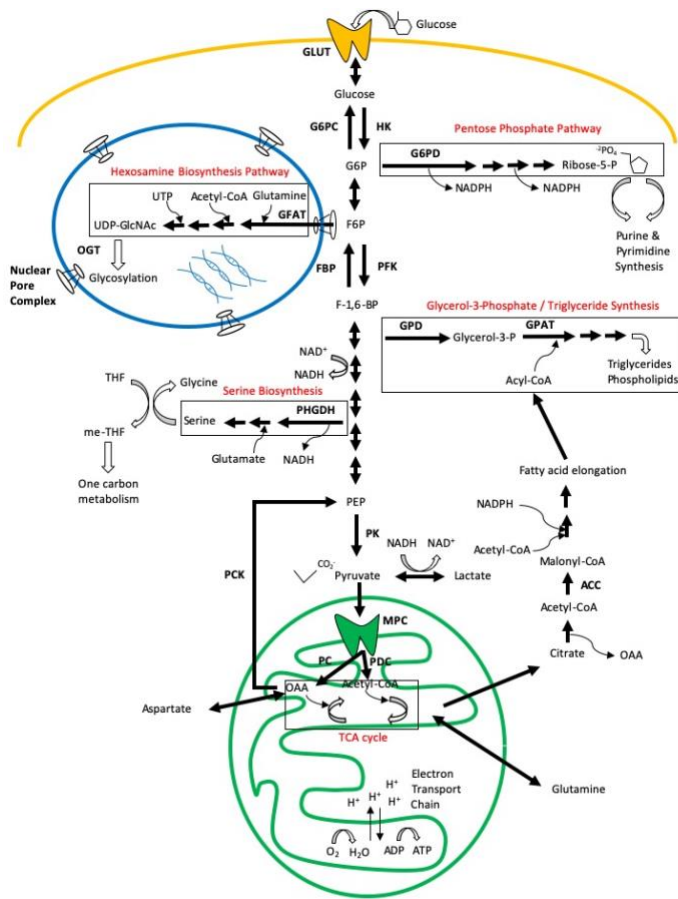
Figure 1.1 – **Major glucose metabolic pathways**. By facilitated diffusion across its concentration gradient, glucose entry into the cell is initially met with phosphorylation by hexokinase. This glucose-6-phosphate is then processed via multiple reactions to produce energy, anabolic precursors, and redox homeostasis necessary for cell function and viability. GLUT: glucose transporter, G6PC: glucose-6-phosphatase catalytic subunit, HK: hexokinase, G6P: glucose-6-phosphate, G6PD: glucose-6-phosphate dehydrogenase, NAD(P)H: nicotinamide adenine dinucleotide (phosphate), F6P: fructose-6-phosphate, GFAT: glucosamine--fructose-6-phosphate aminotransferase, CoA: Coenzyme A, UT(D)P: uridine tri(di)phosphate, GlcNAc: n-acetylglucosamine, OGT: *o*-linked GlcNAc transferase, FBP: fructose-1,6-bisphosphatase, PFK: phosphofructokinase, F-1,6-BP: fructose-1,6-bisphosphate, GPD: glycerol-3-phosphate dehydrogenase, GPAT: glycerol-3-phosphate acyltransferase, PHGDH: 3-phosphoglycerate dehydrogenase, (me-)THF: (methyl-)tetrahydrofolate, PEP: phosphoenolpyruvate, PK: pyruvate kinase, MPC: mitochondrial pyruvate carrier, PDC: pyruvate dehydrogenase complex, PC: pyruvate carboxylase, OAA: oxaloacetate, ACC: acetyl-CoA carboxylase, AT(D)P: adenosine tri(di)phosphate.
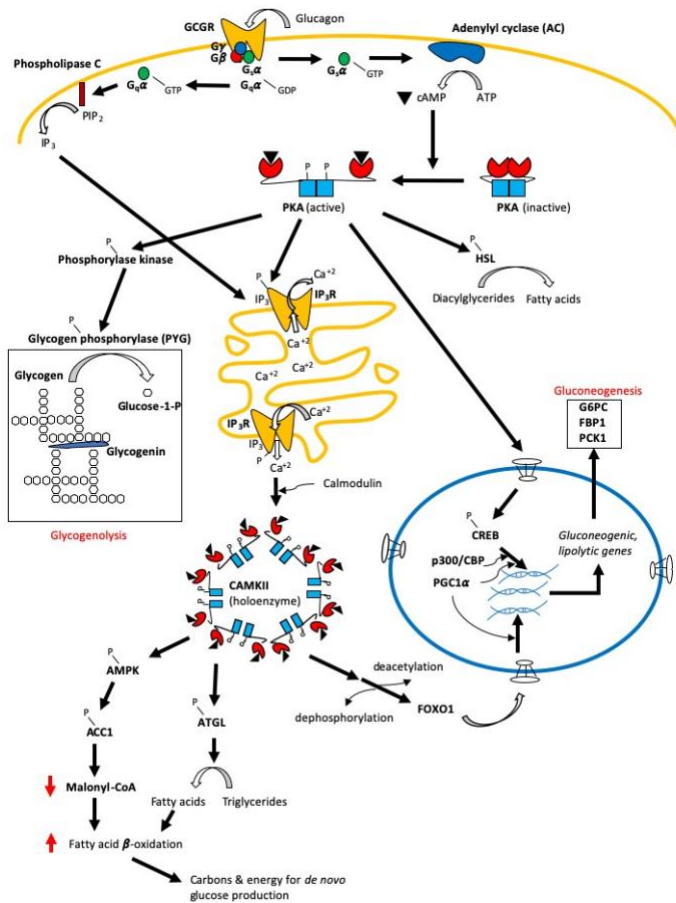
Figure 1.2 – **Glucagon signaling**. Glucagon binds its specific receptor to stimulate heterotrimeric G-protein signaling that produces cAMP and cytosolic Ca^{+2}. Signal transduction is further mediated by PKA and CAMKII to promote glycogenolysis, lipolysis and fatty acid oxidation, and lastly gluconeogenesis. GCGR: g-coupled glucagon receptor, $G_{(s/q)}\alpha/\beta/\gamma$: guanine nucleotide-binding protein alpha$_{(s/q)}$/beta/gamma subunits, GT(D)P: guanosine tri(di)phosphate, AC: adenylyl cyclase, cAMP: cyclic adenosine monophosphate, PKA: protein kinase A, PIP$_2$: phosphatidylinositol-4,5-bisphosphate, IP$_3$: inositol triphosphate, IP$_3$R: inositol triphosphate receptor, HSL: hormone-sensitive lipase, PYG: glycogen phosphorylase, CAMKII: Ca^{+2}/calmodulin-dependent protein kinase II, AMPK: AMP-activated protein kinase, ACC1: acetyl-CoA carboxylase 1, ATGL: adipose triglyceride lipase, FOXO1: forkhead box O1, CREB: cAMP-response element-binding protein, CBP: CREB-binding protein, PGC1α: peroxisome proliferator-activated receptor gamma coactivator 1 alpha.
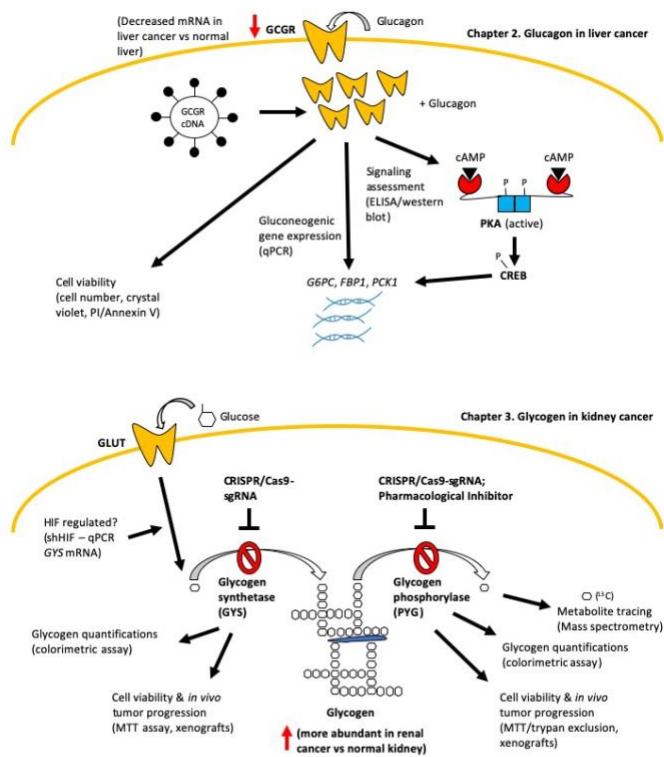
Figure 1.3 – Determining the roles of glucagon in liver cancer & glycogen in kidney cancer. For Chapter 2, our goal is to determine the effects of glucagon signaling in liver cancer. To that end, the glucagon receptor GCGR will be overexpressed in liver cancer cell models, followed by a pathway specific evaluation of signaling and gluconeogenic gene transcription. For Chapter 3, our aim is to characterize the function of elevated glycogen in kidney cancer. To accomplish this, both glycogen synthesis and breakdown will be disrupted via genetic and/or small molecule inhibition, followed by cell viability assessment. Additionally, glycogen-derived glucose tracing will be performed to elucidate how glycogen is utilized under nutrient-deprived conditions.

CHAPTER 2: Glucagon Signaling via Supraphysiologic GCGR can Reduce Cell Viability without Stimulating Gluconeogenic Gene Expression in the Liver Cancer Cells

Portions of this chapter have been adapted from:

(1) Godfrey J, Skuli N, Riscal R, and Simon MC. Glucagon signaling via supraphysiologic GCGR reduces cell viability without stimulating gluconeogenic gene expression in the liver cancer cell line, SNU398. *Manuscript in preparation*.

2.1 Abstract

Downstream biochemical processing of glucose in tumor cells, such as aerobic glycolysis, provides energy, anabolic precursors, reducing power, and other metabolites necessary for mitogenic engagement and environmental adaptability, creating an attractive therapeutic target. Here, we test the hypothesis of whether glucagon signaling can antagonize glycolysis by activating gluconeogenesis to reduce tumor proliferation in models of liver cancer. Liver cancer cell lines were infected with a lentiviral construct driving constitutive expression of the g-coupled glucagon receptor, GCGR. ELISA assays show an increase in cAMP abundance specifically in liver cancer cell lines overexpressing GCGR treated with 100nM glucagon. Western blot analysis of a glucagon-responsive transcription factor downstream of cAMP/PKA, CREB, reveal greater levels of activated S133 phosphorylation localized to the nucleus in SNU398 GCGR cells. However, qPCR data indicate that none of the three major gluconeogenic genes: *G6PC*, *FBP1*, or *PCK1*, are elevated at the mRNA level in SNU398 GCGR cells when treated with glucagon. Moreover, their expression cannot be fully restored to levels measured in primary human hepatocytes even in the presence of multiple epigenetic inhibitors. Regardless, glucagon-treated SNU398 GCGR cells showed a reproducible, two-fold increase in PI/Annexin V staining that was further validated by proliferation assays measuring 50% or more reduction in SNU398 GCGR cell number when exposed to glucagon. Rescue experiments utilizing siRNA or pharmacological inhibition of CREB showed no increase in SNU398 GCGR cell number in the glucagon condition, suggesting a CREB-independent, tumor suppressive function of glucagon signaling in SNU398. Overall, our work describes a novel finding that restrained cell viability of a liver cancer model can be actualized through glucagon signaling.

2.2 Materials and Methods

Cell Lines and Culture

The following liver cancer cell lines were purchased from the American Type Culture Collection (ATCC): SNU182 (hepatocellular carcinoma, P53$^{S215I/S215I}$, catalog # CRL-2235), SNU387 (hepatocellular carcinoma, NRAS$^{Q61K/+}$, P53$^{K164*/K164*}$, catalog # CRL-2237), SNU398 (hepatocellular carcinoma, β-catenin$^{S37C/+}$, catalog # CRL-2233), SNU423 (hepatocellular carcinoma, P53 splice site mutation, catalog # CRL-2238), SNU449 (hepatocellular carcinoma, P53$^{A161T/A161T}$, catalog # CRL-2234), SNU475 (hepatocellular carcinoma, P53$^{N239D,G262D/+}$, catalog # CRL-2236), HepG2 (hepatoblastoma, NRAS$^{Q61L/+}$, catalog # HB-8065), Hep3B (hepatocellular carcinoma, Axin1$^{R146*/R146*}$, catalog # HB-8064), PLC (hepatoma, P53$^{R249S/R249S}$, catalog # CRL-8024), and SKHEP1 (hepatocellular carcinoma, BRAF$^{V600E/+}$, catalog # HTB-52). Huh7 (hepatoma, P53$^{Y220C/Y220C}$) was a gift from Dr. Terence Gade. The patient-derived xenograft cell line, M7571, was a gift from Drs. Terence Gade and Katy Wellen. Top oncogene hotspot mutations listed for each cell line were compiled from the Broad Institute Cancer Cell Line Encyclopedia (https://portals.broadinstitute.org/ccle). 293T cells were purchased from the ATCC (catalog # CRL-3216). All cancer cell lines were maintained in RPMI 1640 medium (Gibco, catalog # 21875034) with 10% fetal bovine serum (Gemini Bio, catalog # 900-108), 1% penicillin/streptomycin (Gibco, catalog # 15140122), and incubated at 21% oxygen/5% carbon dioxide. These cells were passaged by aspirating media, washing with DPBS (Corning, catalog # 21-031-CM), detached from plates with 0.25% trypsin-EDTA (Gibco, catalog # 25200056), and re-plated with fresh 10% FBS-containing RPMI media. Most experiments were performed at 5% FBS. For glucose dependent growth assays, cells were cultured in RPMI medium without glucose (Gibco, catalog # 11879020) with dialyzed

FBS (Gemini Bio, catalog # 100-108). For lipid dependent growth assays, cells were cultured with delipidated FBS (Gemini Bio, catalog # 900-123). Primary human hepatocytes (PHH) obtained from Life Technologies (catalog # HMCS15) and directly lysed for RNA and protein analysis only without prior culturing. Cryoplateable primary human hepatocytes (cPHH) were obtained from Sigma-Aldrich (discontinued, catalog # MTOXH1000), thawed in Human Hepatocyte Thawing Medium from Sigma-Aldrich, (discontinued, catalog # MED-HHTM), and cultured in Human Hepatocyte Culture Medium from Sigma-Aldrich (discontinued, catalog # MED-HHCM) on collagen-coated plates. THLE3 cells (ATCC, catalog # CRL-11233) were seeded on plates coated overnight with 0.03mg/ml bovine collagen type I (Life Technologies, catalog #A1064401), 0.01mg/ml bovine fibronectin (Sigma-Aldrich, catalog # F1141), and 0.01mg/ml BSA (Sigma-Aldrich, catalog # A9576) in modified BEGM medium (Lonza, catalog # CC-3171) without gentamycin, amphotericin, or epinephrine and with an extra 5ng/ml EGF (Corning, catalog # CB-40052), 70ng/ul p-ethanolamine, 1% PenStrep, and 10% FBS.

Compounds

Hormones and inhibitors used in culture for *in vitro* experiments were as follows: Glucagon (Sigma-Aldrich, catalog #) was prepared in 0.05M acetic acid (Sigma-Aldrich, catalog # 6283) at a concentration of 1mg/ml. Forskolin (MedChem Express, catalog # HY-15371) was prepared in DMSO (Sigma-Aldrich, catalog # 2650) at a stock concentration of 10mM. 666-15 (Sigma-Aldrich, catalog # 5383410001) was prepared in DMSO at a stock concentration of 10mM. Palbociclib (Selleck Chemicals, catalog # S1116) was prepared in DMSO at a stock concentration of 10mM. GSK126 (Selleck Chemicals, catalog # S7061) was prepared in DMSO at a stock concentration of 10mM. LBH589 (Selleck Chemicals, catalog # S1030) was prepared in DMSO at an initial

concentration of 10mM and diluted to 0.1mM for a working stock solution. Decitabine (Selleck Chemicals, catalog # S1200) was prepared in DMSO at a stock concentration of 10mM. Sorafenib (Selleck Chemicals, catalog # S1040) was prepared in DMSO at a stock concentration of 10mM. UNC0642 (Selleck Chemicals, catalog # S7230) was prepared in ethanol (Decon labs) at a stock concentration of 10mM.

Plasmid purification and cloning

Bacterial cultures of pLenti-CMV-eGFP-PURO (Addgene, catalog # 17448) and pCR4-TOPO-GCGR (Dharmacon, catalog # MHS6278-202857850) were grown in 1X LB (Difco) plus Carbenicillin (Sigma-Aldrich, catalog # c1389) overnight at 30 degrees Celsius with shaking. DNA plasmid minipreps were performed according to the kit manufacturer (Qiagen, catalog # 27106). GCGR cDNA was PCR-amplified to include XbaI and SalI restriction enzyme sites with the forward primer (5'-GATACTTCTAGAATGCCCCCCTGCCAGCC-3') and reverse primer (5'-GATACTGTCGACTCAGAAGGGGCTCTCAGCCA-3'), respectively. GCGR cDNA and pLent-CMV-eGFP plasmid were digested with XbaI and SalI, and purified following agarose gel electrophoresis with QIAquick gel extraction kit (catalog # 28706). Purified, digested GCGR cDNA and pLenti-CMV vector backbone were then ligated and used to transform TOP10 (OneShot) cells. Colonies with successful ligations were picked and re-streaked on LB-Carbenicillin plates overnight at 30 degrees Celsius. New minipreps were made on a few colonies and validated by Sanger sequencing with the CMV forward primer (CGCAAATGGGCGGTAGGCGTG) at the Children's Hospital of Philadelphia Sequencing Core Facility.

Lentiviral Infection and siRNA Transfection

37

To generate lentivirus for stable integration and expression of eGFP or GCGR, approximately 400,000 293T cells were seeded in 6-well plates without PenStrep. The following day, cells were transfected with 3 plasmids prepared in OPTI-MEM (Gibco, catalog # 31985070): 3μg of pLenti-eGFP or pLenti-GCGR, 3μg of psPAX2, and 0.3μg of pMDG.2 with 3μl FuGENE reagent (Promega, catalog # E2691) per well. The next day, media was aspirated and fresh 10-30% FBS-containing media was added to each well for 24-48hr incubation. Virus was harvested by filtering media through a 0.45μm filter (Millex-HV). Viral solutions were aliquoted into cryovials and stored in -80 degrees Celsius and all supplies in contact with virus were bleached. Liver cancer cells were infected with 250-1000μl of virus in 1.5ml total media, containing 8μg/ml polybrene (Sigma-Aldrich, catalog # 107689). After 24-48hrs, stably expressing eGFP- or GCGR-cells were selected by puromycin (Sigma-Aldrich, catalog # P9620) at a concentration range between 1-5μg/ml. For siRNA transfections, pooled siRNAs were purchased from Dharmacon to target CREB1 (catalog # L-003619-00-0005) and controls, Cyclophilin B (catalog # D-001820-10-20) or a non-targeting sequence (catalog # D-001810-10-05). Transfections were performed according to the manufacturer's recommendation. SNU398 cells were seeded in 6-well plates at approximately 30-40% confluency (50,000 - 100,000 cells) and at the indicated time point were transfected with 25nM of siRNA in OPTI-MEM with 2-6μl lipofectamine (Fisher Scientific, catalog # 13778030) per well. The next day, media was aspirated and cells were given the appropriate, fresh media.

Proliferation (cell # or density) Assays

Cells were seeded in 6-well or 12-well plates at approximately 30-40% confluency (50,000 - 100,000 cells for 6-well and 25,000 - 50,000 cells for 12-well) in 10% FBS-

containing RPMI. The following day, media was aspirated and the experimental conditions were added, with this process repeated over the duration of the experiment, as described in each figure. For cell number quantifications, at the indicated time points, media were aspirated, washed with DPBS, trypsinized with 0.5ml (6-well) or 0.25ml (12-well), and then neutralized with equivalent volumes of 10% FBS-containing media. Next, 10μl of cells was mixed with 10μl of 0.4% Trypan Blue (Gibco, catalog # 15250061) and finally counted in a Countess II (Life Technologies), with live cell/ml concentrations corrected for a 1:1 dilution. Quantifications were further analyzed in Microsoft Excel and Prism 9. For crystal violet colorimetric assays, at the indicated time points, media were aspirated and then 1ml (6-well) or 0.5ml (12-well) of 0.5% crystal violet (Sigma-Aldrich, catalog # C6158)/20% methanol (Sigma-Aldrich, catalog # 179337) solution in ddH$_2$O was added down the sides of each well. Cells were incubated with crystal violet for 10 minutes with gentle rocking. Crystal violet solutions were aspirated and then cells were washed twice with DPBS. For the last wash, cells were gently rocked in DPBS for at least an hour to help remove background staining. Following DPBS aspiration, plates were inverted and dried overnight. Images were taken by a scanner (Epson Perfection 4490 Photo, discontinued) and assembled into figure format in Adobe Photoshop 2020. Quantification of crystal violet staining was performed by adding an equivalent volume of 99.8% methanol, incubating plates at room temperature for at least 1 hour, and then reading absorbance at OD 570nm (Feoktistova et al, 2016)[186].

Viability (ATP-based) Assays

Cells were seeded in white, opaque, flat bottom 96-well plates (Corning, catalog # CLS3917) at approximately 30-40% confluency (1000 - 4000 cells) in 50μl of 10% FBS-containing RPMI. The following day (Day 0), 50μl of experimental media conditions at a

2X concentration were added to the appropriate wells and incubated for the indicated durations. At Day 0, 50µl of normal media was added to a separate plate for a baseline reading. For all readings, 50µl of Cell Titer Glo reagent (Promega, catalog # G9242) was added directly to each well and incubated at room temperature while shaking for 10 minutes. Luminescence was measured by a microplate reader (SpectraMax M2, Molecular Devices) with the settings at white/opaque plate, top read, and 3 reads per sample rate. Further numerical analysis, such as normalization to baseline, were calculated with Microsoft Excel and Prism 9.

Apoptosis (propidium iodide & annexin v-based) Flow Cytometry

Cells were seeded in 6-well plates at approximately 30-50% confluency (50,000 - 200,000 cells) in 10% FBS-containing RPMI. The following day, media was aspirated and the experimental conditions were added, with this process repeated over the duration of the experiment, as described in each figure. At the endpoint, media was collected in 15ml conical tubes, cells were washed with DPBS, which was then collected in the same tubes, and then 0.5ml of trypsin was added to each well. Upon detachment, cells were transferred into their respective tubes and pelleted by centrifugation at 2000rpm for 5min. Supernatants were discarded and rims of tubes dried by kimwipe. Cell pellets were resuspended in 110µl of staining solution containing 5% Annexin V, 5% Propidium Iodide, and 90% 1X binding buffer (BD Bioscence, catalo # 556547). Next, cells were filtered through a 35µm strainer cap in FACS-compatible tubes (MTC Bio, catalog # T9005) and incubated in the dark for 15 minutes at room temperature. 300µl of 1X binding buffer was added, vortexed, and then flow analysis was performed with a BD FACSCalibur. Stained cells were kept on ice and protected from light when not being

processed. Gates were drawn to obtain data for at least 10,000 single cell events. FlowJo software was used to further process data.

Gene Expression Analysis

For patient data, mRNA expression was obtained from The Cancer Genome Atlas (TCGA) (https://www.cbioportal.org). Raw RNA-seq reads were normalized and presented as log2 values by Dr. John Tobias (University of Pennsylvania). These calculations were graphed and statistically analyzed using Prism 9. Kaplan-Meier probability curves for overall survival comparing expression of a given gene was obtained from the website tool, https://kmplot.com (Nagy et al, 2021)[187]. Briefly, a TCGA RNA-seq dataset for liver cancer with 364 patient tumor samples was assessed for most statistically significant correlation between high vs. low gene expression and the probability of patient survival. For experimental studies in general, cells were seeded in 6-well plates in 10% FBS-containing RPMI at approximately 30-50% confluency (50,000 - 200,000 cells) for <24hr durations or at 50-70% confluency (200,000-400,000 cells) for >24hr time points. At the designated endpoint, media was aspirated, cells were washed with 1ml of 1X DPBS on ice, aspirated again, and then RNA extraction was performed with the Qiagen RNeasy kit (Qiagen, catalog # 74104), following the manufacturer's protocol. RNA concentrations were determined using a NanoDrop 1000 (Thermo Fisher Scientific). Next, between 0.25-1μg of RNA was reverse transcribed into cDNA with the High-Capacity RNA-to-cDNA kit (Applied Biosystems, catalog # 4388950). A ratio of 10μl buffer and 1μl enzyme per 20μl total volume was used. Reactions were prepared in strip tubes (Thermo Fisher Scientific, catalog # AB-0773) and a RT-PCR cycle program was run in a C1000 Thermal Cycler (BioRad) with reaction settings of 37/36:00, 95/3:00. cDNA samples were diluted in ddH$_2$O by 10-20-fold depending on the amount of RNA

used. qPCR of target genes was performed in a ViiA7 using 5.4μl of cDNA with 0.6μl

TaqMan primers (Thermo Fisher Scientific) per reaction and 6.6μl (6ul buffer, 0.6ul

enzyme) of TaqMan Fast Advanced Master mix (Life Technologies, catalog # 4444965).

All qPCR reactions were performed in three technical triplicates. Raw Ct values were

converted into $\Delta\Delta$Ct by first subtracting the technical replicate average of the

housekeeping gene (RNA45S) from the Ct value of each target gene (=ΔCt). Then ΔCt

values were converted to expression with the formula =$2^\wedge$-ΔCt. Expression values were

then normalized to the triplicate average of the vehicle or primary human hepatocyte

sample (=$\Delta\Delta$Ct). Taqman primers used for this work are the following: housekeeping

gene *RNA45SR* (catalog # Hs03928985_g1), *GCGR* (catalog # Hs00164710_m1),

G6PC (catalog # Hs02560787_s1), *FBP1* (Hs00983323_m1), *PCK1* (catalog #

Hs00159918_m1).

Protein Analysis

For experimental studies in general, cells were seeded in 6-well plates in 10% FBS-

containing RPMI at approximately 30-50% confluency (50,000 - 200,000 cells) for <24hr

durations or at 50-70% confluency (200,000-400,000 cells) for >24hr time points. At the

designated endpoint, media was aspirated, cells were washed with 1ml of 1X DPBS on

ice, aspirated again, and then 50-200μl of whole cell extract lysis buffer (3% of 5M NaCl,

1% of 1M Tris pH 7.6, 0.1% SDS, 1% of 0.5M EDTA, and 1X protease/phosphatase

inhibitor cocktail (Thermo Fisher Scientific, catalog # 78444) in ddH$_2$O) was added to

each well and incubated on ice for at least 10min. Cells were scraped and transferred

into a 1.5ml microfuge tube. Following 10s sonication pulses per tube, samples were

spun down at 13,000 RPM for 10min in 4 degrees Celsius. Protein supernatants were

pipetted into new 1.5ml microfuge tubes. For subcellular fractionation, nuclear and cytosolic protein samples were extracted using the NE PER kit (Thermo Fisher Scientific, catalog # 78833), following the manufacturer's protocol. Sample concentrations were performed by BCA (Pierce), following the manufacturer's protocol, and calculated in Microsoft Excel using trendline analysis comparing the OD 562nm of samples to a standard curve of BSA. For western blots, depending on the concentration, between 5-40μg of protein (in 1X sample buffer, 1% beta-mercaptoethanol (Sigma-Aldrich, catalog # M3148)) were loaded into SDS-acrylamide PAGE gels (4% stacking, 10-12% running) and ran at 100-130V for 60-90 minutes. Proteins were then transferred onto nitrocellulose membranes in a transfer apparatus at 0.1A overnight in 4 degrees Celsius. Membranes were blocked with 5% nonfat milk in 1X TBST for approximately 1hr at room temperature. Following a few washes with 1X TBST, membranes were cut with scissors at the appropriate sizes and incubated with the corresponding primary antibodies (prepared in 1X TBST, 5% BSA, 0.01% sodium azide) overnight at 4 degrees Celsius with rocking. The following day, antibody solutions were pipetted into original tubes for future use, membranes washed 2-3 times with 1X TBST, and then incubated with 1:10,000 secondary antibody conjugated to HRP for 1hr at room temperature with rocking. Antibody solutions were discarded and membranes were washed 3 times with 1X TBST over the course of an hour. Autoradiography film processing of membranes were performed in a dark room. Films were scanned and protein band images were cropped for figure production by Adobe Photoshop. Primary antibodies used for this work are the following: β-Actin (Cell Signaling Technology, catalog # 3700), GAPDH (Cell Signaling Technology, catalog # 2118), GCGR (Invitrogen, catalog # PA5-50668), eGFP (Thermo Fisher Scientific, catalog # CAB4211), p-PKA substrates (Cell Signaling

43

Technology, catalog # 9624S), p-CREB S133 (Cell Signaling Technology, catalog # 9198), total CREB (Cell Signaling Technology, catalog # 9197), H3K27me3 (Cell Signaling Technology, catalog # 9733), H3K27Ac (Cell Signaling Technology, catalog # 8173), total H3 (Cell Signaling Technology, catalog # 14269), DNMT1 (Cell Signaling Technology, catalog # 5032), cleaved PARP (Cell Signaling Technology, catalog # 5625), cleaved Caspase-3 (Cell Signaling Technology, catalog # 9664), Cyclophilin B (Abcam, catalog # ab16045), p-CaMKII T286 (Cell Signaling Technology, catalog # 12716).

ELISA Assays

For cAMP quantification, cells were seeded in 6-well plates in 10% FBS-containing RPMI at approximately 30-50% confluency (50,000 - 200,000 cells) for <24hr durations or at 50-70% confluency (200,000-400,000 cells) for >24hr time points. At the designated endpoint, media was aspirated, cells were washed with 1ml of 1X DPBS on ice, aspirated again, and then 200μl of 1N HCl was added to each well for lysis. The remaining steps were carried out according to the manufacturer's protocol (Enzo Life Sciences, catalog # ADI-900-066). For serum glucagon quantification, blood was initially collected by retroorbital draw and allowed to clot at room temperature for one hour. Samples were then centrifuged at 3000RPM for 10min in 4 degrees Celsius and serum supernatant was transferred into a new 1.5ml microfuge tube. From here, quantification of glucagon was determined by following the manufacturer's protocol (R&D Systems, catalog # DGCG0). Sigmoidal regression analysis and extrapolations were calculated in Prism for final concentrations.

Mouse Experiments

All experiments described were approved by IACUC at the University of

Pennsylvania. All mice used for xenograft experiments were 4-6 weeks old Nu/J females

(Jackson Laboratory, catalog # 002019). Following a few days of acclimation, mice were

anesthetized with isofluorane and 1-2 million SNU398 liver cancer cells (in a 1:1 mixture

of DPBS:matrigel) were subcutaneously injected into both flanks. After approximately 2-

3 weeks, xenograft tumors reached an average of 100mm^3, caliper measured, at which

point experimental treatments began. The EZH2 inhibitor, GSK126, and pan-HDAC

inhibitor, LBH589, were prepared at the indicated concentration in 20% 2-hydroxypropyl-

β-cyclodextrin (Cayman Chemical, catalog # 16169) pH 4.5 either as a single agent or in

combination. 200μl of the drug solutions was intraperitoneally injected once daily unless

mice displayed toxicity symptoms, such as severe weight loss and lethargy, at which

point drugs were administered irregularly following weight recovery. Once tumors

reached 2000mm^3, mice were euthanized by CO_2, followed by cervical dislocation.

Tumors were resected and frozen on dry ice for further processing. Tumor volumes were

calculated by the following equation: $(\pi/6)$ x (width^2) x (length), where width is always the

shorter parameter.

2.3 Results

Gluconeogenic Proteins are Downregulated in Glucose-Dependent Liver Cancer Models

To provide a rationale for targeting glucose metabolism via glucagon-stimulating

gluconeogenesis in liver cancer, we probed the necessity of glucose for cell viability. Cells

that require more glucose may exhibit increased vulnerability to agents stimulating

gluconeogenesis, such as glucagon. To that end, 11 established cell line models of liver

cancer, with various disease etiology and oncogenic driver mutations (see **Table 2.1; pgs. 68 and 69**), were cultured *in vitro* under glucose-limiting conditions and cell numbers were quantified after approximately one week of growth. All cell lines tested were unable to proliferate in 0mM glucose conditions, and in particular, SNU398, SNU182, and SNU475 cells were unable to fully recover even in physiological 5mM glucose concentrations (**Fig. 2.1A**, and **Supp. Fig. 2.1A; pgs. 60 and 61**).

Previous studies have demonstrated the key role of hepatic lipolysis, via the activation of inositol triphosphate receptor 1 and adipose triglyceride lipase, in glucagon-stimulated gluconeogenesis (Perry et al, 2020)[120]. Moreover, the metabolic effects of glucagon contribute to hepatic fat clearance in fatty liver disease models (Finan et al, 2016)[188], suggesting glucagon-induced depletion of lipid stores may reduce viability in liver cancer cells that demand more fatty acids for growth. To examine lipid dependency, we compared endpoint proliferation between cells cultured with normal serum, delipidated serum, or delipidated serum with oleic acid supplementation. Unlike glucose, more varied results were obtained across cell lines (**Fig. 2.1A**, and **Supp. Fig. 2.1B; pgs. 60 and 61**). This lipid phenotypic distribution did not appear to be due to relative growth rate or oncogenic driver (data not shown), which may simply indicate that not all cell lines are able to perform adequate *de novo* lipogenesis under nutrient deprivation. Short-term cell viability assessment of growth recapitulated these findings across all cell lines tested, reinforcing the conclusion that all liver cancer cells require glucose but not lipids (**Supp. Fig. 2.1C, D; pg. 61**). At the very least, this highlights a critical role of glucose in the growth of established liver cancer cells, which is not ubiquitously observed in all cancers, like soft tissue sarcomas (Lee et al, 2020)[88].

The inability of liver cancer cells to proliferate under 0mM glucose supports the hypothesis that any process that antagonizes glucose utilization, such as gluconeogenesis, may suppress tumor growth. Gluconeogenesis is the direct biochemical reversal of glycolysis, whereby three rate-limiting enzymes, PCK1, FBP1, and G6PC, work to synthesize glucose and ultimately release it from the hepatocyte (**Supp. Fig. 2.1E; pg. 61**). In both liver cancer cell lines and patients, all major gluconeogenic genes are significantly downregulated in tumors compared to normal liver tissue (**Supp. Fig. 2.1F, G; pg. 61**). In contrast, this expression pattern was not observed across all glycolytic genes (data not shown), suggesting that gluconeogenic dampening may be more vital than direct glycolytic acceleration in liver cancer development. We hypothesized that silencing across all gluconeogenic genes involved a deficient upstream node of the pathway.

Physiologically, hepatocytes initiate production of glucose upon prolonged glucagon signaling via its receptor, GCGR, which stimulates a cascade of signaling events mediated by cAMP and PKA that activate transcription factors, such as CREB, to induce gluconeogenic and lipolytic gene expression (**Fig 2.1B; pg. 60**). Similar to the gluconeogenic enzymes, *GCGR* is also significantly downregulated at the mRNA level in both liver cancer patient samples and cell lines (**Fig. 2.1C, D; pg. 60**). Whereas normally, GCGR is most abundant in the liver versus any other tissue type, we also detected a comparable decrease in *GCGR* expression in the immortalized, normal hepatocyte cell line, THLE-3 (data not shown). This data suggests that either artefactual contributions from 2D growth or early mutagenic events inhibiting tumor suppressor genes may account for *GCGR* repression in liver cancer. Regardless, based on RNA-seq data analyzed by the website tool, https://kmplot.com (see Methods), tumors with lower gene expression of

GCGR and the gluconeogenic enzymes correlate with shorter overall survival in liver cancer patients (**Fig. 2.1E** and **Supp. Fig. 2.1H**, respectively; **pgs. 60 and 61**).

Overexpression of GCGR Activates Glucagon-Mediated Signaling Transduction via cAMP in SNU398 Cells

Based on strict glucose requirements for cell growth, a ubiquitous decrease in *GCGR* mRNA in liver cancer samples, and the positive correlation between *GCGR* expression and patient survival, we hypothesized that glucagon signaling downstream of GCGR may restore gluconeogenic expression and drive anti-tumorigenic effects. To examine this possibility, *GCGR* cDNA was overexpressed in the human hepatocellular carcinoma cell line SNU398, which notably harbors a constitutively active mutation in β-catenin. RNA and protein analysis verified the supraphysiologic overexpression of GCGR in SNU398 cells (**Fig. 2.2A, B; pg. 62**). To determine whether ectopic overexpression of GCGR can effectively promote adenylyl cyclase activity in response to glucagon, control (eGFP-expressing) or GCGR-overexpressing cells (referred to as SNU398 GCGR cells) were treated with glucagon and assayed for cAMP. SNU398 GCGR cells reproducibly generated cAMP in response to glucagon exposure, which in some cases was as high as the positive control condition, forksolin, an agonist of adenylyl cyclase (**Fig. 2.2C, Supp. Fig. 2.2A; pgs. 62 and 63**), thus confirming that glucagon/GCGR signaling was functional in this system.

To further investigate glucagon signaling, cAMP-dependent PKA activity was assessed by phosphorylation of PKA-substrates. SNU398 GCGR cells stimulated with glucagon showed rapid increases in phosphorylation of PKA targets, including p-CREB S133 (**Fig. 2.2D; pg. 62**). Because G-coupled protein receptors can also activate

phospholipase C and the subsequent release of calcium ions from the endoplasmic reticulum, we probed for a common effector of glucagon and Ca^{+2} signaling, CAMKII, but did not observe any difference in any of its activated isoforms (**Fig. 2.2D; pg. 62**). However, we further validated the phosphorylation of CREB by GCGR stimulation over a longer period of time and range of glucagon concentrations. Phosphorylation of CREB at S133 was maximally measured with 100nM glucagon, specifically in SNU398 GCGR cells, with no change in total CREB (**Supp. Fig. 2.2B; pg. 63**). Although there are other post-translational modifications reported for CREB, the phospho-S133 site is thought to enhance the recruitment of necessary transcriptional co-activators (Johannessen et al, 2004)[189]. Since previous studies in cancer models have demonstrated instances of mitochondrial CREB localization (Steven et al, 2016)[190], we performed nuclear fractionations on SNU398 eGFP or GCGR cells treated with glucagon to verify if activated p-CREB S133 was spatially capable of facilitating gluconeogenic gene transcription. The glucagon/GCGR-dependent increase in p-CREB was detected in the nuclear fraction (**Fig. 2.2E; pg. 62**), suggesting that the canonical cAMP-PKA-CREB pathway downstream of glucagon signaling was functionally intact in SNU398 GCGR cells.

With increased activated CREB in the nucleus, we next quantified the relative mRNA abundance of *G6PC*, *FBP1*, and *PCK1*, the transcriptional output of glucagon-mediated gluconeogenesis. Upon glucagon treatment of SNU398 GCGR cells for either 3 or 5 days, *G6PC* mRNA levels did not significantly increase relative to control cells (**Fig. 2.2F, Supp Fig. 2.2C; pgs. 62 and 63**). Moreover, both *FBP1* and *PCK1* mRNA expression was undetected, regardless of condition (data not shown). These data imply that glucagon signaling in SNU398 GCGR cells, was unable to transmit completely to gluconeogenic gene transcription. Other cell line models employing this GCGR overexpression strategy

were similarly examined, and whereas we did measure comparable *GCGR* expression (**Supp. Fig. 2.2D; pg. 63**) and elevated cAMP concentrations upon glucagon treatment (**Supp. Fig. 2.2E; pg. 63**), PKA activity and p-CREB were not discernably increased compared to SNU398 (**Supp. Fig. 2.2F; pg. 63**).

In contrast to SNU398 GCGR cells, primary human hepatocytes treated with glucagon displayed trends (1.5-3-fold) towards an increase in gluconeogenic gene expression for all 3 enzymes, alongside a drop in *GCGR* mRNA abundance (**Supp. Fig. 2.2G; pg. 63**). However, it is unclear if this level of change accurately reflects the physiological response to glucagon in humans, as studies in zebrafish, rat, and murine hepatocytes have measured increases in *PCK1* mRNA anywhere from 4-to-20-to-500-fold upon glucagon treatment, respectively (Karanth et al, 2018; Zhang et al, 2011; Taddeo et al, 2017)[191-193]. Of note, we did not observe a decrease in *GCGR* expression with glucagon treatment in SNU398 or other liver cancer cell lines, but rather a consistent increase (data not shown). We hypothesize this could be due to increased levels of the transcription factor, carbohydrate-responsive element binding protein (ChREBP), in liver cancer (Ribback et al, 2018)[194] that has been shown to positively regulate *GCGR* expression in rat hepatocytes (Iizuka et al, 2012)[195]. Collectively, our data indicate that glucagon cannot induce a uniform augmentation in gluconeogenic gene expression in liver cancer cell lines and that SNU398 cells are most responsive to glucagon upon GCGR overexpression, in terms of downstream signaling.

Co-Treatment of SNU398 GCGR Cells with Glucagon and Epigenetic Inhibitors Cannot Fully Restore Gluconeogenesis

Our data shows a signaling cascade from extracellular glucagon to nuclear CREB in SNU398 GCGR cells, yet this fails to effectively induce gluconeogenic gene transcription, which we hypothesized would antagonize glycolysis to reduce tumor growth. One approach to promote transcriptional activation is through inhibiting heterochromatic epigenetic modifications. Previous studies on the *FBP1* loci have indicated that the presence of biochemical alterations to histones and DNA functionally correlate with heterochromatin formation and gene silencing. Specifically, promoter-rich methylated cytosine residues (Chen et al, 2011)[196], non-acetylated histone 3 lysine 27 in enhancer regions (Yang et al, 2017)[197], and the chromatin interaction of the histone methyltransferase, EZH2 (Liao et al, 2020)[198], have all been identified as mechanisms of epigenetic repression for *FBP1* in liver cancer. Therefore, we hypothesized that glucagon/GCGR signaling requires chromatin accessibility in order to fully activate gluconeogenic gene expression and the accompanying metabolic program.

To that end, we tested the efficacy of 3 epigenetic inhibitors targeting either EZH2-specific histone methylation (GSK126), HDAC-mediated histone deacetylation (LBH589), or DNMT-catalyzed cytosine methylation (Decitabine) (**Fig. 2.3A; pg. 64**). For GSK126, reduced EZH2 catalytic activity has been shown to reduce the trimethylation of lysine 27 in histone 3 (H3K27me3) (McCabe et al, 2012)[199]. For LBH589, pan-HDAC inhibition results in broad increases in histone acetylation (Scuto et al, 2008)[200]. And lastly, for Decitabine, it has been shown that reduction of DNA methylation is at least partially through the degradation of DNMTs (Ghoshal et al, 2005)[201]. As determined by western blot probing of these specific effects, all 3 compounds were found to be effective in SNU398 (**Fig. 2.3B; pg. 64**). To further confirm their efficacy, we treated SNU398 and

other cell lines at ranges of drug concentrations for different durations and found similar effectiveness on their respective target enzymes (data not shown).

Since previous studies have performed experiments assessing gluconeogenic gene expression following treatment with the above epigenetic drugs as single agents in liver cancer models, we first tested whether combinations of epigenetic inhibitors themselves could restore gluconeogenic gene expression to any meaningful degree. After 24hr of drug treatment, we measured approximately 20-fold increases in expression of *FBP1* and *PCK1* with the triple combination in SNU398, while *G6PC* mRNA level was largely unchanged across all drug permutations (**Fig. 2.3C; pg. 64**). Next, we tested whether GCGR-overexpressing SNU398 cells stimulated with glucagon would be more amenable to gluconeogenic gene expression with the epigenetic inhibitors. Interestingly, we observed a different effect on mRNA levels for each gluconeogenic enzyme: (1) *G6PC* expression, again, remained unchanged regardless of glucagon/GCGR signaling or epigenetic inhibition, (2) *FBP1* abundance was more dependent on epigenetic regulation than glucagon/GCGR stimulation, and (3) *PCK1* mRNA levels were substantially elevated only when both glucagon/GCGR signaling and epigenetic inhibition were present (**Fig. 2.3D; pg. 64**). Importantly, the relative 200-fold increase in *PCK1* expression with the triple combination plus glucagon/GCGR is still at least an order of magnitude less than the *PCK1* levels in normal hepatocytes (data not shown).

We next examined a patient-derived xenograft cell line, M7571, to determine whether a more patient-proximal liver cancer model was amenable to restoration of gluconeogenic gene expression after treatment with glucagon and our panel of epigenetic inhibitors. We quantified a maximal 2-fold increase in gene expression of the gluconeogenic enzymes under any condition tested in M7571 cells (**Fig. 2.3E; pg. 64**). However, contrary to the

established SNU398 cell line, M7571 has vastly greater mRNA quantities of all 3 gluconeogenic enzymes, which was more comparable to primary human hepatocytes. That being the case, M7571 cells do display reduced *GCGR* expression, akin to other liver cancer cell lines (data not shown). This may explain why neither the epigenetic inhibitors nor glucagon treatment substantially increased gluconeogenic gene expression, as little epigenetic repression at the gluconeogenic gene loci coupled with low *GCGR* expression would predictably make M7571 cells less responsive to epigenetic inhibitors and glucagon, respectively.

Although the epigenetic inhibitors failed to fully restore gluconeogenic gene expression in SNU398, cell growth was noticeably affected at specific drug concentrations and combinations. To provide a systematic analysis of this effect, the viability of multiple liver cancer cell lines was measured by relative ATP abundance across pharmacologically relevant doses of each epigenetic drug (**Supp. Fig. 2.3A; pg. 65**). We included the FDA-approved receptor tyrosine kinase inhibitor, Sorafenib, as a clinically meaningful comparison, as well as another experimental inhibitor, UNC0642, targeting the histone methyltransferase, G9a, which has garnered recent appreciation for its contributions to cancer progression (Kato et al, 2020)[202]. Our data reveal a broad scope of responses across liver cancer cell lines. In general, cell lines like SNU449 exhibited increased tolerance to epigenetic inhibitor treatment, whereas other cell lines like SNU398 displayed greater sensitivity. Interestingly, SNU398 cells showed severe growth reduction with the dual treatment of the EZH2 inhibitor (GSK126) and the pan-HDAC inhibitor (LBH589), suggesting a potential therapeutic window for the drug combination (**Supp. Fig. 2.3B; pg. 65**).

53

To further characterize the *in vivo* effects of EZH2/HDAC inhibition on SNU398 cells, we generated xenograft tumors in Nu/J mice. Once tumor volume reached an average of 100-200cm^3, mice were treated intraperitoneally with the epigenetic drugs at doses previously published by other groups. Although treatment with anti-EZH2/HDAC compounds suppressed the growth of SNU398 xenografts, significant toxicity was prevalent, as measured by greater than 20% decreases in mouse body weight (**Supp. Fig. 2.3C, D; pg. 65**).

Overall, our data indicates that while various epigenetic inhibitors may be effective in attenuating heterochromatin repression of specific gluconeogenic gene loci under certain conditions in liver cancer cells, we conclude that epigenetic inhibition is not sufficient for glucagon-stimulated gluconeogenesis. Furthermore, although the epigenetic drugs present potential therapeutic avenues from viability data in multiple cell lines *in vitro*, it is unclear if this can be translated into clinical strategies or if patients would experience better quality of life over currently deployed targeted therapies, such as Sorafenib.

SNU398 GCGR Cells Display Reduced Viability upon Glucagon Treatment through CREB-Independent Mechanisms

Similar to the epigenetic inhibitors, while glucagon/GCGR stimulation was unable to restore gluconeogenic gene expression to physiological levels, we did observe a reproducible, apoptotic phenotype in SNU398 GCGR cells when treated with glucagon. The apoptotic protein markers, cleaved PARP and cleaved Caspase-3, were both induced specifically in SNU398 cells overexpressing GCGR upon glucagon exposure (**Fig. 2.4A; pg. 66**). Additionally, overall cell number was significantly decreased in SNU398 GCGR cells with persistent glucagon treatment (**Fig. 2.4B; pg. 66**). This reduction in cell growth

was comparable to treatment with the cell cycle inhibitor, Palbociclib, and also more pronounced than daily forskolin treatment, suggesting glucagon/GCGR may be either more efficient in signal transduction via cAMP or engage other pathways aside from cAMP signaling to enact tumor suppressive properties. Further validation of apoptosis engagement in these conditions was supported by increases in PI/Annexin V-positivity (**Fig. 2.4C; pg. 66**).

According to previous studies, glucagon ligand binding to GCGR approaches saturation at the mid nanomolar range (Han et al, 2015)[203]. Indeed, we observed a dose-dependent decrease in cell number with increasing glucagon concentration that plateaued at 100nM and began displaying anti-proliferative effects around 3-4 days (**Fig. 2.4D; pg. 66**). Because serum concentration can have an impact on drug efficacy *in vitro*, upon continued examination of this glucagon/GCGR phenotype, we observed an optimal difference in growth at 5% serum, a lack of phenotype at 10% serum, and a highly unconducive condition to cell growth at 1% serum (**Fig. 2.4D**, data not shown; **pg. 66**). We tested this phenotype in numerous other liver cancer cell lines for glucagon/GCGR robustness but did not measure equivalent changes in cell number compared to SNU398 at 100nM glucagon (**Supp. Fig. 2.4A; pg. 67**). These data suggest that SNU398 possesses a unique vulnerability to glucagon signaling, which may represent a subset of patients.

We have previously shown that SNU398 is the only cell line tested that shows an increase in p-CREB S133 with glucagon/GCGR (**Supp. Fig. 2.2F; pg. 67**). Therefore, we surmised that CREB may be critical for a gluconeogenic-independent transcriptional program inducing cell death, specifically in SNU398. A siRNA knockdown of CREB protein did not rescue SNU398 GCGR cell proliferation with glucagon treatment (**Supp.**

Fig. 2.4B; pg. 67), despite reasonable reductions in levels of active p-CREB S133

(**Supp. Fig. 2.4C; pg. 67**). Even though we did not observe a substantial effect on

viability from siCREB, we switched to a pharmacological approach with the CREB

inhibitor, 666-15, which has been shown to disrupt binding critical for transcriptional

activity (Xie et al, 2015)[204] and reduce phosphorylation in AML models (Kang et al,

2015)[205]. However, no decrease in p-CREB S133 with drug treatment was observed

(**Supp. Fig. 2.4D; pg. 67**), and likewise, no rescue of cell death under the

GCGR/glucagon/666-15 condition was measured (**Supp. Fig. 2.4E; pg. 67**).

2.4 Discussion

Our study indicates that the liver cancer cell line SNU398 can be partially re-sensitized

to glucagon, in terms of downstream signaling and biological effect, upon supraphysiologic

levels of ectopic GCGR. This re-sensitization was unique to this specific liver cancer cell

line as others did not show a similar phenotype. Concordantly, we hypothesize that liver

cancer cells themselves would be largely unaffected by circulating glucagon directly.

Although, it remains to be seen if normal hepatocytes stimulated to synthesize glucose by

glucagon secretion could provide local glucose, as tumor cells are thought to regulate

metabolism of others cells within the microenvironment to suit their nutritional needs

(Comito et al, 2020)[206]. In this manner, gluconeogenesis could actually be oncogenic at

the systemic level through nutrient partitioning and/or competition between normal and

tumor cells. Diabetes is a risk factor for liver cancer development and is commonly

characterized by abnormally high glucagon signaling, likely as a result of decreased insulin

sensitivity (Haedersdal et al, 2018)[207]. In diabetic patients with liver cancer, we believe it

important to study the potential cell non-autonomous effects of normal, glucagon-

responsive hepatocytes as to their ability to facilitate tumor cell growth by releasing glucose into the tumor microenvironment.

In terms of inducing gluconeogenesis within tumor cells themselves, our data suggests that this may be an unlikely therapeutic approach for liver cancer. The mRNA expression of *GCGR*, *G6PC*, *FBP1*, and *PCK1* are decreased in patient tumors and heavily silenced in many established liver cancer cell lines. For these cell lines, neither epigenetic agents nor stimulation of glucagon signaling was sufficient to restore physiological gluconeogenic gene expression (which we infer does not reduce glycolytic flux), suggesting multiple and/or redundant mechanisms of transcriptional repression. In addition, modulation of protein stability and enzyme activity should also be considered. Taken together, this regulatory complexity may account for why cell lines are still unable to fully engage the entire gluconeogenic pathway despite enforced glucagon/GCGR signaling and inferred improvement of chromatin accessibility.

However, this is not to say that individual gluconeogenic enzymes could not have distinct roles under certain metabolic circumstances. For example, PCK1 expression and activity could be induced to funnel extra anaplerotic intermediates from the TCA cycle into serine/glycine biosynthesis to support one-carbon metabolism. FBP1-catalyzed production of fructose-6-phosphate can enter the pentose phosphate pathway to support nucleotide, lipid, and antioxidant synthesis. However, it is not clear how G6PC-regulated loss of intracellular glucose could promote survival under any situation. Interestingly, *G6PC* was the only gene not increased upon any combination of glucagon/GCGR or epigenetic inhibition, suggesting that the de-phosphorylation of glucose-6-phosphate, and its subsequent loss or lack of utilization, has no advantage for cell viability under cellular stress.

57

Three unresolved questions pertain to (1) the lack of gluconeogenic gene expression in glucagon-treated SNU398 GCGR cells, (2) mechanistic nature of the GCGR/glucagon phenotype in SNU398, and (3) this discrepancy between other liver cancer cell lines tested. While p-CREB S133 has been shown to be important for stimulating *G6PC* and *PCK1* expression through recruitment of transcriptional coactivators such as CBP (Kwok et al, 1994)[208], there are certainly a number of other transcription factors, aside from epigenetic modifiers, that can also directly regulate gluconeogenic gene expression. Chromatin interactions between FOXO1 and PGC1α (Puigserver et al, 2003)[209], HNF4a and PGC1α (Rhee et al, 2003)[210], as well as nuclear glucocorticoid receptors with RXRs (Grontved et al, 2013)[211], can also localize at gluconeogenic gene promoters to positively control expression. A successful gluconeogenic response in normal hepatocytes may require inputs from all of these factors, whereas insufficient components of these transcriptional machineries may embody cancer cells. This may explain why glucagon signaling alone is not enough in a SNU398 GCGR cells.

Mechanistically, CREB inhibition was insufficient to rescue the growth phenotype of glucagon-stimulated SNU398 GCGR cells. This may imply that another factor downstream of PKA, or multiple factors including CREB, are responsible. Utilizing pharmacological approaches, we attempted to target PKA, which has many other targets besides CREB, and Ca^{+2}-activated CAMKII, which has also been shown to be an important effector of glucagon signaling. However, neither inhibition of PKA nor CAMKII resulted in an increase in SNU398 GCGR cell proliferation upon glucagon treatment.

Because glucagon signaling has widespread pleotropic effects on cell metabolism, including glycogenolysis and lipid processing, it may be necessary to unbiasedly address metabolic rewiring before performing precise rescue experiments. Therefore,

future studies on glucagon signaling in liver cancer could analyze metabolomics profiling

of SNU398 GCGR cells with or without glucagon, compared to a cell line that is

unresponsive, regardless of glucagon treatment. Differential analysis of metabolites may

reveal the likely cause of sensitivity in SNU398 cells, answering a potentially impactful

question of how glucagon signaling could disrupt cell viability independent of

gluconeogenesis.
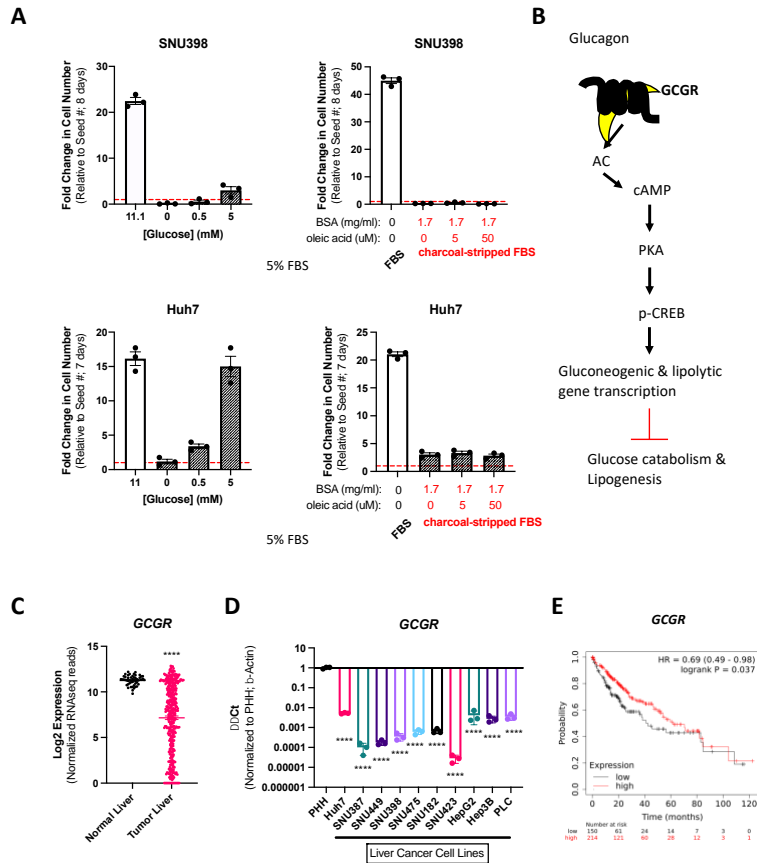
Figure 2.1 – HCC cell lines are dependent on exogenous glucose / lipid dependency and express low levels of the glucagon receptor, GCGR. (**a**) Cell proliferation assays of two cell lines, SNU398 and Huh7, at the indicated time point and nutrient conditions. Data represents a single experiment with 3 biological replicates. Red dashed line denotes fold change of 1, which refers to the starting number of cells. (**b**) Simplified Glucagon/GCGR signaling transduction. GCGR: g-coupled glucagon receptor, Ac: adenyly cyclase, cAMP: cyclic adenosine monophosphate, PKA: protein kinase A, p-CREB: phosphorylated cAMP-response element binding protein. (**c**) Normalized RNA-seq values for GCGR in human HCC compared to normal liver. Data obtained from TCGA. ****: $p<0.0001$, unpaired two-tailed t test. n = 50(normal) and 374(tumor). (**d**) qPCR mRNA expression of GCGR in HCC cell lines compared to Primary Human Hepatocytes (PHH). Data represent a single experiment with 3 biological replicates (3 separate RNA samples). ****: $p<0.0001$, ordinary one-way ANOVA with Dunnett's multiple comparisons test. (**e**) Kaplan-Meier plot of overall survival probability between high and low GCGR expression in liver cancer patients. Graph was generated using the website: https://kmplot.com.
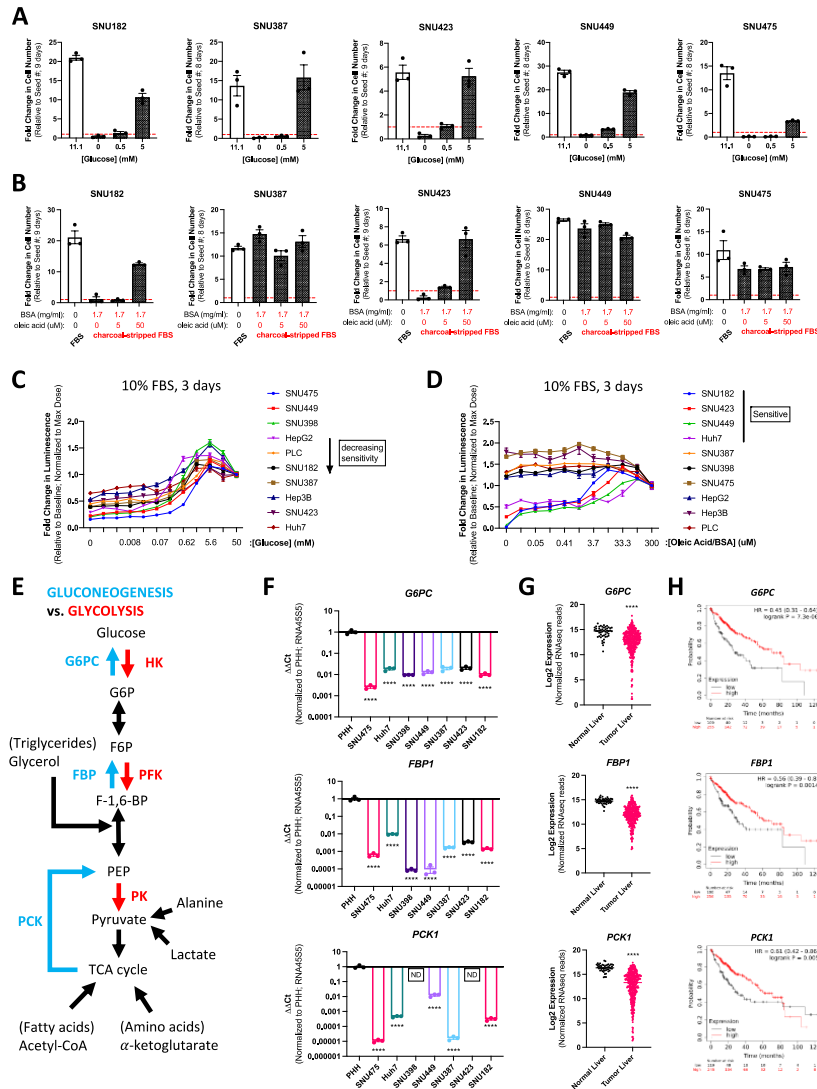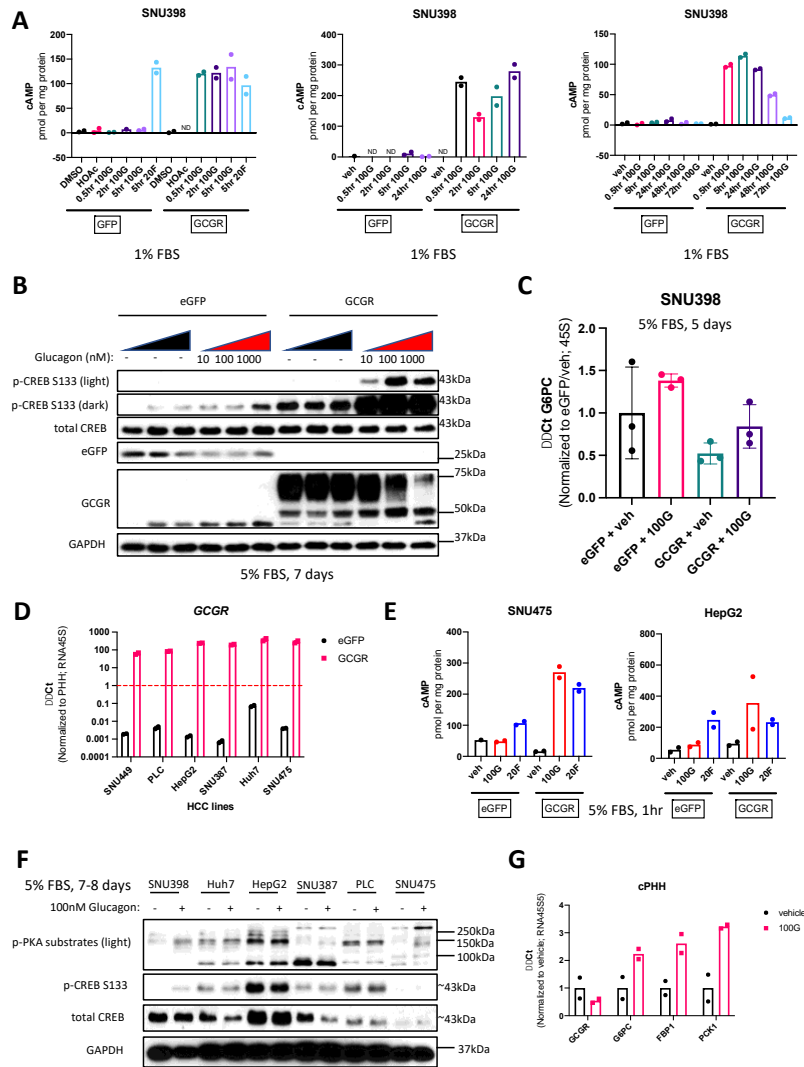
Supplementary Figure 2.1. **Liver cancer cells display hypersensitivity to long- and short-term glucose and lipid withdrawal, potentially explained by low gluconeogenic gene expression. (a)** Cell number-based proliferation assays of HCC cell lines cultured in different concentrations of glucose at the indicated time point. Data represent a single experiment with 3 biological replicates. **(b)** Cell number-based proliferation assays of HCC cell lines cultured in different concentrations of lipids (oleic acid) at the indicated time point. Data represent a single experiment with 3 biological replicates. **(c)** ATP-based cell viability assay of HCC cell lines cultured across a wide range of glucose concentrations. Data points represent the average of 6 biological replicates. **(d)** ATP-based cell viability assay of HCC cell lines cultured across a wide range of oleic acid concentrations. Data points represent the average of 6 biological replicates. **(e)** Simplified schematic of opposing glycolytic (red) and gluconeogenic (blue) pathways. G6PC: glucose-6-phosphatase, HX: hexokinase, G6P: glucose-6-phosphate, FBP1: fructose-1,6-bisphophatase 1, PFK: ATP-dependent 6-phosphofructokinase, F-1,6-BP: fructose-1,6-bisphophatase, PCK1: phosphoenolpyruvate carboxykinase (cytosolic), PK: pyruvate kinase. **(f)** qPCR mRNA expression of gluconeogenic genes in HCC cell lines compared to Primary Human Hepatocytes (PHH). Data represent a single experiment with 3 biological replicates (3 separate RNA samples). ****: p<0.0001, ordinary one-way ANOVA with Dunnett's multiple comparisons test. **(g)** Normalized RNA-seq values for gluconeogenic genes in human HCC compared to normal liver. Data obtained from TCGA. ****: p<0.0001, *: p<0.05, unpaired two-tailed t test. n = 50(normal) and 374(tumor). All error bars: +/- SEM. **(h)** Kaplan-Meier plot of overall survival probability between low and high expression of gluconeogenic enzymes. Graphs were generated using the website: https://kmplot.com.

61
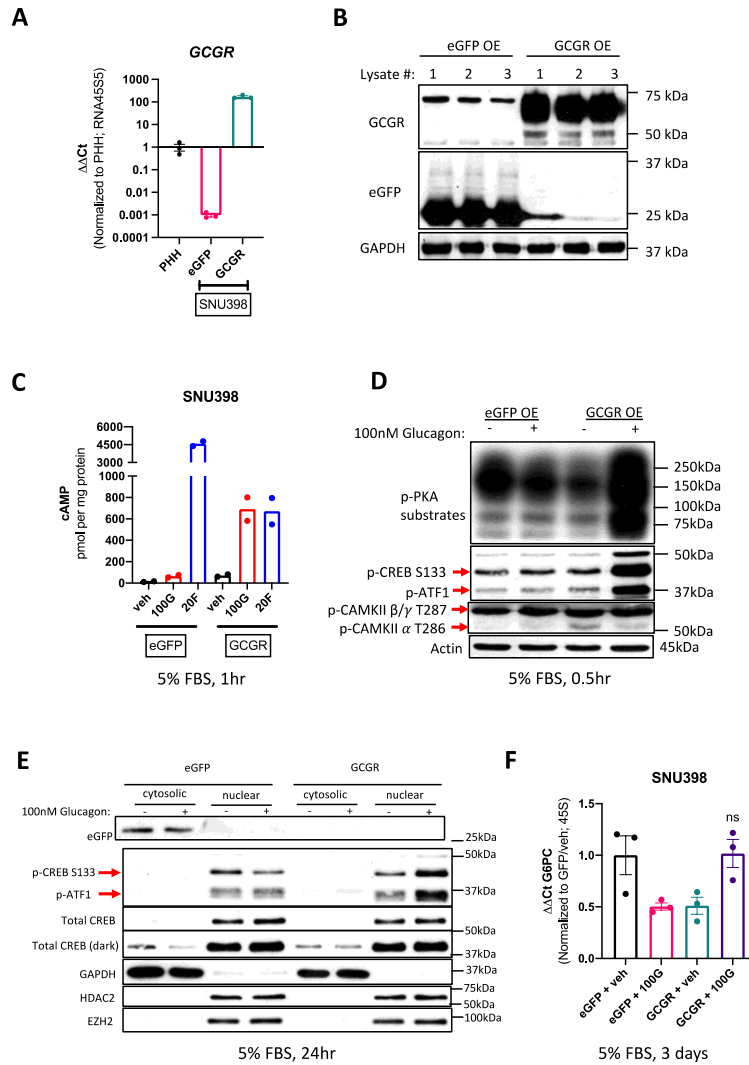
Figure 2.2. **GCGR overexpression partially sensitizes SNU398 to glucagon signaling. (a)** qPCR mRNA levels of *GCGR* in SNU398, following lentiviral CMV-driven mammalian expression, compared to Primary Human Hepatocytes (PHH). Data represent a single experiment with 3 biological replicates (3 separate RNA samples). eGFP used as a control. **(b)** Protein assessment of GCGR and eGFP overexpression in SNU398. Lysate number denotes independent protein sample. **(c)** Quantification of cAMP in SNU398 expressing either eGFP or GCGR and treated with 100nM glucagon (100G) at the indicated condition and time. Data points represent a single experiment of 2 technical replicates. veh: vehicle (0.05M acetic acid), 20F: 20uM forskolin (positive control). **(d)** Protein analysis of downstream effectors of cAMP signaling in SNU398 cells expressing either eGFP or GCGR and treated with 100nM glucagon (+) at the indicated condition and time. (-): vehicle treated. **(e)** Protein localization of p-CREB following glucagon treatment of SNU398 cells expressing either eGFP or GCGR. **(f)** qPCR mRNA expression of *G6PC* in SNU398 cells expressing either eGFP or GCGR and treated with 100nM glucagon (100G) at the indicated condition and time. Data represent a single experiment with 3 biological replicates (3 separate RNA samples). Error bars: +/- SEM. veh: vehicle (0.05M acetic acid). ns: not significant, p>0.05, ordinary one-way ANOVA with Tukey's multiple comparisons test.

Supplementary Figure 2.2. **Constitutive GCGR expression in SNU398, but not other liver cancer cell lines, stimulates PKA activity in response to glucagon without inducing gluconeogenic gene expression. (a)** Quantification of cAMP in SNU398 expressing either eGFP or GCGR and treated with 100nM glucagon (100G) at the indicated condition and times. Each graph represents an independent experiment with 2 technical replicates. DMSO: dimethylsulfoxide, HOAc: 0.05M acetic acid, 20F: 20uM Forskolin (positive control), veh: vehicle (0.05M acetic acid), 20F: 20uM forskolin (positive control). **(b)** Long-term protein analysis of downstream effectors of cAMP signaling in SNU398 cells expressing either eGFP or GCGR and treated with 3 different concentrations of glucagon. Black triangles denote increasingly equivalent concentrations of vehicle compared to glucagon (red triangles). **(c)** qPCR mRNA expression of *G6PC* in SNU398 cells expressing either eGFP or GCGR and treated with 100nM glucagon (100G) at the indicated condition and time. Data represent a single experiment with 3 technical replicates (1 RNA sample). Error bars: +/- SD. veh: vehicle (0.05M acetic acid). **(d)** qPCR mRNA levels of *GCGR* in HCC cell lines compared to Primary Human Hepatocytes (PHH). Same pLenti-CMV-GCGR or pLenti-CMV-eGFP lentivirus as SNU398 was used for stable expression. Data represent a single experiment with 2 biological replicates (2 separate RNA samples). **(e)** Quantification of cAMP in HCC cell lines expressing either eGFP or GCGR and treated with 100nM glucagon (100G) at the indicated condition and time. Data points represent a single experiment of 2 technical replicates. veh: vehicle (0.05M acetic acid), 20F: 20uM forskolin (positive control). **(f)** Protein analysis of downstream effectors of cAMP signaling (PKA substrates) in HCC cell lines expressing GCGR and treated with either vehicle (0.05M acetic acid, (-)) or 100nM glucagon (+) at the indicated condition and time. **(g)** qPCR mRNA levels of *GCGR* and gluconeogenic enzyme genes in cryopreserved primary human hepatocytes (cPHH) treated with 100nM glucagon (100G) at the indicated condition and time. Data represent a single experiment with 2 biological replicates (2 separate RNA samples).
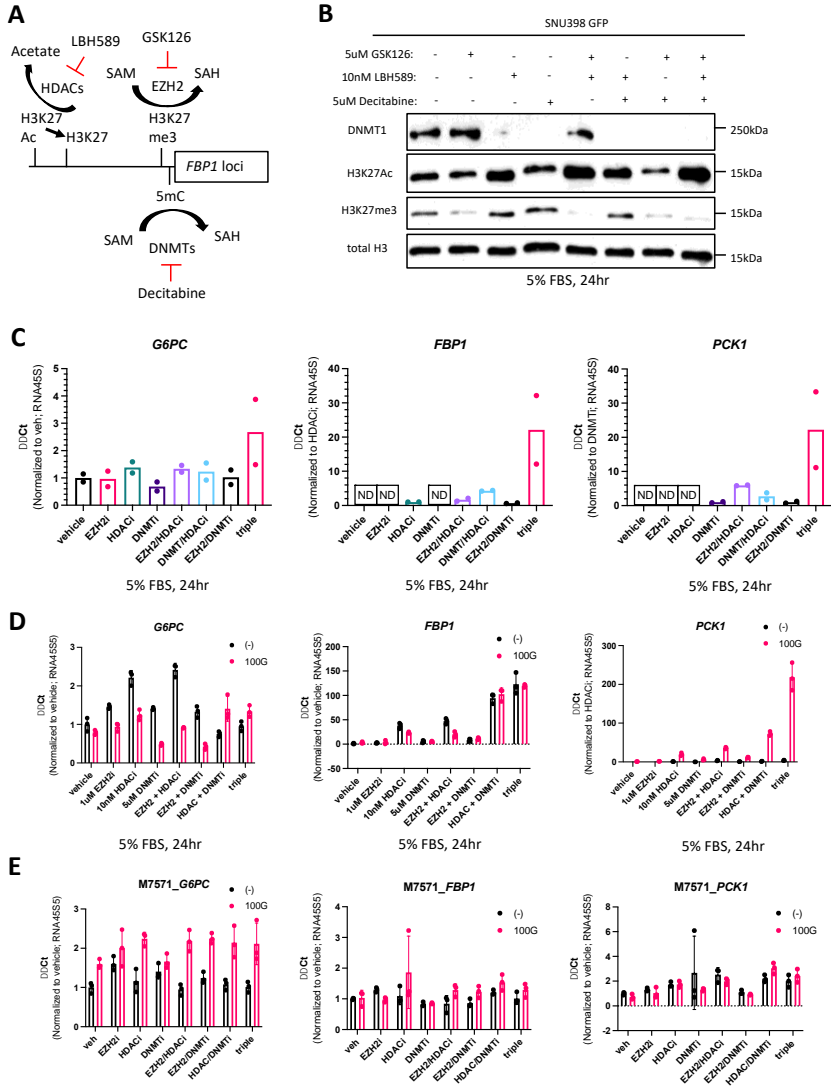
Figure 2.3. **Epigenetic inhibitors fail to fully restore gluconeogenic gene expression with or without glucagon. (a)** Diagram of epigenetic drugs and their targets. GSK126: EZH2 (enhancer of zeste homolog 2) inhibitor, SAM: S-adenosyl-L-methionine, SAH: S-adenosyl homocysteine, H3K27me3: histone 3 lysine 27 trimethylated, LBH589: pan-HDAC (histone deacetylase) inhibitor, H3K27Ac: histone 3 lysine 27 acetylated, Decitabine: DNA methylation (DNMT - DNA methyltransferase) inhibitor, 5mC: 5-methylcytosine. **(b)** Protein analysis of epigenetic inhibitor efficacy in SNU398 eGFP-expressing cells at the indicated drug concentrations, culture conditions, and time. **(c)** qPCR mRNA levels of gluconeogenic genes in SNU398 expressing eGFP and treated with epigenetic inhibitors at the concentrations used in (b), condition, and time. Data represent a single experiment with 2 biological replicates (2 separate RNA samples). ND: not detected. **(d)** qPCR mRNA levels of *G6PC*, *FBP1*, and *PCK1* in SNU398 GCGR-overexpressing cells treated with glucagon plus combinations of epigenetic drugs at the indicated condition and time. Data represent a single experiment with 3 technical replicates (1 RNA sample). Error bars: +/- SD. (-): no drug, 100G: 100nM glucagon, vehicle: 0.035% of 0.05M acetic acid, EZH2i: 1uM GSK126, HDACi: 10nM LBH589, DNMTi: 5uM Decitabine, triple: 1uM GSK126 + 10nM LBH589 + 5uM Decitabine. **(e)** Same qPCR mRNA analysis as in (d) but using the liver cancer patient-derived cell line, M7571.

64
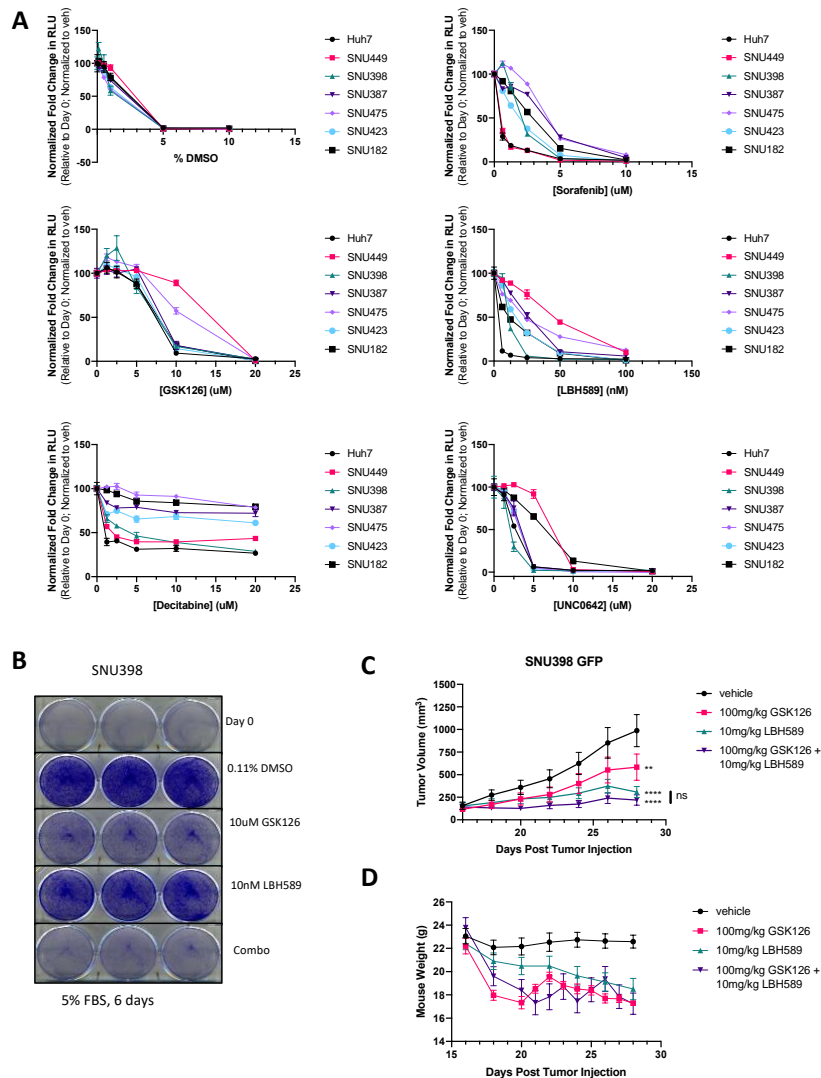
Supplementary Figure 2.3. **Epigenetic inhibitors reduce cell viability across multiple HCC cell lines but display high toxicity in vivo. (a)** ATP-based cell viability assays performed on HCC cell lines treated with serially diluted (1:3) concentrations of epigenetic inhibitors at the indicated condition and time. Data points represent the average of 6 biological replicates. Error bars: +/- SEM. DMSO used a vehicle control. Note, no maximal drug concentration included greater than 0.2% (1:500) of DMSO. Sorafenib used as a clinically relevant drug comparison. UNC0642 (G9a inhibitor (H3K9 dimethylation)) used as an emerging epigenetic target comparison. **(b)** Crystal violet assay on SNU398 cells treated with EZH2 and pan-HDAC inhibitors at the indicated concentrations, condition, and time. Each well represents a biological replicate. **(c)** Tumor volume measurements of SNU398 xenografts in Nu/J mice treated with EZH2 (GSK126) and pan-HDAC (LBH589) inhibitors at the indicated dosage. Treatments were performed at irregular intervals (due to loss/recovery of weight) over the course of the experiment by intraperitoneal injection. vehicle: 20% 2-HP-B-CD (hydroxypropyl-beta-cyclodextrin), pH 4.5. N=5 mice per treatment cohort with 2 tumors per mouse. Data points represent average volume of 10 tumors. Error bars: +/- SEM. **(d)** Body weight measurements of mice treated with EZH2 (GSK126) and pan-HDAC (LBH589) inhibitors at the indicated dosage in same experiment as (c). Data points represent average weights of 5 mice. Error bars: +/- SEM.
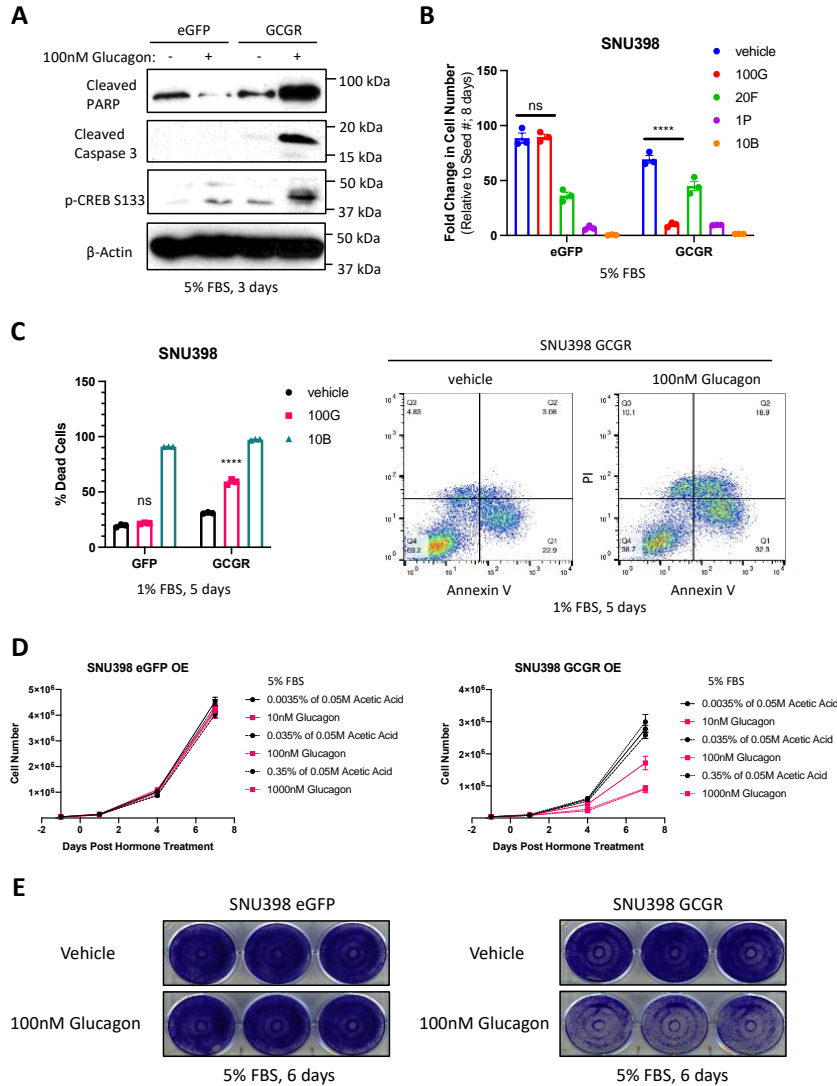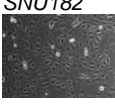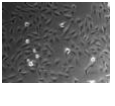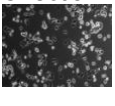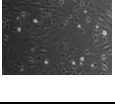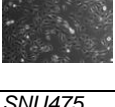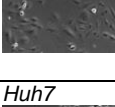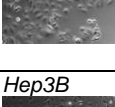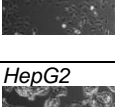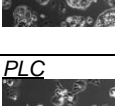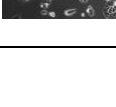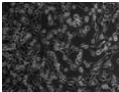
Figure 2.4. **Glucagon treatment reduces in vitro cell viability of GCGR-overexpressing SNU398. (a)** Protein assessment of apoptotic markers in SNU398 cells either expressing eGFP or GCGR and treated with 100nM glucagon at the indicated condition and time. **(b)** Cell proliferation assay of SNU398 cells either expressing eGFP or GCGR and treated with 100nM glucagon (100G) at the indicated condition and time. Vehicle, 100G, and 20F were added daily in fresh media. Data represent a single experiment of 3 biological replicates. Error bars: +/- SEM. ns: not significant, ****: p<0.0001, two-way ANOVA with Tukey's multiple comparisons test. 20F: 20uM forskolin, 1P: 1uM palbociclib (cell cycle inhibitor), 10B: 10ug/ml blasticidin (cell death inducer). **(c)** (Left panel) Histogram of flow cytometry analysis of gated, single cells staining positive for Annexin V/Propidium iodide in SNU398 cells either expressing eGFP or GCGR and treated with 100nM glucagon (100G) at the indicated condition and time. Data represent a single, independent experiment of 3 biological replicates. Error bars: +/- SEM. ns: not significant, ****: p<0.0001, two-way ANOVA with Sidak's multiple comparisons test. 10Blast: 10ug/ml blasticidin (positive control). (Right panel) Representative PI/Annexin V scatter plots for SNU398 GCGR with or without glucagon treatment. **(d)** Cell proliferation assay on SNU398 cells either expressing eGFP or GCGR and treated with glucagon at the indicated concentrations, condition, and time. Data represent a single experiment with 3 biological replicates. Error bars: +/- SEM. **(e)** Crystal violet assay on SNU398 cells either expressing eGFP or GCGR and treated with 100nM glucagon (100G) at the indicated conditions and time.
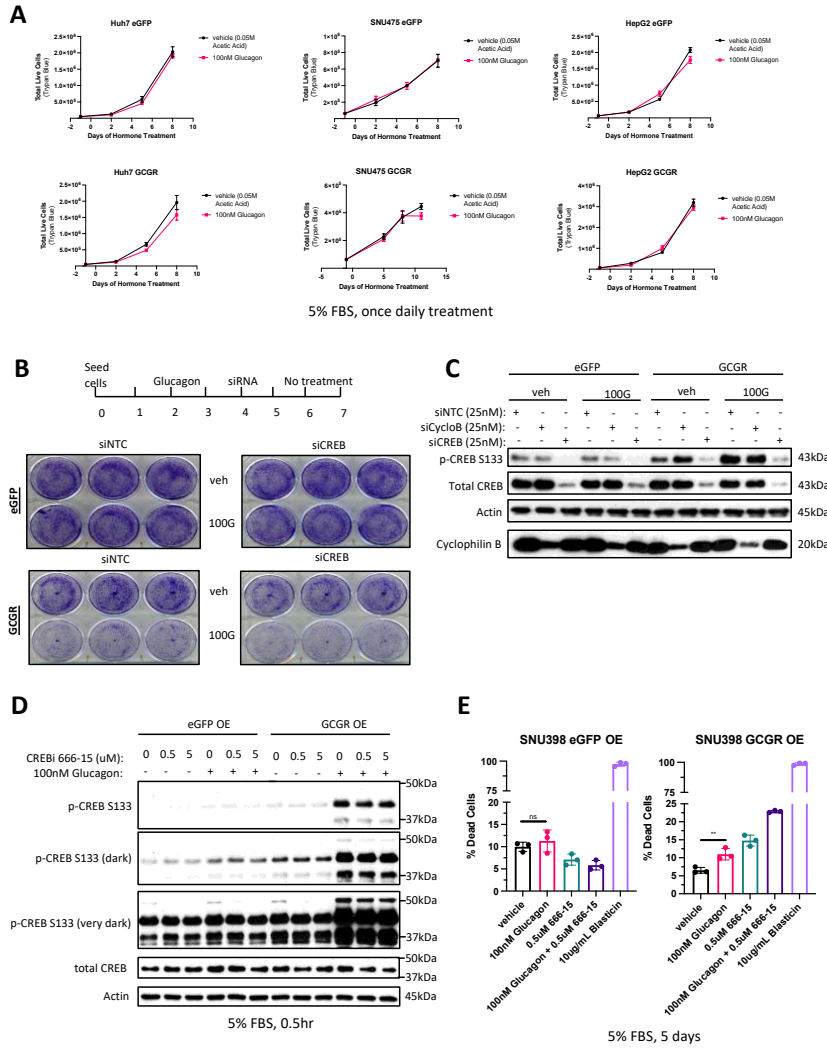
Supplementary Figure 2.4. Glucagon/GCGR only decreases cell viability in SNU398 through an unknown mechanism independent of CREB. (a) Cell proliferation assays on liver cancer cell lines either expressing eGFP or GCGR and treated with 100nM glucagon at the indicated condition and time. Data points represent 3 biological replicates. Error bars: +/- SEM. **(b)** Crystal violet assay on SNU398 cells either expressing eGFP or GCGR, treated with 100nM glucagon (100G), and transfected with 25nM of a small interfering RNA molecular targeting CREB1 (siCREB). Cells were initially treated with glucagon for 3 days and then transfected with siCREB without any further treatment. siNTC (25nM): non-targeting control, veh: vehicle (0.05M acetic acid). **(c)** Protein analysis of siRNA efficacy in SNU398 cells either expressing eGFP or GCGR and treated with 100nM glucagon. Samples harvested at the 7-day time point as illustrated in the previous figure panel. siCycloB (25nM): Cyclophilin B (positive control for transfection protocol). **(d)** Protein assessment of the target efficacy of CREB antagonist, 666-15, in SNU398 cells either expressing eGFP or GCGR and treated with or without 100nM glucagon. (e) PI/Annexin V flow cytometry analysis of SNU398 cells expressing either eGFP or GCGR and treated with either 100nM glucagon, 0.5uM 666-15, or the combination. Data points represent average of 3 biological replicates. Error bars: +/- SEM. 10ug/ml blasticidin used as a positive control. ns: not significant, **: adjusted p=0.0055, ordinary one-way ANOVA with Tukey's multiple comparisons test.

67

Table 2.1 – **Cell line models of liver cancer**.

Cell Line	Sex, ethnicity, age	Cancer subtype, grade, treatment status	Hepatitis B status	Hotspot mutations (putative drivers)	Telomerase amplification (promoter mutation)	Chromosome Y loss
SNU182	M, Asian, 24	HCC, (?), naive	+	P53$^{S215I/S215I}$	WT	No
SNU387	F, Asian, 41	Pleomorphic HCC, (?), post-TACE with doxorubicin / mitomycin-C	+	NRAS$^{Q61K/+}$ P53$^{K164*/K164*}$	AMP (-124C>T)	No
SNU398	M, Asian, 42	HCC, (?), post-TACE with doxorubicin + mitomycin-C	+	CTNNB1$^{S37C/+}$	WT	Yes
SNU423	M, Asian, 40	Pleomorphic HCC, III/IV, post-TAC with doxorubicin	+	P53$^{SS/SS}$ (splice site)	AMP (-124C>T)	No
SNU449	M, Asian, 52	HCC, II-III/IV, naive	+	P53$^{A161T/A161T}$	WT	Yes
SNU475	M, Asian, 43	HCC, (?), naive	+	P53$^{N239D, G262D/+}$	AMP (-124C>T)	Yes
Huh7	M, Asian, 57	Hepatoma, (?), (?)	-	P53$^{Y220C/Y220C}$	WT	No
Hep3B	M, Black, 8	HCC, (?), (?)	+	Axin1$^{R146*/R146*}$	WT	Yes
HepG2	M, White, 15	Hepatoblastoma, (?), (?)	-	NRAS$^{Q61L/+}$	AMP (-124C>T)	No
PLC	M, Black, 24	Hepatoma, (?), (?)	+	P53$^{R249S/R249S}$	WT	Yes

SK-HEP-1	M, White, 52	Adenocarcinoma (liver endothelial origin), (?), naive	(-)	BRAF$^{V600E/+}$	WT	Yes

CHAPTER 3: Glycogen Metabolism is Dispensable for Tumor Progression in Clear Cell Renal Cell Carcinoma

This chapter has been adapted from:

(1) Hong X, Song J, Godfrey J, Riscal R, Skuli N, Nissim I, and Simon MC. Glycogen metabolism is dispensable for tumor progression in clear cell renal cell carcinoma. *Nat Metab*. 2021. Mar;3(3):327-336. doi: 10.1038/s42255-021-00367-x.

Additionally, I would like to clearly state that the majority of experiments performed, as described in this chapter, were done by the lead authors of the aforementioned paper (Hong Xie, and Jun Song). Following their departure from the laboratory, I completed the final xenograft experiment (with significant help from Nico Skuli and Romain Riscal), submitted the manuscript, performed experiments based on reviewer feedback, and wrote the final version of the manuscript.

3.1 Abstract

Glycogen accumulation is a highly consistent, distinguishable characteristic of clear cell renal cell carcinoma (ccRCC) (Ericsson and Seljelid, 1966)[212]. While elevated glycogen pools might be advantageous for ccRCC cells in nutrient deprived microenvironments to sustain tumor viability, data supporting a biological role for glycogen in ccRCC are lacking. Here, we demonstrate that glycogen metabolism is not required for ccRCC proliferation *in vitro* nor xenograft tumor growth *in vivo*. Disruption of glycogen synthesis by CRISPR-mediated knockout of glycogen synthase 1 (GYS1) has no effect on proliferation in multiple cell lines, regardless of glucose concentrations or oxygen levels. Similarly, prevention of glycogen breakdown by deletion or pharmacological inhibition of glycogen phosphorylases B and L (PYGB and PYGL) has no impact on cell viability under any condition tested. Lastly, *in vivo* xenograft experiments using the ccRCC cell line, UMRC2, reveal no significant alteration in tumor size or volume when glycogen metabolism is altered, largely phenocopying our *in vitro* observations. Our findings suggest glycogen buildup in established ccRCC tumor cells is likely to be a secondary, and apparently dispensable, consequence of constitutively active HIF-1α signaling.

3.2 Materials and Methods

Primary Patient Samples

Deidentified fresh-frozen matched ccRCC tumor/normal samples were obtained from the Cooperative Human Tissue Network (CHTN), which operates with the review and approval of their local Institutional Review Boards.

Cell Culture and Cell Proliferation Assays

Human ccRCC cell lines (UMRC2, 786-O, RCC4, and UOK101) were obtained from the American Type Culture Collection (ATCC) and cultured in DMEM supplemented with 10% FBS and Penn/Strep. All cells were routinely confirmed to be *Mycoplasma* negative (MycoAlert; tested every 3 months). For culture conditions with various glucose concentrations, cells were maintained in glucose-free DMEM supplemented with 10% dialyzed FBS (cat. 100-108, GeminiBio) and indicated concentrations of glucose. Hypoxic conditions (0.5% O_2 and 1% O_2) were achieved in a Baker Ruskinn *in vivo$_2$* workstation, by supplementing ambient air with balanced N_2 and CO_2. For lipid depletion experiments, cells were cultured in charcoal-stripped FBS (cat. 900-123, GeminiBio). Cell proliferation assays were performed using WST-1 reagent (cat. 5015944001, Sigma-Aldrich): cells were plated in 96-well plates at 800-1,500 cells/well and allowed to attach overnight. The medium was changed according to indicated culture conditions on the following day, which was considered as Day 0. Cells were subjected to WST-1 assay following manufacturers protocol on each day. Cell proliferation rate was represented by relative absorbance, which was determined by normalizing to the absorbance number at Day 0 of the assay. Additional proliferation assays were performed using Trypan Blue exclusion and labeled as "Total Live Cells" on the Y axis (see Figure 3.3j and Extended

data figure 3.4h (upper panel)). Cells were plated in 6-well plates at 50,000-100,000 cells/well and allowed to adhere overnight. The next day, cells were given fresh medium and cultured in the experimental conditions. At each time point, cells were trypsinized and resuspended in FBS-containing medium. Cell/trypan blue mixtures were counted by a Countess II (Life Technologies) and corrected for dilutions.

Boyden Chamber Cell Migration Assay

50,000 UMRC2 cells were seeded in 0.1 ml of 0% FBS, DMEM (0mM glucose) per transwell polycarbonate insert with 8μm pores (cat. 3422, Corning). Approximately 0.6 ml of either 0% or 10% FBS DMEM (25 mM glucose) was added to each bottom well. Following overnight incubation, inserts were washed with PBS and then gently scraped with a cotton swab (topside only). Next, membrane inserts were incubated in approximately 0.6 ml of 0.5% crystal violet (cat. C6158, Sigma-Aldrich) in 20% methanol for 10 minutes. Transwells were washed twice with PBS and allowed to dry overnight. Membrane inserts were cut out and mounted on a microscope slide for imaging.

Plasmids, Lentivirus Production, and Viral Transduction

For shRNAs, the lentiviral vector pLKO.1 SCR (scrambled shRNA plasmid no. 17920) was from Addgene. shRNAs targeting *HIF1A* (shHIF1A_52, shHIF1A_9) and *EPAS1* (shHIF2A_6, shHIF2A_7) were described previously[9]. For genetic knockout using CRISPR/Cas9, the lentiviral vector LentiCRISPR v2 (plasmid no. 52961) and LentiCRISPRv2GFP (plasmid no. 82416) were obtained from Addgene. Human single-guide RNAs (sgRNA) targeting *GYS1* #1 (GAACGCAGTGCTCTTCGAAG), #3 (CTACACGGTGCTGCAGACGA); *PYGL* #1 (GAAGCTGCTCCCTCGACATT), #3 (TAGCCACGCCATTCACAGCA), and #4 (GAGGACCCGGGAGATGTTCT) along with a

control sgRNA targeting mouse *Rosa26* locus (AAGATGGGCGGGAGTCTTCT) were cloned into LentiCRISPR v2 plasmid, while sgRNAs targeting *PYGB* #1 (CAACGTGGGAGACTACATCG) and #4 (CCACCTTCTCCACGTCCACC) along with a control sgRNA targeting *LacZ* (TCGTTTTACAACGTCGTGAC) were cloned into LentiCRISPRv2GFP plasmid. To produce lentiviruses, 293T cells were co-transfected with shRNA or CRISPR plasmid of interest along with packaging plasmids psPAX2 and pMD2.G using FuGENE 6 transfection reagent (cat. E2691, Promega). Lentiviruses were collected 48 hours after transfection. Viruses were used with 8 µg/ml polybrene for infection. For the LentiCRISPR v2 system, cells were selected with 4 µg/ml puromycin for 5 days to establish stable cell lines, while for LentiCRISPRv2GFP system, top 50% GFP positive cells were sorted for future culture and analysis. For PYGB overexpression analyses, 25 µl of pre-made, constitutive expression lentiviral vector, pLOC-PYGB (cat. OHS5899-202619959, Dharmacon), were added to 1.5 ml of UMRC2 cells. Cells were selected with 5 µg/ml blasticidin for 4 days prior to subsequent experimentation.

Western Blot Analysis

Cells and tumor tissue samples were lysed in RIPA lysis and extraction buffer (cat. 89900, ThermoFisher Scientific) containing Roche complete ULTRA Protease/Phosphatase Inhibitor (cat. 05892791001). Protein concentration was quantified with Pierce BCA Protein Assay Kit (cat. 23225, ThermoFisher Scientific). Isolated proteins were resolved by SDS-PAGE, and Western blot analysis was performed. All primary antibodies were diluted 1:1,000 in 5% w/v nonfat milk. Blots were incubated with primary antibodies overnight at 4°C. GYS1 (cat. ab40810) and ACTIN (cat. ab3280) antibodies were from abcam; HIF-1α antibody was from Cayman (cat. 10006421); HIF-2α antibody was from Novus Biologicals (cat. NB100-122); GAPDH

74

antibody was from Cell Signaling Technology (cat. 2118); PYGL antibody was from Sigma (cat. HPA000962); PYGB antibody was from proteintech (cat. 12075-1-AP). Primary antibodies were detected using horseradish peroxidase–conjugated secondary antibodies from Cell Signaling Technology (cat. 7074) followed by exposure to enhanced chemiluminescence substrate (cat. NEL103001EA, PerkinElmer) or SuperSignal West Femto Maximum Sensitivity Substrate (cat. 34095, ThermoFisher Scientific).

Reagents

GPi (pan-glycogen phosphorylase inhibitor) CP316819 was purchased from Tocris (cat. 3542).

TCGA RNA-seq Analysis

RNA-seq data for ccRCC and normal kidney samples were downloaded and analyzed from the TCGA on April 2, 2013 as previously described[17]. Differential gene expression analysis of tumor and normal samples were performed using DeSeq (Bioconductor Version 2.12). Box and whisker plots correspond to 5-95th percentiles (bars), 25-75th percentiles (box), and median (line in box).

RNA Extraction, Real-Time Quantitative RT-PCR Analysis

Total RNA was isolated using the RNeasy Mini Kit (cat. 74104, QIAGEN), and cDNA was synthesized using the High-Capacity RNA-to-cDNA Kit (cat. 4387406, ThermoFisher Scientific). Quantitative reverse-transcription PCR (qRT-PCR) was performed on a ViiA7 Real-Time PCR system from Applied Biosystems. Predesigned TaqMan primers were obtained from ThermoFisher Scientific for the following genes: *TBP* (Hs00427620_m1), *ACTB* (Hs01060665_g1), *HIF1A* (Hs00153153_m1), *HIF2A*

(Hs01026149_m1), *CCND1* (Hs00765553_m1), *PDK1* (Hs00176853_m1), *GYS1*
(Hs00157863_m1), *PYGB* (Hs00765686_m1), *PYGL* (Hs00958087_m1), *PYGM*
(Hs00989942_m1), and *RNA18S/45S* (Hs03928985_g1).

Glycogen Quantification

Glycogen levels were measured using the Glycogen Assay Kit II (Colorimetric) from
abcam (cat. Ab169558). Briefly, cells or tumor tissues were homogenized with dH2O on
ice and then boiled for 10 min. Homogenates were then spun at 13,000 rpm for 10 min
and supernatants were assayed for glycogen content. Results were normalized by
protein content.

Matrigel-Based Spheroid Growth Assay

Matrigel-based 3D spheroids formation technique was described previously (Vinci et
al, 2012)[213]. Briefly, 3,000 cells per well were plated in a 96-well ultra-low attachment
plate (cat. CLS3474, Sigma) along with DMEM plus 10% FBS and 2.5% matrigel (cat.
354234, Corning). Plates were centrifuged at 1,500 rpm to promote spheroid formation,
and then imaged at indicated time points using the EVOS FL Imaging System. Final
pictures were taken at 40X magnification. Spheroid volume was calculated using a
previously published ImageJ macro (Ivanov et al, 2014)[214].

Metabolites and Glycogen Tracing

Mass spectrometry-based metabolomics analysis of primary ccRCC was performed
with Metabolon (Extended Data Figure 3.1b), as previously described (Li et al, 2014)[137].
In addition, publicly available metabolomics data from Hakimi, et al.[215] were downloaded
and values normalized to normal kidney tissue (Figure 3.1c). For the glycogen tracing

experiment, cells were seeded at 50-70% confluency in 15 cm dishes (Day 0). The following day (Day 1), media was changed to 1% dialyzed FBS, 0 mM glucose DMEM, to deplete unlabeled glycogen stores, and incubated at 1% O_2 overnight. The next day (Day 2), 25mM of uniformly labeled ^{13}C ([U-^{13}C]) glucose (cat. CLM-1396-1, Cambridge Isotope Lab.) was added to cells, to regenerate glycogen with labeled glucose, and cultured overnight at 1% O_2. The following day (Day 3), media was aspirated and cells were washed twice with 1X PBS to remove labeled glucose. Cells were then incubated at 1% O_2 overnight in fresh 1% dialyzed FBS, 0 mM glucose DMEM with 10 μM of GPi (see reagents) to prevent the breakdown of labeled glycogen. On the last day (Day 4), media was changed to either DMSO control or 10 μM GPi in fresh 1% dialyzed FBS, 0 mM glucose DMEM and cultured for 0, 3, or 6 hrs. At these time points, cell metabolites were extracted by (1) aspirating media, (2) washing twice with cold PBS, (3) adding 0.5 ml of 4% perchloric acid, and (4) transferring semi-frozen supernatant to microfuge tubes. All samples were submitted to the Metabolomic Core at the Children's Hospital of Philadelphia for LC/MS analysis. Data are normalized to internal metabolite controls and presented as atomic percent excess (APE) to describe the percentage of a ^{13}C-labeled metabolite relative to its unlabeled form.

Periodic Acid Schiff Staining

Glycogen was detected in tumor sections following a standardized periodic acid Schiff (PAS) staining technique, which was performed by the Molecular Pathology & Imaging Core at the University of Pennsylvania.

Mice and Xenograft Experiments

Xenograft tumor experiments were approved by the Animal Care and Use
Committee at the University of Pennsylvania. 200μL of 5 million UMRC2 control or
knockout cells were subcutaneously injected into opposing flanks of the same 4-6 week
old female NIH-III nude mouse (strain code 201, Charles River), in a 1:1 mixture of
DMEM and matrigel. Once palpable tumors were established, tumor volume was
monitored by caliper measurements. Upon completion of the experiment, the animals
were sacrificed by CO_2 inhalation, followed by cervical dislocation, and xenograft tumors
were dissected for downstream analyses.

Statistics and Reproducibility

Experimental significance was determined by *P* value, whereby any value 0.05 or
below was considered mathematically unlikely to be random. Unpaired, two-tailed
Student's *t* test was used for simple column analyses between two conditions, unless
comparing matched samples, such as from same patient or mouse, in which case paired
t tests were employed. Two-way ANOVA with Sidak's multiple comparison correction
test was used for more complex group analyses and multiple conditions (see individual
figure legends). All graphs and statistical inquiries were generated using GraphPad
Prism versions 7.0 - 9.0.1 (current). For all qRT-PCR and glycogen quantifications, data
is derived from technical replicates, presented as mean +/- standard deviation (SD), and
represents results of reproducible experiments. For all growth curves and metabolite
tracing, data is derived from biological replicates and presented as mean +/- standard
error of the mean (SEM). For box plots, graphs are shown with all points, center line as
the median, box bounds as 25th and 75th percentiles, and whiskers as either 5th and 95th
percentiles or minimum and maximum values (see individual figure legends). For all

experiments shown, similar results were obtained across multiple cell lines (see

Extended Data for additional cell lines) and reproduced at least once by multiple authors.

3.3 Results

Glycogen Synthesis and Breakdown are Hyperactive in ccRCC Tumors

To address whether the glycogen pathway (**Fig. 3.1a; pg. 90**) is consistently altered

in ccRCC, elevated glycogen levels were confirmed in patient tumors compared to

matched normal kidney tissue (**Fig. 3.1b; pg. 90**). Comparable quantities of glycogen

were also detected in six cell line models of ccRCC: 786-O, UOK101, 769P, UMRC2,

RCC4, and RCC10 (**Extended Data Fig. 3.1a; pg. 91**). To provide a more

comprehensive and informative picture of glycogen production and degradation, we

queried our previously generated metabolomic data**[137]** on the same patient paired tumor

and normal samples for glycogen-related metabolites. Many products of glycogen

metabolism were relatively increased in ccRCC, including glucose-1-phosphate, and

oligosaccharide branch intermediates, i.e. maltose, maltotriose, and maltotetraose (**Fig.**

3.1c; pg. 90). These findings are consistent with a separate metabolomics assessment

of 138 matched ccRCC/normal tissue pairs we further analyzed[215] (**Extended Data Fig. 3.1b; pg. 91**). Lastly, TCGA RNA-seq analysis revealed that all genes involved in glycogen metabolism are differentially expressed, including overexpression of those encoding critical synthetic enzymes (*PGM1*, *GYS1*, and *GBE1*), and catabolic enzymes (*PYGL* and *PYGM*) (**Fig. 3.1d, e; pg. 90**). Some patients appear to stratify into high or low levels of expression (relative to normal kidney), which may indicate that elevated glycogen abundance is a result of a variety of transcriptional inputs. This was also consistent with our patient samples, where tumors sometimes showed higher or lower expression of a given gene related to glycogen metabolism compared to normal tissue (**Extended Data Fig. 3.1c; pg. 91**). Nevertheless, based on increased glycogen content, elevated glycogen-derived metabolites, and differential expression of glycogen modifying genes, we concluded that glycogen metabolism is significantly deregulated in ccRCC tumors.

Elevated Glycogen Synthesis Enzyme, GYS1, is Regulated by HIF1α, but has No Effect on Tumor Proliferation in ccRCC Models

To determine whether glycogen serves a key biological role in ccRCC, the rate-limiting enzyme, glycogen synthase, was initially evaluated as it directly controls glycogen synthesis (**Fig. 3.2a; pg. 92**). In mammalian cells, glycogen synthase has two isoforms, GYS1 (expressed in skeletal muscle and other tissues) and GYS2 (expressed predominately in the liver) (Zois et al, 2016)[216]. Analysis of TCGA RNA-seq database and primary samples revealed that *GYS1* mRNA and protein levels were significantly increased in tumor samples (**Fig. 3.2b, c; pg. 92**). Since constitutive activation of HIF-α proteins through pVHL loss of function is a major driver of ccRCC pathogenesis[176], the capability of HIFs to facilitate increased *GYS1* transcription was assessed. Based on

shRNA knockdown, *GYS1* mRNA levels and glycogen deposition were selectively controlled by HIF-1α in HIF-1α expressing cells (H1H2) (**Extended Data Fig. 3.2a, b; pg. 93**), and HIF-independent mechanisms in HIF-2α only expressing cells (H2) (**Extended Data Fig. 3.2c; pg. 93**). Based on previous transcriptomic analyses[4], expression levels of *GYS1*, *PYGB*, *PYGL*, and *PYGM* were not significantly different between H1H2 and H2 ccRCC tumors. Additionally, 786-O cells stably re-expressing pVHL did not show altered expression of glycogen metabolic enzymes (**Extended Data Fig. 3.2c; pg. 93**), confirming regulation by pathways other than the HIF-prolylhydroxylation-pVHL system when HIF-1α is absent.

In addition to transcriptional regulation, post-translational control of GYS is achieved through phosphorylation, alternating between the phosphorylated inactive state and dephosphorylated active state (**Extended Data Fig. 3.2d; pg. 93**)[216]. GYS dephosphorylation is catalyzed via hydrolysis by protein phosphatase-1 (PP1) which is bound to glycogen targeting subunit proteins, protein phosphatase 1 regulatory subunit 3 (PPP1R3) (Munro et al, 2005)[217]. At least seven distinct genes encode PPP1R3: *PPP1R3A-G*, that are differentially expressed across tissues[216]. Previous studies demonstrated that PPP1R3C overexpression promotes glycogen accumulation in different tissues, suggesting its essential role in activating GYS and subsequent glycogen buildup (Shen et al, 2010; Yang et al, 2015; Jurczak et al, 2007; Greenberg et al, 2003)[218-221]. In ccRCC tumors, *PPP1R3B* and *PPP1R3C* expression was elevated in all tumor stages (**Extended Data Fig. 3.2e; pg. 93**). Consistent with glycogen buildup, these data suggest that elevated *GYS1* mRNA and protein levels in ccRCC is a result of HIF-1α stabilization, whereas enhanced GYS1 activity is due to greater expression of accessory proteins important for GYS1 dephosphorylation.

To assess the functional consequences of elevated GYS1 expression and glycogen accumulation in ccRCC, GYS1 protein was reduced using two independent sgRNAs in multiple cell lines with variable baseline glycogen levels (UMRC2, 786-O, RCC4, and UOK101, **Extended Data Fig. 3.1a; pg. 91**). As shown in Figure 3.2d and Extended data figure 3.3a, both sgRNAs targeting *GYS1* robustly decreased GYS1 protein levels, resulting in rapid glycogen depletion in these cells (**Fig. 3.2e**, **Extended Data Fig. 3.3b; pgs. 92 and 94**). We hypothesized that cell proliferation would be inhibited if cells were unable to store glucose as glycogen for future use under acute conditions of nutrient deprivation. Surprisingly, *GYS1* KO did not affect growth in UMRC2 cells, regardless of culture conditions (25mM vs. 0mM glucose, 21% vs. 1% O_2, 1% FBS) (**Fig. 3.2f; pg. 92**). UMRC2 *GYS1* WT and KO cells were also embedded in Matrigel for spheroid growth to better mimic nutrient gradients and tissue pressure observed within the tumor environment. Again, *GYS1* KO did not affect spheroid volume during the course of this assay (**Fig. 3.2g; pg. 92**). The same trend was observed in spheroid assays for 786-O cells, as well as in 2-D proliferation assays for RCC4 and UOK101 cells (**Extended Data Fig. 3.3c, d; pg. 94**). Of note, both *GYS1* WT and KO UOK101 cells were particularly sensitive to growth in 25mM glucose at 1% O_2 after 2 days due to lactic acid accumulation. These results suggest that although *GYS1* mRNA and protein levels are overexpressed in ccRCC patient tumors and cell lines and associated with a concomitant accumulation in glycogen, neither GYS1 nor glycogen production is required for 2-D or 3-D growth under normal and tumor-relevant stress conditions.

Glycogen Breakdown Requires Both PYGL and PYGB but is Irrelevant for ccRCC Cell Growth, Despite Glycolytic Entry of Glycogen-Derived Glucose

The data showing that glycogen depletion does not affect *in vitro* ccRCC cell proliferation were rather unexpected, since it had been shown that GYS1 inhibition reduces cell proliferation of other types of cancer, such as leukemia (Bhanot et al, 2015)[222]. An alternative hypothesis to explain this apparent lack of phenotype upon GYS1 inhibition in ccRCC cells proposes that increased GYS1 expression and glycogen accumulation is a collateral effect of HIF-1α activation and other factors, simply making glycogen generation a byproduct. Cells may need to simultaneously increase activity of the breakdown pathway to maintain glycogen homeostasis and avoid aberrant glucose storage into glycogen. Therefore, pVHL-deficient ccRCC cells may require enzymes involved in glycogen breakdown to balance enhanced GYS1 activity for metabolic homeostasis.

To investigate this further, glycogen catabolism (glycogenolysis) was functionally examined in ccRCC (**Fig. 3.3a; pg. 95**). Glycogen phosphorylase is the rate-limiting enzyme for glycogen degradation and comprises three isoforms in mammals: liver (PYGL), muscle (PYGM), and brain (PYGB)[216]. As shown in Figure 3.1e, both *PYGL* and *PYGM* mRNA abundance were elevated in ccRCC. Since *PYGM* expression at baseline was much lower than *PYGL*, *PYGL* was initially evaluated. Similar to *GYS1*, *PYGL* mRNA levels were amplified in all tumor stages (**Fig. 3.3b; pg. 95**). To genetically block glycogenolysis, two independent sgRNAs were pooled to target PYGL, producing a nearly complete loss of PYGL protein (**Extended Data Fig. 3.4a, b; pg. 96**). Because glycogen was depleted *in vitro* within 12 hours following glucose deprivation (**Extended Data Fig. 3.4c; pg. 96**), glycogen levels were measured at 6 hours in glucose-free medium. This time point allows cells to engage glycogenolysis without complete depletion before glycogen could be harvested. *PYGL* KO was unable to protect glycogen

from degradation during this time frame (**Extended Data Fig. 3.4d; pg. 96**), suggesting

that these cells either did not utilize PYGL to mobilize glycogen under glucose deprived

conditions or there exists redundancy in this process. Consistent with our finding, Favaro

et al.[184] showed that in a GBM cell line U87, *PYGL* knockdown did not increase glycogen

content under normoxia. However, they obtained the opposite result under hypoxia,

where glycogen accumulated and proliferation decreased in sh*PYGL* cells. To examine

whether this can be recapitulated in ccRCC cells, *PYGL* WT/KO cells were subjected to

hypoxia treatment (0.5% O_2). In contrast to U87 cells, PYGL depletion in ccRCC cells did

not accumulate more glycogen under hypoxia (**Extended Data Fig. 3.4e; pg. 96**). In

addition, there was no difference in cell growth between WT and *PYGL* KO cells when

cultured in any condition tested (replete, low serum, low glucose, low oxygen)

(**Extended Data Fig. 3.4f; pg. 96**). Taken together, these data suggest that although

PYGL expression is upregulated in ccRCC, it is not necessary for glycogenolysis, nor it

is required for *in vitro* cell growth.

   As PYGL was insufficient to control glycogen breakdown, other isoforms were

analyzed for functional redundancy. Although *PYGB* expression was downregulated in

ccRCC tumors, it had comparable baseline mRNA levels as *PYGL* (**Fig. 3.1e; pg. 90**).

Neither genetic knockout or constitutive overexpression of PYGB protein disrupted

proliferation of UMRC2 under metabolic stress conditions (**Extended Data Fig. 3.4g, h;

pg. 96**). Upon reduction of PYGB protein, PYGL protein levels were increased,

suggesting possible compensation (**Extended Data Fig. 3.4g; pg. 96**). Consistent with

TCGA patient data, *PYGM* mRNA abundance was very low compared to the other two

isoforms in UMRC2 (**Extended Data Fig. 3.4i; pg. 96**), and PYGM was not evaluated

further. Therefore, PYGL and PYGB were simultaneously depleted with sgRNAs to avoid

compensation from either enzyme (**Fig. 3.3c**, **Extended Data Fig. 3.5a; pgs. 95 and 97**). Notably, *PYGB/L* DKO completely prevented glycogenolysis under glucose deprivation, suggesting both these isoforms are active in ccRCC (**Fig. 3.3d**, **Extended Data Fig. 3.5b; pgs. 95 and 97**). However, *PYGB/L* DKO cells did not exhibit higher glycogen content than WT cells under hypoxia, despite a trend towards increased deposition of glycogen with low oxygen exposure (**Extended Data Fig. 3.5c; pg. 97**). This result suggests that ccRCC cells do not use any glycogen-derived glucose under hypoxic conditions, perhaps due to the increased uptake of extracellular glucose downstream of even greater hypoxia-mediated HIF stabilization. In addition, *PYGB/L* DKO did not affect cell proliferation under any conditions (**Fig. 3.3e**, **Extended Data Fig. 3.5d; pgs. 95 and 97**). To verify this result independently, a selective glycogen phosphorylase inhibitor, GPi, was employed. GPi dose-dependently maintained glycogen content in glucose-free culture condition (**Fig. 3.3f**, **Extended Data Fig. 3.5e; pgs. 95 and 97**), and during a long-term treatment, GPi blocked glycogen degradation when cells were cultured in low glucose (2mM) or no glucose (0mM) conditions, regardless of oxygenation (**Fig. 3.3g**, **Extended Data Fig. 3.5f; pgs. 95 and 97**). Consistent with *PYGB/L* DKO, GPi treatment did not affect *in vitro* ccRCC cell growth (**Fig. 3.3h**, **Extended Data Fig. 3.5g; pgs. 95 and 97**). These findings indicate that ccRCC tumor cells do not rely on glycogen breakdown for growth.

Despite no observable role in maintaining ccRCC viability, glycogen is rapidly broken down under low glucose conditions (**Extended Data Fig. 3.4c; pg. 96**), suggesting that glycogen-derived glucose is metabolized in some way. Therefore, glycogen was labeled with [U-^{13}C] glucose and then either allowed to or prevented from breakdown to specifically determine how glycogen-derived glucose was utilized (**Fig. 3.3i**, and

Extended Data Fig. 3.6a, b; pgs. 95 and 98). As a proof of principle, the percentage of intracellular, labeled glucose relative to unlabeled glucose was greater in cells that can properly catabolize glycogen under low glucose conditions (**Extended Data Fig. 3.6c; pg. 98**). Mass spectrometry results indicated that glycogen-derived glucose was diffusely processed into various metabolites (**Extended Data Fig. 3.6d; pg. 98**), but perhaps more concentrated in glycolytic intermediates and serine rather than the TCA cycle (**Fig. 3.3i**, **Extended Data Fig. 3.6d; pgs. 95 and 98**).

Due to increased glyceraldehyde-3-phosphate (G3P), serine/glycine, and very slightly ribose-5-phosphate labeling, additional experiments were designed to test potential proliferation defects in cells that lack glycogenolysis under nutrient conditions pertaining to these metabolites. Aside from the obvious role of G3P in glycolysis, G3P can also be catalyzed to generate glycerol, which is necessary for lipid synthesis. Serine/glycine and the pentose phosphate pathways both produce NAPDH, also needed for lipid synthesis. Therefore, UMRC2 control or *PYGB/L* DKO cells were subjected to lipid starvation and assessed for relative cell numbers over 7 days. Although UMRC2 cells typically grow poorly without an exogenous source of lipids, this was exacerbated somewhat in cells that cannot break down glycogen (**Fig. 3.3j; pg. 95**) (see below for further discussion).

To evaluate whether these metabolic perturbations could also affect other cellular functions aside from growth, such as migration, Boyden chamber assays were performed using control or *PYGB/L* DKO UMRC2 cells. Similar to the lack of a proliferation phenotype, no observable change in migration was detected between cells that can or cannot engage in glycogenolysis (**Extended Data Fig. 3.7a, b; pg. 99**).

Glycogen Metabolism has No Substantial Role in Tumor Progression of ccRCC

Xenograft Models

Lastly, to determine whether glycogen metabolism is important for ccRCC tumor progression *in vivo*, we systematically transplanted our UMRC2 models into both flanks of nude mice. For glycogen synthesis, no significant difference was evident between the growth of *GYS1* KO and WT tumors (**Fig. 3.4a; pg. 100**), despite robust glycogen and GYS1 protein depletion (**Fig. 3.4b, c; pg. 100**). Similarly, for glycogen breakdown, no consistent statistically significant effects on tumor volume or weight were observed when both PYGL and PYGB were effectively eliminated, and glycogen levels were either maintained or slightly elevated in *PYGB/L* DKO tumors (**Fig. 3.4d-f; pg. 100**). Collectively, these results indicate that neither glycogen accumulation nor homeostasis plays a major role in ccRCC tumor models.

3.4 Discussion

In this study, we demonstrated that glycogen is largely unnecessary for ccRCC cell growth in a variety of models and stress conditions, clarifying an important clinical distinction for a classical biological feature of the disease. Only under low oxygen and low lipid conditions did inhibition of glycogen breakdown appear to modestly reduce cell growth. One explanation for this phenotype could be that ccRCC cells metabolize glycogen-derived glucose in pathways important for lipid synthesis, which is why no phenotype was observed in lipid replete culture conditions. It remains perplexing why 25mM exogenous glucose could not compensate for the lack of glycogen-derived glucose during lipid starvation. Nevertheless, since this phenotype was not observed in

transplantable *in vivo* models, it is likely that overall deregulated glycogen metabolism in ccRCC is a side effect of constitutive HIF-1α signaling with minimal biological importance under conventional stress conditions (i.e. low glucose, low oxygen). In other cancer types, such as GBM11 and NSCLC12, data does exist supporting a pro-tumorigenic role of glycogen. Whether these tumor microenvironments have reduced fatty acid or triglyceride availability is unknown. Therefore, a key unanswered question remains in how cancer cells of distinct metabolic dependencies and microenvironments utilize glycogen. In our ccRCC models, we reproducibly observe glycogen degradation in low glucose and, conversely, glycogen retention in PYGB/L DKO cells exposed to glucose deprivation. This indicates ccRCC cells mobilize glycogen-derived glucose for some metabolic processes. Based on the glycogen labeling experiment, potential metabolic pathways include glycolysis, serine/glycine biosynthesis, and the pentose phosphate pathway. More in depth metabolite analyses, such as antioxidant readouts or lipidomics, could clarify and connect a metabolic role of glycogen to a specific stress condition. *In vivo* models of PYGB/L DKO tumor growth in either a low- or high-fat diet to mimic changes in serum lipids, or with antiangiogenic treatment to intensify a hypoxic tumor microenvironment, could also be examined.

Future work on glycogen in ccRCC could identify distinct destinations of glycogen-derived glucose under specific culture conditions. This may reveal synthetic lethality approaches between GYS1 or PYGB/L inhibition, tailored to a patient's unique tumor metabolism. For example, tumors addicted to glutamine, fatty acid, or acetate availability may become vulnerable when glycogen cannot feed glucose-1-phosphate into the central carbon pathway (Varnier et al, 1995; Lundsgaard et al, 2018; Hardin et al, 1997)[223-225]. Additionally, it has recently been described that glycogen breakdown in the

nucleus can regulate gene expression through altering histone acetylation in non-small cell lung cancer[185]. Whether or not nuclear glycogen impacts the epigenetic landscape, or if the epigenetic profile itself can alleviate any proliferation defects from the loss of glycogen metabolism in ccRCC, has yet to be explored. Another avenue of synthetic lethality could be in serine/glycine biosynthesis (**Extended Data Fig. 3.6d; pg. 97**). Nevertheless, we suggest that elevated glycogen content in ccRCC patient tumors should not be considered a therapeutic target on its own.
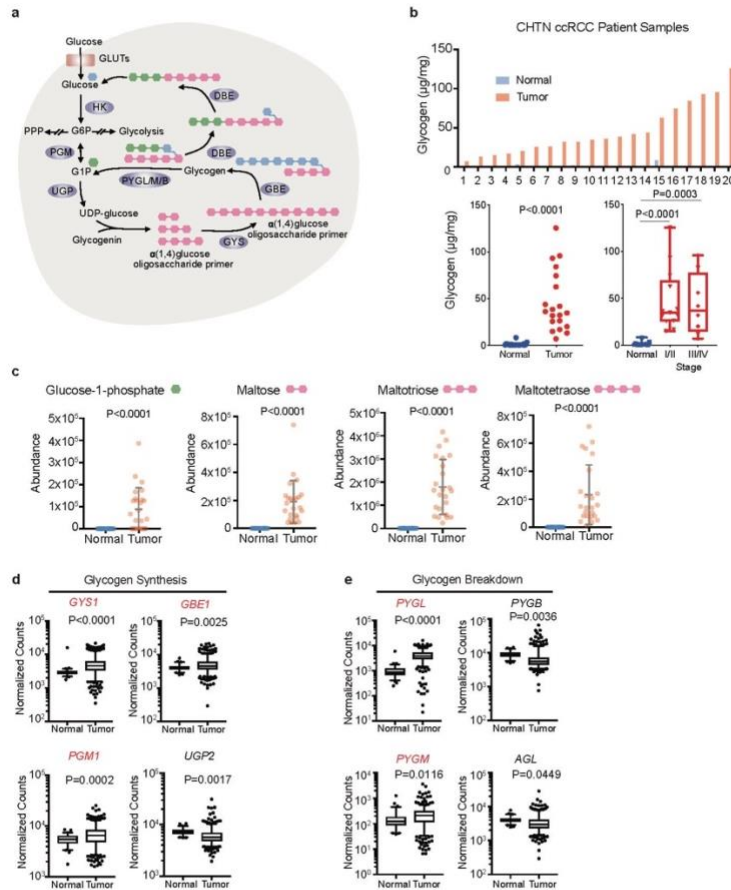
Figure 3.1. **Glycogen synthesis and breakdown are hyperactive in ccRCC tumors. a**. Schematic representation of glycogen synthesis and breakdown pathway in the cytosol. Briefly, glucose conversion into glucose-1-phopshate (G1P) is added or subtracted from oligosaccharide chains scaffolded by the core protein, glycogenin. Green hexagon: singly added glucose-1-phosphate; Pink hexagon: polysaccharide molecules added; Blue hexagon: units added as new branch. **b**. Upper panel: Glycogen extracted from 20 pairs of fresh frozen ccRCC patient tumors and adjacent normal kidneys and then quantified using glycogen assay kit (see Methods). Lower panels: Summary of tumors analyzed for glycogen levels, and subdivided according to tumor stage; n=20 biologically independent human ccRCC tumor/normal paired samples. Box plots (min. to max. all points): center=median, bounds=25th and 75th percentiles, whiskers=min. and max. values. **c**. Abundance of glycogen metabolism related metabolites in same human ccRCC tumor/normal paired samples. Data presented as mean +/- SEM. **d, e.** Normalized RNA-seq reads of glycogen synthesis genes (*PGM1*, *UGP2*, *GYS1*, and *GBE1*) and glycogen breakdown genes (*PYGL*, *PYGB*, *PYGM*, and *AGL*) in ccRCC (n=428) and normal kidney (n=66) samples; n denotes biologically independent human tissue samples. RNA-seq data obtained from TCGA. Box plots (min. to max. all points): center=median, bounds=25th and 75th percentiles, whiskers=5th and 95th percentiles. *P* values determined by two-tailed Student's *t* test. GLUT: glucose transporter; HK: hexokinase; PPP: pentose phosphate pathway PGM: phosphoglucomutase; UGP: UDP-glucose pyrophosphatase; UDP-glucose: uridine diphospho-glucose; GYS: glycogen synthase; GBE: glycogen branching enzyme; PYGL/M/B: glycogen phosphorylase, liver/muscle/brain; DBE (encoded by *AGL*): debranching enzyme. Red denotes gene expression increase.
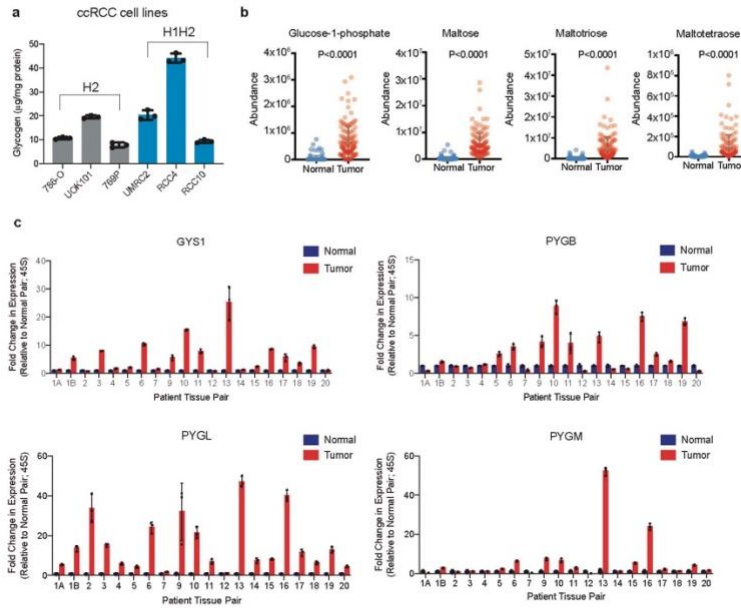
Extended Data Figure 3.1 (related to Figure 3.1). **Glycogen synthesis and breakdown are hyperactive in ccRCC tumors. a.** Glycogen quantification of six ccRCC cell lines in replete conditions (10% FBS, 25mM glucose DMEM) normalized to protein mass; n=3 technical replicates as an example of reproducible experiments. Data presented as mean +/- SD. "H2": cell lines exclusively expressing HIF-2α. "H1H2": cell lines expressing both HIF-1α and HIF-2α. **b**. Abundance of glycogen metabolism-related metabolites (glucose-1-phosphate, maltose, maltotriose, and maltotetraose) in n=138 biologically independent human ccRCC tumor/normal paired samples; data extracted from Hakimi AA, et al[16]. Data presented as mean +/- SEM. **c**. qRT-PCR of *GYS1*, *PYGB*, *PYGL*, and *PYGM* in 20 matched ccRCC and adjacent normal kidney tissues; n=3 technical replicates per tissue sample as an example of reproducible experiments. Data presented as mean +/- SD. Ribosomal subunit 45S RNA (*45S*) utilized as the endogenous control gene. *P* values determined by two-tailed Student's *t* test.

91
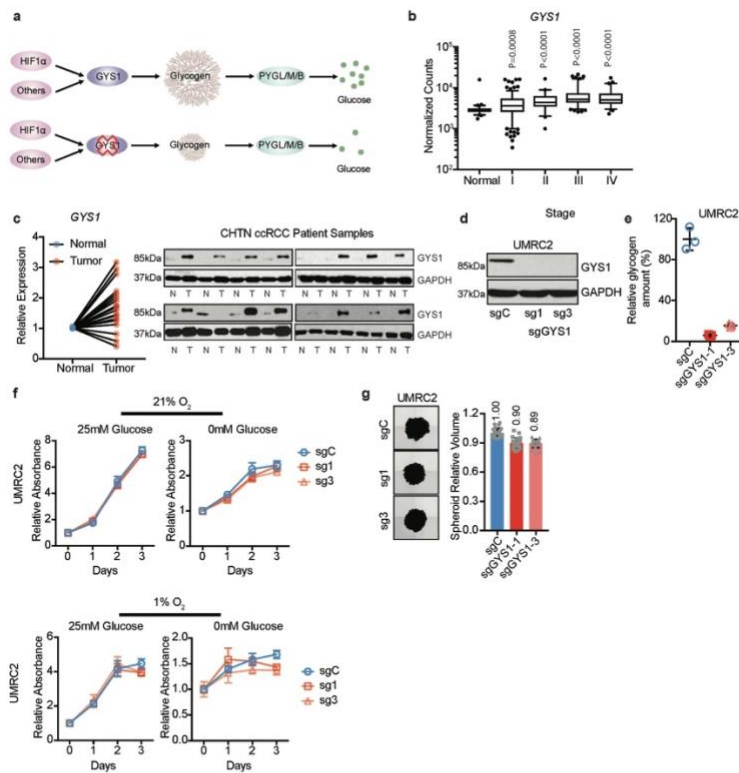
Figure 3.2. **Elevated glycogen synthesis enzyme, GYS1, in ccRCC tumors does not affect proliferation *in vitro*. a**. Schematic model of simplified glycogen metabolism pathway and hypothetical effect of GYS1 blockade on glycogen and free glucose. **b**. Normalized RNA-seq reads of *GYS1* in stage-stratified ccRCC (n=428) and normal kidney (n=66) samples; n denotes biologically independent human tissue samples. RNA-seq data obtained from TCGA. Box plots (min. to max. all points): center=median, bounds=25th and 75th percentiles, whiskers=5th and 95th percentiles. Center line=median. **c**. qRT-PCR (left) and immunoblots (right) of GYS1 in matched ccRCC and normal kidney samples; n=20 biologically independent human ccRCC tumor/normal paired samples. For qRT-PCR, *TBP* and *ACTB* utilized as endogenous control genes. Relative mRNA expression determined by normalizing to expression in normal tissues. **d**. UMRC2 ccRCC cells transduced with two independent sgRNAs against *GYS1* (sg1 and sg3) or a control sgRNA (sgC). Western blot analysis performed 7 days after virus infection to assess GYS1 expression. **e**. Glycogen content measured in cells described in **d** on day 14 after virus infection; n=3 technical replicates as an example of reproducible experiments. Data presented as mean +/- SD. Relative glycogen amount determined by normalizing to glycogen level in sgC cells. **f**. Growth curves for cells described in **d** cultured in medium containing 1% FBS combined with indicated glucose and oxygen concentrations; n=6 biologically independent cell populations. Data presented as mean +/- SEM. Relative absorbance determined by normalizing to values at Day 0. **g**. Representative images acquired at 40X magnification and relative volumes of spheroids formed by cells described in **d** after 19 days culture; n=24 biologically independent spheroids. Data presented as mean +/- SEM. Relative volume determined by normalizing to that of sgC spheroids. Numbers denote average relative volumes. *P* values determined by two-tailed Student's *t* test. For panels **f** and **g**, data are presented as mean values +/- SEM.
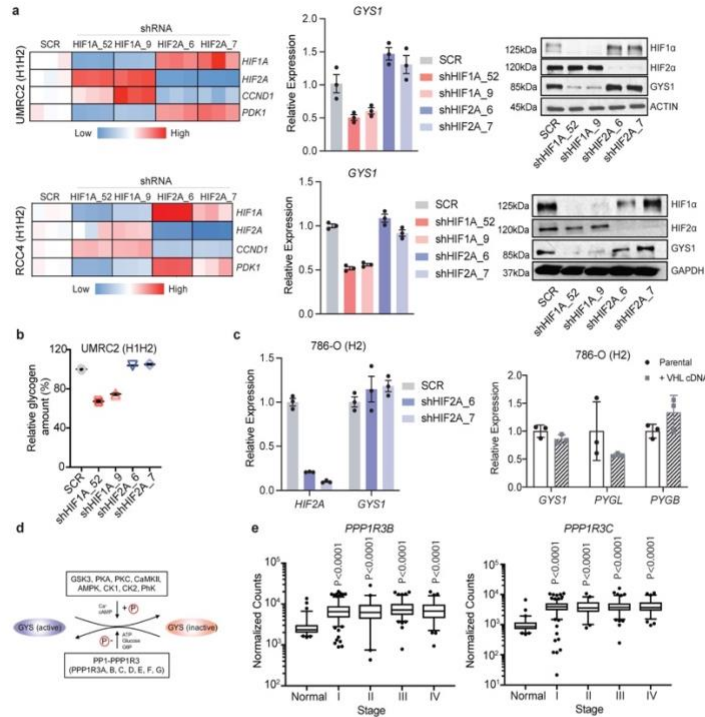
Extended Data Figure 3.2 (related to Figure 3.2). **Glycogen synthesis enzyme GYS1 is overrepresented in ccRCC and regulated by HIF-1α. a.** UMRC2 and RCC4 (H1H2) ccRCC cells transduced with two independent shRNAs against *HIF1A* (shHIF1A_52 and shHIF1A_9), *EPAS1* (shHIF2A_6 and shHIF2A_7), or a SCR (scrambled shRNA) control. qRT-PCR and Western blot for GYS1 shown. *PDK1* and *CCND1* included as positive controls for HIF-1α and HIF-2α suppression, respectively. For qRT-PCR, *TBP* and *ACTB* utilized as endogenous control genes, and relative mRNA expression determined by normalizing to expression in SCR samples; n=3 technical replicates as an example of reproducible experiments. Data are presented as mean +/- SD. **b.** Glycogen quantification in UMRC2 cells transduced with indicated shRNAs after 4 days; n=3 technical replicates as an example of reproducible experiments. Data are presented as mean +/- SD. Relative glycogen amount determined by normalizing to levels in SCR samples. **c.** (Left panel) *EPAS1* (HIF-2A) depleted by two independent shRNAs (shHIF2A_6 and shHIF2A_7) or (right panel) ectopic VHL expression in 786-O (H2) ccRCC cells. Expression relative to *ACTB* shown by qRT-PCR; n=3 technical replicates as an example of reproducible experiments. Data are presented as mean +/- SD. **d.** Schematic representation of GYS regulation by PP1 and PPP1R3 (see text for details). **e.** Normalized RNA-seq reads of *PPP1R3B* and *PPP1R3C* in stage-stratified ccRCC (n=428) and normal kidney (n=66) samples; n denotes biologically independent human tissue samples. RNA-seq data obtained from TCGA. Box plots (min. to max. all points): center=median, bounds=25th and 75th percentiles, whiskers=5th and 95th percentiles. *P* values determined by two-tailed Student's *t* test.

93
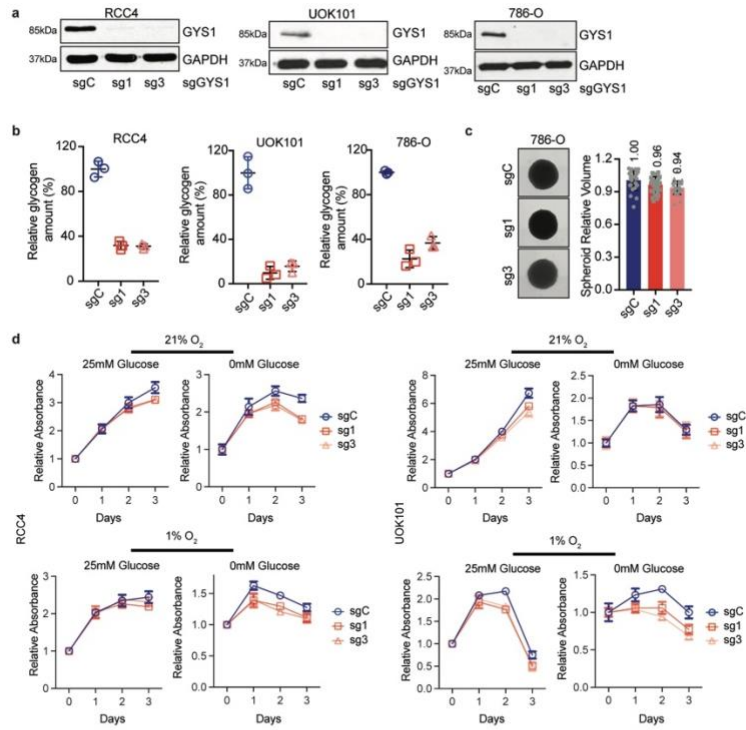
Extended Data Figure 3.3 (related to Figure 3.2). **Glycogen is dispensable for ccRCC cell growth *in vitro*. a.** RCC4, UOK101, and 786-O ccRCC cells transduced with two independent sgRNAs against *GYS1* (sg1 and sg3) or a control sgRNA (sgC). Western blot analysis performed 7 days after virus infection to assess GYS1 expression. **b.** Glycogen levels measured in cells described in **a** on day 7 after virus infection; n=3 technical replicates as an example of reproducible experiments. Data presented as mean +/- SD. Relative glycogen amount was determined by normalizing to glycogen level in sgC cells. **c.** Representative images acquired at 40X magnification and relative volumes of spheroids formed by 786-O cells described in **a** after 19 days culture; n=24 biologically independent spheroids. Data presented as mean +/- SEM. Relative volume was determined by normalizing to that of sgC spheroids. Numbers denote average relative volumes. **d**. Growth curves for cells described in **a** cultured in medium containing 1% FBS combined with indicated glucose and oxygen concentrations; n=6 biologically independent cell populations. Data presented as mean +/- SEM. Relative absorbance was determined by normalizing to values at Day 0.
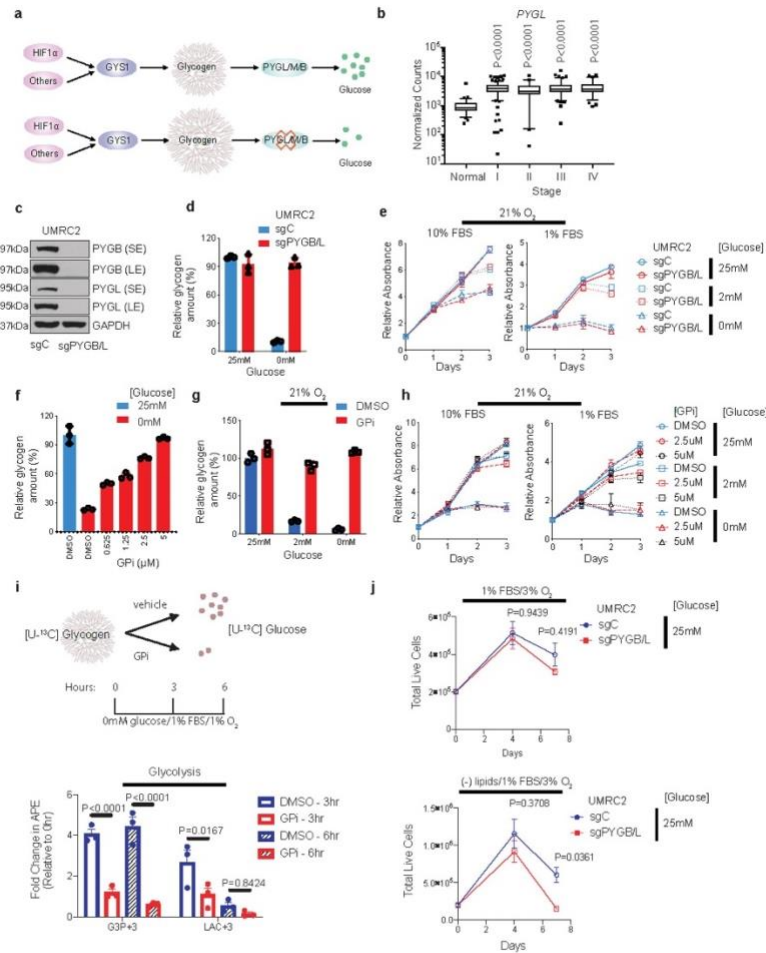
94

Figure 3.3. **ccRCC tumor cells do not rely on glycogen breakdown for growth *in vitro* despite glycolytic entry of glycogen-derived glucose. a.** Hypothetical effect of PYGL/M/B blockade on glycogen breakdown. **b.** Normalized TCGA RNA-seq reads of *PYGL* in stage-stratified ccRCC (n=428 tumors) and normal kidney (n=66 tissue) samples. *P* values determined by two-tailed Student's *t* test. **c.** Protein assessment comparing WT UMRC2 cells and PYGL KO UMRC2 cells described in Extended Data Figure 4b transduced with a control sgRNA against *LacZ* (sgC) or combined two sgRNAs targeting *PYGB* (sgPYGB/L), respectively. SE, short exposure; LE, long exposure. **d.** Glycogen quantification of cells described in **c** cultured in 25mM or 0mM glucose for 6 hours. Normalized to sgC in 25mM glucose. **e**. Growth curves for cells described in **c** cultured in indicated conditions; n=6. Normalized to Day 0. **f.** Glycogen quantification of UMRC2 cells cultured in 25mM (blue) or 0mM (red) glucose, treated with indicated concentrations of DMSO or GPi for 6 hours. Normalized to 25mM glucose. **g**. Glycogen quantification of UMRC2 cells cultured in 25mM, 2mM, or 0mM glucose and treated with DMSO (blue) or 5µM GPi (red) in 21% O_2 for 48 hours. Normalized to 25mM glucose condition plus DMSO. **h**. Growth curves for UMRC2 parental cells treated with DMSO, 2.5µM, or 5µM GPi and cultured in indicated conditions; n=6 biologically independent cell populations. Normalized to Day 0. **i**. Upper panel: schematic of uniformly ^{13}C-labeled ([U-^{13}C]) glucose release from glycogen. Bottom panel: fold change in atomic percent excess (APE) of key glycolytic metabolites. Normalized to 0 hr; n=3. G3P+3: Glyceraldehyde-3-phosphate with three ^{13}C carbons. LAC+3: Lactate with three ^{13}C carbons. GPi concentration was 10µM (bottom panel). **j**. Growth curves for UMRC2 under the indicated culture conditions; n=3 biologically independent cell populations. For I and J, two-way ANOVA with Sidak's multiple comparison test was used to determine significance. For all glycogen measurements, data from n=3 technical replicates and presented as mean +/- SD. For all growth curves, data from biologically independent cell populations and presented as mean +/- SEM.

95
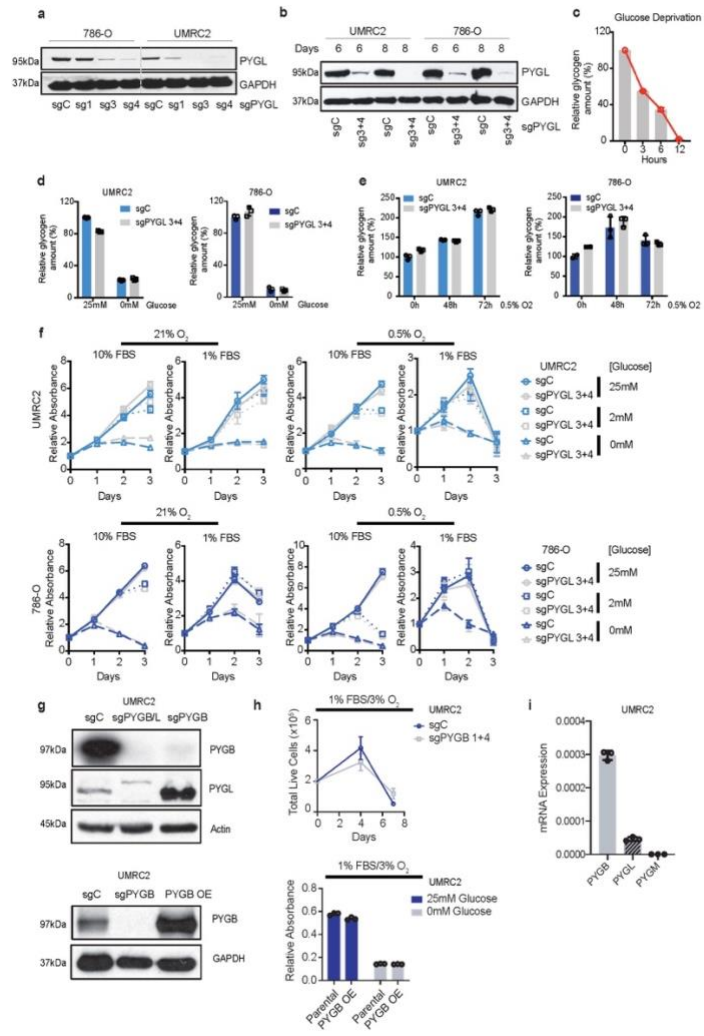
Extended Data Figure 3.4 (related to Figure 3.3). **PYGL is not required for glycogen breakdown and *in vitro* ccRCC cell growth. a**, **b**. Protein assessment of 786-O and UMRC2 ccRCC cells transduced with three independent or two pooled sgRNAs against *PYGL* (sg1, sg3, sg4, or sg3+4) or a control sgRNA (sgC). Samples collected at 7 (a) or 6,8 (b) days after lentiviral infection. **c**. UMRC2 cells cultured in glucose-free medium for indicated time points, glycogen extracted and quantified. Relative glycogen amount determined by normalizing to glycogen level in cells at 0 hour. **c**. Cells described in **b** cultured in medium with 25mM glucose or starved in glucose-free medium for 6 hours, glycogen extracted and quantified. Relative glycogen amount determined by normalizing to glycogen level in sgC cells cultured in medium with 25mM glucose. **e.** Cells described in **b** cultured in 0.5% O_2 for indicated time points, glycogen extracted and quantified. Relative glycogen amount determined by normalizing to glycogen level in sgC cells cultured in 21% O_2. **f**. Growth curves for cells described in **b** cultured in indicated conditions; n=6 biologically independent cell populations. Relative absorbance determined by normalizing to values at Day 0. **g**. Protein assessment of pooled sgRNAs 1+4 targeting *PYGB* (sgPYGB) or overexpression of *PYGB* (PYGB OE), upper and bottom panels respectively. sgC: control (guide targeting *LacZ*); sg*PYGB/L*: double knockout. **h**. Growth assays of UMRC2 under the indicated conditions. Live cell numbers were measured by Trypan Blue exclusion, and finalized values adjusted for dilution; n=3 biologically independent cell populations. PYGB knockout and PYGB overexpression (upper and bottom panels respectively). Parental refers to uninfected UMRC2 cells. I. qRT-PCR on UMRC2 cells for glycogen phosphorylase isoforms; n=3 technical replicates. Data presented as mean +/-SD. Ribosomal subunit 45S RNA (*45S*) utilized as the endogenous control gene. For all glycogen measurements, data from n=3 technical replicates and presented as mean +/- SD. For all growth curves, data are presented as mean +/- SEM.

96
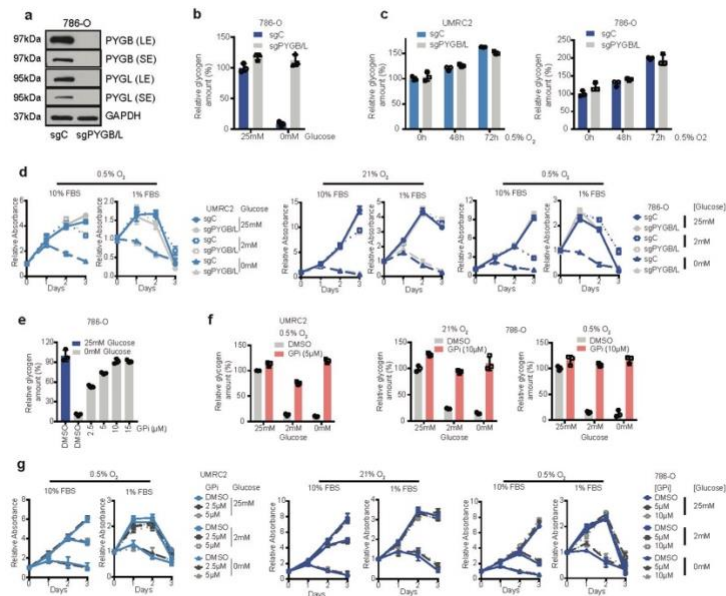
Extended Data Figure 3.5 (related to Figure 3.3). **ccRCC tumor cells do not rely on glycogen breakdown for growth.**
a. WT and PYGL KO 786-O cells transduced with a control sgRNA against *LacZ* (sgC) or combined two sgRNAs targeting *PYGB* (sgPYGB/L), respectively. Top 50% GFP positive cells sorted for culture. Western blot analysis performed 14 days after virus infection to assess PYGL and PYGB expression. SE, short exposure; LE, long exposure. **b**. Cells described in **a** cultured in medium with 25mM glucose or starved in glucose-free medium for 6 hours, glycogen extracted and quantified. Relative glycogen amount determined by normalizing to glycogen level in sgC cells cultured in medium with 25mM glucose. **c**. UMRC2 and 786-O sgC vs. sgPYGL/B ccRCC cells cultured in 0.5% O_2 for indicated time points, glycogen extracted and quantified. Relative glycogen amount determined by normalizing to glycogen level in sgC cells cultured in 21% O_2. **d**. Growth curves for UMRC2 cells described in Figure 3c and 786-O cells described in **a** cultured in indicated conditions. Relative absorbance determined by normalizing to values at Day 0. **e**. 786-O cells cultured in medium with 25mM or 0mM glucose, treated with indicated concentrations of DMSO or GPi for 6 hours. Glycogen extracted and quantified. Relative glycogen amount determined by normalizing to glycogen level in cells cultured in 25mM glucose condition. **f.** UMRC2 and 786-O cells cultured in medium with 25mM, 2mM, or 0mM glucose, treated with DMSO or 10μM GPi in 21% O_2 or 0.5% O_2 for 48 hours. Glycogen extracted and quantified. Relative glycogen amount determined by normalizing to glycogen level in cells cultured in 25mM glucose condition treated with DMSO. **g**. Growth curves for UMRC2 and 786-O parental cells treated with DMSO, 5μM, or 10μM GPi and cultured in indicated conditions. Relative absorbance determined by normalizing to values at Day 0. For all glycogen measurements, data from n=3 technical replicates and presented as mean +/- SD. For all growth curves, data from n=6 biologically independent cell populations and presented as mean +/- SEM.

97
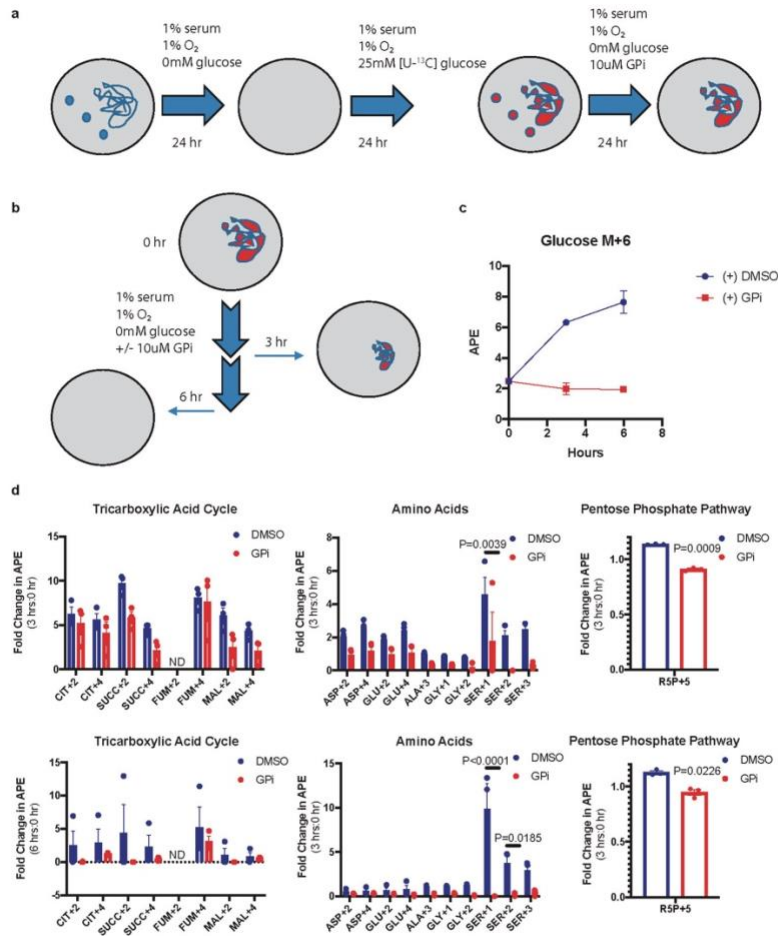
Extended Data Figure 3.6 (related to Figure 3.3). **Glycogen-derived glucose broadly enters the central carbon pathway during glucose starvation. a**. Glycogen labeling experimental design. [U-^{13}C]: uniformly labeled heavy carbon (^{13}C); GPi: glycogen phosphorylase inhibitor. Small blue or red circles denote free, unlabeled or labeled glucose, respectively. Large blue or red undefined shapes denote unlabeled or labeled glycogen, respectively. **b**. Sample collection scheme for metabolomic analysis following labeled glycogen breakdown or retention. **c**. Percentage of labeled glucose (Glucose M+6) relative to unlabeled glucose in cells over 6 hours of glycogen breakdown or retention; n=3 biologically independent cell populations. **d**. Fold change in APE relative to time 0 for indicated metabolites after 3 hours (upper panel) and 6 hours (bottom panel) of glycogen breakdown or retention; n=3 biologically independent cell populations. For all metabolite measurements, data presented as mean +/- SEM. CIT: citrate; SUCC: succinate; FUM: fumarate; MAL: malate; ASP: aspartate; GLU: glutamate; ALA: alanine; GLY: glycine; SER: serine; R5P: ribose-5-phosphate. ND: not detectable. (+1,2,3 denotes number of ^{13}C carbons). Two-way ANOVA with Sidak's multiple comparison test was used to determine significance.
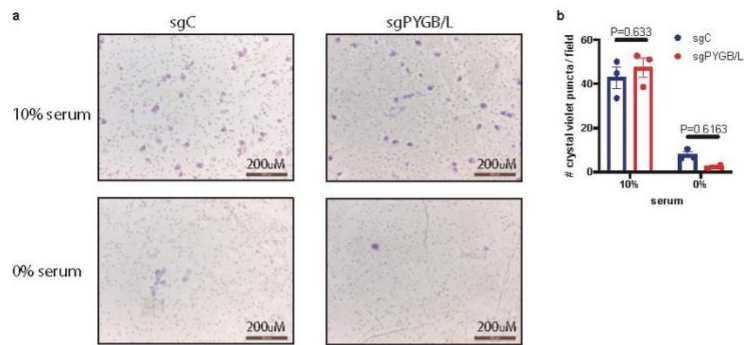
Extended Data Figure 3.7 (related to Figure 3.3). **Glycogen availability does not alter cell migration**. **a**. Representative field image of crystal violet-stained UMRC2 cells under the specified conditions and genetic alterations. Scale bar=200µm. **b**. Quantification of cell migration calculated as average cell number per field; n=3 biologically independent cell populations (average count of 4 center-oriented fields per sample). Data presented as mean +/- SEM. sgC: UMRC2 control sgLacZ; sgPYGB/L: UMRC2 *PYGB/L* double knockout. Two-way ANOVA with Sidak's multiple comparison test was used to determine significance.

99
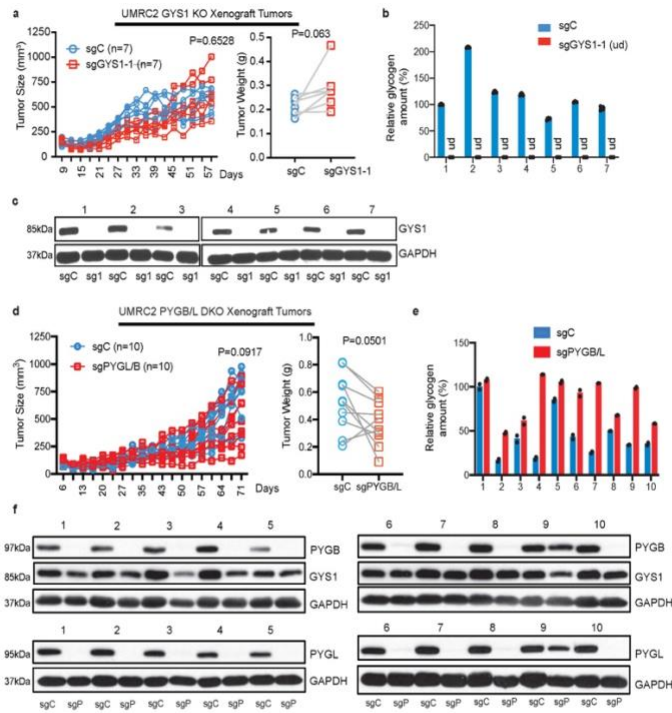
Figure 3.4. **Genetic perturbation in glycogen metabolism does not alter ccRCC xenograft progression *in vivo*. a.** Tumor volume measurements for UMRC2 control (sgC) and *GYS1* KO (sg1) subcutaneous xenograft tumors (in opposing flanks of each animal) at indicated time points (left); n=7 biologically independent tumors. Tumor weights at harvest determined (right). Note: some points overlap. **b.** Glycogen quantification of 7 pairs of sgC and sg1 xenograft tumors at harvest; n=3 technical replicates per tumor sample. Relative glycogen amount determined by normalizing to glycogen level in #1 sgC tumor. **c.** Western blot analysis for GYS1 in xenograft tumors. **d**. Tumor volume measurements for UMRC2 control (sgC) and *PYGL/B* KO (sgPYGL/B) subcutaneous xenograft tumors (in opposing flanks of each animal) at indicated time points (left); n=10 biologically independent tumors. Tumor weights at harvest determined (right). Note: some points overlap. **e**. Glycogen quantification of 10 pairs of sgC and sgPYGL/B xenograft tumors at harvest; n=2 technical replicates per tumor sample. Relative glycogen amount determined by normalizing to glycogen level in #1 sgC tumor. **f**. Western blot analysis for PYGL and PYGB protein in xenograft tumors. sgC: UMRC2 control sgLacZ; sgP: UMRC2 sgPYGB/L. For tumor volume and weight measurements, two-way ANOVA with Sidak's multiple comparison test and paired t test were used to determine significance, respectively. For all glycogen measurements, data are presented as mean +/- SD.

CHAPTER 4: Conclusions and Future Directions

This final chapter will summarize and critically assess the pertinent results described in the previous two chapters. I hope to convey an honest interpretation of the data juxtaposed to propositions of new experimentation that will deepen our scientific understanding whilst outlining a practical path forward for clinical progress. Lastly, I will aim to connect our findings and my perspective with the broader field of glucose metabolism in cancer, as discussed in the introduction, to provide a navigational blueprint for the future of translational research in liver and kidney cancer.

4.1 Overall Summary: Return to the Role of Glucose Metabolism in Cancer

Glucose utilization provides cancer and cancer-associated cells in the local milieu with the energy, metabolite derivatives, and antioxidant balance to drive tumor progression. Thus, understanding precisely how glucose is catabolized in cancer relative to normal tissue is an attractive targeted therapy. Historically, the initial wave of targeted therapies was developed against various mitogenic kinases harboring oncogenic mutations, namely: Imatinib inhibition of Bcr-Abl in chronic myelogenous leukemia (O'Brien et al, 2003)[226], Vemurafenib inhibition of BRAF in melanoma (Chapman et al, 2011)[227], and Crizotinib inhibition of ALK in non-small cell lung cancer (Shaw et al, 2013)[228]. However, many patient tumors possess *de novo* or acquired resistance through secondary mutations or activation of parallel pathways, which has directed the field towards identifying next-generation drugs and combination strategies (Aldea et al, 2021)[229].

Ultimately, sustained growth signaling or avoidance of cell death mechanisms, intrinsically- or immunologically-mediated, are major obstacles to the future of targeted therapy. This is further compounded by the substantial genetic and transcriptomic heterogeneity between patients, primary and metastatic sites within a single patient, or clonally within an individual tumor (Dagogo-Jack and Shaw, 2017)[230]. Therefore, in an effort to develop novel cancer treatments with greater efficacy across a general population, drug discovery and translational research is currently investigating role of metabolism in tumors: a complex yet fundamental network of biochemical processes that integrate oncogenic drivers with nutrient availability. In particular, the central carbon pathway, which as its nomenclature suggests is principal for all components of cellular metabolism, provides numerous catabolic fates of glucose and dictates cell survival.

Specifically, our work focused on aspects of glucagon-regulated glucose metabolism in liver and kidney cancer, gluconeogenesis and glycogenolysis, respectively. From these studies, we identified two main conclusions: (1) glucagon signaling can be experimentally manipulated to antagonize HCC, through an unknown mechanism independent of gluconeogenic gene expression; and (2) glycogenolysis is not required for ccRCC progression but may contribute to cell viability under specific lipid and oxygen stress conditions. These data represent interesting cases of metabolic vulnerabilities in cancer that can and should be further explored within a precise framework. Similar to the importance of biomarker distinction and patient stratification in clinical trials (Goossens et al, 2015)[231], prioritizing future experiments is necessary to optimize both scientific and medical benefits. I advise that direct continuation of both projects is not currently justified by the data; however, incorporating glucagon, gluconeogenesis, and glycogen metabolism into the context of tumor microenvironment or clinical research may yield more promising results for glucagon treatments or inhibitors of glycogen breakdown in liver or kidney cancer, respectively.

4.2 Criticisms and Future Directions

Glucagon/GCGR in Hepatocellular Carcinoma

To summarize our research into glucagon and GCGR in hepatocellular carcinoma, we report 5 major findings: (1) liver cancer cells are robustly dependent on exogenous glucose for growth; (2) the glucagon receptor, GCGR, is downregulated at the mRNA level in both patient liver tumors and cell line models; (3) supraphysiologic levels of GCGR can re-sensitize SNU398 cells to glucagon treatment by enhancing cAMP

103

production, PKA activity, and nuclear CREB phosphorylation; (4) neither glucagon/GCGR nor epigenetic inhibitors are sufficient to completely restore gluconeogenic gene expression to that of primary human hepatocytes; and (5) SNU398 cells over-expressing GCGR uniquely, but reproducibly, display reduced viability upon glucagon treatment that appears to be independent of CREB and gluconeogenic gene expression. These results were obtained over the course of 2 years and address an, as of yet, uncharacterized area of hormone-dependent glucose metabolism in cancer.

My critical assessment of the data is mainly that glucagon signaling is not a reliable tumor suppressor pathway. Supporting this interpretation, only one cell line showed a consistent phenotype of increased cell death and decreased cell proliferation. Moreover, this isolated effect was only observed at a non-physiological setting with 100-fold overexpression of *GCGR* in SNU398 relative to normal human hepatocytes. No parental cell line was affected by glucagon exposure in any measurable way. Additionally, we examined whether glucagon could reduce SNU398 GCGR tumor progression in a xenograft model, but measured no significant difference in tumor volume (data not shown). GCGR tumor volumes and weights were actually larger on average compared to eGFP controls, which was unexpected given that they grow at equivalent rates *in vitro*.

Technical errors aside, it is concerning that the glucagon/GCGR phenotype *in vitro* failed to translate *in vivo*, a closer proxy to the human patient. Discrepancies in glucagon stability and concentration could provide an explanation; however, this was not evaluated in sufficient detail to conclusively determine. If the *in vitro* phenotype was robust, meaning a majority of cell lines displayed a similar reduction in proliferation with glucagon treatment and GCGR overexpression, then I believe it would have been more

reasonable to elucidate the precise *in vivo* conditions and pharmacodynamics of glucagon. Of course, it is also plausible that a phenotype in other cell lines or *in vivo* could have been created with combination strategies (i.e. glucagon/GCGR + Sorafenib) or specific surgical procedures (i.e. transarterial chemoembolization with glucagon on GCGR tumors). However, given the substantial amount of negative data, as well as an undetermined mechanism for the phenotype in SNU398 GCGR cells, I believe further study into glucagon signaling within cancer cells themselves is not an effective use of time and resources.

However, I do strongly believe that glucagon signaling should be further characterized in the context of liver cancer in two ways: (1) GCGR silencing in early tumor initiation; and (2) the glucagon-induced effects of hyperglycemia in diabetic liver cancer patients. In the next section, I will describe the rationale and potential experimental design to support these research queries.

The cell-of-origin of most forms of primary liver cancer is hepatocytes and is diagnosed as hepatocellular carcinoma (HCC); the other subtype being cholangiocarcinoma of the hepatic bile duct. However, hepatocytes are effectively categorized into metabolic zonations, depending on spatiotemporal factors within the vascular architecture of the liver, such as differential oxygen gradients, as well as expression of the Wnt/β-catenin pathway (Birchmeier, 2016; Droin et al, 2021; Manco and Itzkovitz, 2021)[232-234]. In zone 1, hepatocytes are responsive to glucagon and regulate blood glucose homeostasis, whereas zone 3 hepatocytes are dominated by Wnt signaling and glycolysis.

It would be interesting to determine whether GCGR-expressing zone 1 hepatocytes are the cell-of-origin for specific etiologies of liver cancer, and if downregulation of *GCGR* mRNA is an early event required for tumor initiation. To test this, lineage tracing of both zone 3 (*Axin2-Cre^ERT2*; *Rosa26-Lox-Stop-Lox-tdTomato*) (Kurosaki et al, 2021)[235] and zone 1 (*GCGR-Flp^ERT2*; *Rosa26-FRT-Stop-FRT-GFP*) hepatocytes could specifically label cells green that express *GCGR* and red that express *Axin2* when treated with tamoxifen. Then, mice can be assigned into various cohorts of liver tumorigenesis models, particularly those that reflect the rising incidences of hepatic steatosis (Anstee et al, 2019)[236], and monitored for tumor development. Upon dissection, if more green tumors are observed than red, indicating a predominance of zone 1-derived hepatocytes, then we could conclude that GCGR-expressing cells may directly undergo neoplastic transformations. Finally, qPCR can be performed to quantify the relative expression of *GCGR* in these green tumors, hypothesized to be decreased relative to pre-tumorigenesis. In this regard, biopsies of at-risk patients could be monitored for *GCGR* mRNA by fluorescent in situ hybridization over time.

Further validation would address whether *GCGR* add back, potentially by hydrodynamic DNA injection, could restore glucagon signaling and gluconeogenesis to slow or revert early tumor onset. As liver cancer prevention and imaging becomes more refined, the efficacy of additional hormones, such as glucagon, and pharmacological agents, such as epigenetic inhibitors, could be evaluated. From these hypothetical experiments and their results, we could provisionally conclude that certain risk factors are associated with zone 1 liver cancer, a subsequent repression of *GCGR*, and that stabilizing glucagon signaling with or without other therapeutics could contribute to reducing HCC burden.

Another avenue of research pertaining to glucagon signaling is in cell non-autonomous crosstalk between glucagon-responsive, normal hepatocytes and liver cancer cells. Type II diabetes is a major risk for HCC development, and hyperglycemia is at least partially maintained by excessive glucagon activity and gluconeogenic output. Therefore, in liver cancer patients with diabetes, does elevated glucagon signaling promote tumor progression by sustaining high levels of circulating or local glucose? I believe this is critical to understand because in this sense glucagon signaling would be oncogenic rather than tumor suppressive. Moreover, it is feasible that antagonists of GCGR, currently under investigation for diabetes, could then be readily utilized for hyperglycemic liver cancer patients.

To test this, liver tumors could be generated in obesity-induced, insulin-resistance mouse models of type II diabetes (*Lep^db*) (Luo et al, 2020)[237]. Then, one cohort would receive the phase I-tested, monoclonal anti-GCGR antibody, REGN1193 (Okamoto et al, 2017; Kostic et al, 2017)[238,239], and the other cohort administered saline as a control. At endpoint, tumor parameters would be quantified, as well as plasma and intratumoral glucose concentrations. I hypothesize that REGN1193 would decrease tumor volume and positively correlate with reduced glucose levels, both systemically and within the tumor. For a mechanistic validation, *Lep^db* mice could be crossed to a strain that harbors a constitutively expressed *G6PC* gene (*Rosa26-G6PC*)(Landau et al, 2016)[240]. These *Lep^db*; *Rosa26-G6PC* mice would hypothetically display enhanced G6PC-mediated glucose export independent of GCGR activity. Following the same tumorigenesis protocol, if tumor reduction by REGN1193 is indeed due to dampened gluconeogenesis, then mice with constitutive expression of the gluconeogenic enzyme G6PC could be insensitive to treatment.

Furthermore, experiments can be designed to test whether the glucose produced from GCGR activity is specifically from normal hepatocytes. I predict this to be the case because GCGR expression is decreased in liver cancer cells, as described previously, and should not be capable of synthesizing new glucose directly. Rather, adjacent zone 1 hepatocytes within the tumor microenvironment could generate and export glucose locally for uptake by tumor cells, as well as by tumor-associated cells, such as macrophages or hepatic stellate cells.

To test this possibility, conditioned media experiments can be performed with purified hepatocytes and cancer cells derived from the *Lep^{db}* diabetic tumor model. First, hepatocytes can be incubated with ^{13}C-labeled pyruvate, a gluconeogenic carbon source, and stimulated with glucagon to convert pyruvate to ^{13}C-labeled glucose for 24-48 hours to fully engage the gluconeogenic pathway. Then, the media from these cells, hypothetically containing ^{13}C-labeled glucose could be transferred to tumor cells without any other source of glucose. I predict that this hepatocyte-originated labeled glucose would be swiftly imported and catabolized in cancer cells. The same experiment could be repeated with other tumor-associated cell types. While not an exact replica of the *in vivo* setting, from these hypothetical data, I would conclude that it is technically plausible for glucagon-responsive hepatocytes to directly feed local tumor cells.

Overall, these studies are important to consider, as they may optimize patient delineation for clinical trials in diabetic vs. non-diabetic liver cancer. In addition, it would shed light on our understanding of exactly which cells are turning cancerous, and how GCGR and gluconeogenesis as a whole metabolic process regulate HCC progression.

Glycogenolysis in ccRCC

Our work in glycogen metabolism in kidney cancer revealed 2 key pieces of data: (1) neither glycogen deposition nor lysis is required for cell viability *in vitro* or *in vivo*, despite its elevated abundance in tumor tissue; and (2) glycogen is rapidly depleted during glucose starvation and contributes carbons to lactate, ribose-5-phosphate, and serine. Although a few late experiments suggested that glycogenolysis may provide a protective effect against simultaneous lipid and oxygen depletion, through unknown mechanisms, the vast majority of the data supports a HIF-driven, inconsequential role of glycogen accumulation in kidney cancer.

While my specific contribution to this project was minor and largely relegated to the revisions and manuscript preparation, I can provide a brief discussion of future translational research in renal carcinoma glycogen, and how our own results could serve as a basis. Generally, I believe subsequent studies should focus on reactive oxygen species (ROS) and non-metabolic functions of glycogen in ccRCC, rather than further examining the role of glycogen with other nutrient stress conditions (i.e. not glucose, oxygen, and lipid availability (what we have done)).

Glycogen metabolism, by definition, is a highly dynamic and fluid process. So far as I know, glycogen has only been described as a storage mechanism for glucose, especially under low oxygen. The prevention of glucose catabolism via glycogen synthesis during temporary ischemia would hypothetically save glucose for maximal energy production, through complete oxidation, once blood flow and nutrient availability are restored. This is not unlike the metabolism of glycogen in skeletal muscle, whereby glycogen is predominantly utilized for ATP generation by oxidative phosphorylation, during higher intensity exercises between 1 minute and a few hours (Hargreaves and Spriet, 2020)[241]. Additionally, since hypoxia is known to increase ROS (Chandel et al, 1998)[242], glycogen storage and breakdown could also be coordinated with the pentose

phosphate pathway to generate NADPH for antioxidant synthesis. Indeed, a recent

report studying the benefit of hypoxia responses in ischemic injury models showed that

Enarodustat, a compound that stabilizes hypoxia-inducible factors (HIFs), mitigated

kidney damage partially through elevated glycogen metabolism and antioxidant

synthesis (Ito et al, 2020)[243].

While the precise relationship between mitochondrial ROS and glycogen processing

is unclear, I believe future experiments could examine the temporal role of glycogen

metabolism in the context oxidative stress, either *in vitro* or in physiologically-relevant

orthotopic models of kidney cancer and ischemia. In our glycogen tracing experiment,

we measured a slight increase in glycogen-derived ribose-5-P. However, we did not

assess ROS levels, which I hypothesize would likely have been increased in the cells

treated with a glycogenolysis inhibitor. In this regard, I believe it is worth preliminarily

testing whether glycogen metabolism could sustain viability during instances of oxidative

stress. A simple experiment could be to treat glycogenolysis-deficient (sgPYGL/B, see

Chapter 3) ccRCC cells with inhibitors of the electron transport chain, which are known

to leak electrons and create superoxide species if decoupled (Raimondi et al, 2020)[244],

and measure ROS and cell viability levels. Further mechanistic experiments can utilize

exogenous antioxidants, such as N-acetyl-cysteine, to rescue the hypothesized

reduction in viability in the absence of glycogen breakdown.

It is possible that our subcutaneous xenograft tumor models did not experience

significant oxidative stress, and therefore may explain why glycogen metabolism

appeared to be dispensable. To stress the potential clinical advantages of studying

glycogen metabolism and ROS, multiple clinical trials are currently investigating the anti-

HIF2-α drug, Belzutifan (NCT04195750, NCT03634540, NCT04489771, NCT04626518,

NCT04586231, etc.), in advanced ccRCC. HIF inhibition is highly relevant to ROS, as

previous work from our lab has demonstrated that HIF2-α siRNA increased the

abundance of ROS, particularly in combination with ionizing radiation (Bertout et al,

2009)[245]. Thus, if clinical HIF2-α antagonists leads to ROS accumulation, then glycogen

levels could functionally correlate to response rates and should be closely evaluated.

Lastly, a very novel, and perhaps antithetical, area of study is the potential non-

metabolic function of glycogen. Nuclear localization of glycogen synthetase (GYS) has

been reported in the absence of glycogen or when mutated, suggesting that glycogen

may also act as a somewhat cytosolic GYS-chelator (Cid et al, 2005; Diaz et al,

2011)[246,247]. This implies that glycogen could also bind and trap other proteins not

necessarily involved in its synthesis or catabolism. We also mentioned previously in

Chapter 3 that glycogen and its catabolic enzymes have been observed in the nucleus. It

would be extremely curious if glycogen, as a macromolecule, also possessed a

scaffolding or signaling role independent of its metabolism (hypothesized by one of the

co-first authors of Xie et al. 2021, Jun Song). As a pilot experiment, glycogen could be

purified, in a method similar to immunoprecipitation, and interacting proteins analyzed by

mass spectrometry. Protein identifications would then be queried for potential

involvement in signaling networks outside of strict glycogen metabolism. While this is

more basic research, if glycogen is found to interact with proteins that predict drug

response or patient outcome, pharmacological approaches targeting those interactions

could lead to new forms of therapies.

Additionally, in pondering recent reports of glycogen metabolism in immune cells,

including memory CD8^{+} T cells (Ma et al, 2018)[248], antigen-presenting dendritic cells

(Thwe et al, 2017)[249] innate neutrophils (Sadiku et al, 2021)[250], it occurs to me that

glycogen could also feasibly act as a damage-associated molecular pattern, or DAMP.

The immune system has multiple detection mechanisms of identifying dying or infected

cells, including the release of certain molecules that would normally not be present outside of the cell. Cytosolic DNA and secreted nuclear proteins are well established DAMPs that can elicit an immune response. Similar to DAMPs are pathogen-specific molecules, like lipopolysaccharide, which can distinguish self from foreign by the immune system.

Therefore, glycogen, which to my knowledge has not be observed outside of the mammalian cell, could act as signal or ligand indicating cellular apoptosis, following its leakage into the extracellular space via porous membranes. To test this, microscopy analysis on ccRCC cells induced to undergo programmed cell death could be performed and visualized for extracellular glycogen. If glycogen is present, then the efficiency of immune cell-mediated clearance of apoptotic ccRCC cells that either release or lack glycogen could be addressed via co-culture experiments. This potential immunomodulatory role of glycogen could also explain why we did not observe any substantial effect on cell viability *in vitro* or in athymic xenograft models because there was effectively no immune component in either system. Clinically, this could be extremely interesting to know whether a tumor cell that has more glycogen would be better recognized by the immune system and synergize with immunotherapies, which are also highly studied in ccRCC (Motzer et al, 2020; Braun et al, 2021)[251,252].

Closing Remarks

In conclusion, we have shown that aspects of glucose metabolism can have context specific roles in cancer. While not entirely positive, our results warrant further investigation into the role of glucagon in liver cancer and glycogen in kidney cancer, as discussed above, with a strong emphasis on translationally applicable models. I thank everyone who has helped me with my research, as well as my mentor, Dr. Celeste

Simon, for giving me the opportunity to pursue some of these less mainstream ideas. I have learned a lot about scientific research, particularly the endless onslaught of challenges, and how important is to strive towards honesty, commitment, and critical thinking. Ultimately, I hope that I have provided a comprehensive (and comprehendible) account of my research in the Simon lab and that any reader finds the information useful.

BIBLIOGRAPHY

1. Berg JM, Tymoczko JL, and Stryer L. Biochemistry, 5th edition. 2002.

2. Chang L, Chiang S-H, and Saltiel AR. Insulin signaling and the regulation of glucose transport. Mol Med. Jul-Dec 2004;10(7-12):65-71. doi: 10.2119/2005-00029.Saltiel.

3. Zhu J and Thompson CB. Metabolic regulation of cell growth and proliferation. Nat Rev Mol Cell Biol. 2019 Jul;20(7):436-450. doi: 10.1038/s41580-019-0123-5.

4. Boukouris AE, Zervopoulos SD, and Michelakis ED. Metabolic Enzymes Moonlighting in the Nucleus: Metabolic Regulation of Gene Transcription. Trends Biochem Sci. 2016 Aug;41(8):712-730. doi: 10.1016/j.tibs.2016.05.013. Epub 2016 Jun 23.

5. Huangyang P and Simon MC. Hidden features: exploring the non-canonical functions of metabolic enzymes. Dis Model Mech. 2018 Jul 6;11(8):dmm033365. doi: 10.1242/dmm.033365.

6. Vander Heiden MG, Plas DR, Rathmell JC, et al. Growth factors can influence cell growth and survival through effects on glucose metabolism. Mol Cell Biol. 2001 Sep;21(17):5899-912. doi: 10.1128/MCB.21.17.5899-5912.2001.

7. Bouvier N, Fougeray S, Beaune P, et al. The unfolded protein response regulates an angiogenic response by the kidney epithelium during ischemic stress. J Biol Chem. 2012 Apr 27;287(18):14557-68. doi: 10.1074/jbc.M112.340570. Epub 2012 Mar 8.

8. Espinoza-Rojo, Iturralde-Rodriguez KI, Chanez-Cardenas ME, et al. Glucose transporters regulation on ischemic brain: possible role as therapeutic target. Cent Nerv Syst Agents Med Chem. 2010 Dec 1;10(4):317-25. doi: 10.2174/187152410793429755.

9. Sun D, Nguyen N, DeGrado TR, et al. Ischemia induces translocation of the insulin-responsive glucose transporter GLUT4 to the plasma membrane of cardiac myocytes. Circulation. 1994 Feb;89(2):793-8. doi: 10.1161/01.cir.89.2.793.

10. Kuo T, McQueen A, Chen T-C, and Wang J-C. Regulation of Glucose Homeostasis by Glucocorticoids. Adv Exp Med Biol. 2015;872:99-126. doi: 10.1007/978-1-4939-2895-8_5.

11. Sherwin RS and Sacca L. Effect of epinephrine on glucose metabolism in humans: contribution of the liver. Am J Physiol. 1984 Aug;247(2 Pt 1):E157-65. doi: 10.1152/ajpendo.1984.247.2.E157.

12. Kim K, Cho SC, Cova A, et al. Alterations of epinephrine-induced gluconeogenesis in aging. Exp Mol Med. 2009 May 31;41(5):334-40. doi: 10.3858/emm.2009.41.5.037.

13. Sandler MP, Robinson RP, Rabin D, et al. The effect of thyroid hormones on gluconeogenesis and forearm metabolism in man. J Clin Endocrinol Metab. 1983 Mar;56(3):479-85. doi: 10.1210/jcem-56-3-479.

14. Del Guercio MJ, Natale B, Gargantini L, et al. Effect of somatostatin on blood sugar, plasma growth hormone, and glucagon levels in diabetic children. Diabetes. 1976 Jul;25(7):550-3. doi: 10.2337/diab.25.7.550.

15. MacDonald PE, El-Kholy W, Riedel MJ, et al. The multiple actions of GLP-1 on the process of glucose-stimulated insulin secretion. Diabetes. 2002 Dec;51 Suppl 3:S434-42. doi: 10.2337/diabetes.51.2007.s434.

16. Koch C, Augustine RA, Steger J, et al. Leptin rapidly improves glucose homeostasis in obese mice by increasing hypothalamic insulin sensitivity. J Neurosci. 2010 Dec 1;30(48):16180-7. doi: 10.1523/JNEUROSCI.3202-10.2010.

17. Coleman SK, Rebalka IA, D'Souza DM, et al. Myostatin inhibition therapy for insulin-deficient type 1 diabetes. Sci Rep. 2016 Sep 1;6:32495. doi: 10.1038/srep32495.

18. Yuan H-Y, Xiong Y, and Guan K-L. Nutrient sensing, metabolism, and cell growth control. Mol Cell. 2013 Feb 7;49(3):379-87. doi: 10.1016/j.molcel.2013.01.019.

19. Glimcher LH and Lee A-H. From sugar to fat: How the transcription factor XBP1 regulates hepatic lipogenesis. Ann N Y Acad Sci. 2009 Sep;1173 Suppl 1(Suppl 1):E2-9. doi: 10.1111/j.1749-6632.2009.04956.x.

20. Liamis G, Liberopoulos E, Barkas F, and Elisaf M. Diabetes mellitus and electrolyte disorders. World J Clin Cases. 2014 Oct 16;2(10):488-96. doi: 10.12998/wjcc.v2.i10.488.

21. Centers for Disease Control and Prevention. National Diabetes Statistics Report, 2020. Atlanta, GA: Centersfor Disease Control and Prevention, U.S. Dept of Health and Human Services; 2020.

22. Muoio DM and Newgard CB. Mechanisms of disease:Molecular and metabolic mechanisms of insulin resistance and beta-cell failure in type 2 diabetes. Nat Rev Mol Cell Biol. 2008 Mar;9(3):193-205. doi: 10.1038/nrm2327.

23. Kawamori D, Kurpad AJ, Hu J, et al. Insulin signaling in alpha cells modulates glucagon secretion in vivo. Cell Metab. 2009 Apr;9(4):350-61. doi: 10.1016/j.cmet.2009.02.007.

24. Gromada J, Duttaroy A, and Rorsman P. The insulin receptor talks to glucagon? Cell Metab. 2009 Apr;9(4):303-5. doi: 10.1016/j.cmet.2009.03.008.

25. Said G. Diabetic neuropathy--a review. Nat Clin Pract Neurol. 2007 Jun;3(6):331-40. doi: 10.1038/ncpneuro0504.

26. Dhatariya KK, Glaser NS, Codner E, and Umpierrez GE. Diabetic ketoacidosis. Nat Rev Dis Primers. 2020 May 14;6(1):40. doi: 10.1038/s41572-020-0165-1.

27. Yang C, Coker KJ, Kim JK, et al. Syntaxin 4 heterozygous knockout mice develop muscle insulin resistance. J Clin Invest. 2001 May;107(10):1311-8. doi: 10.1172/JCI12274.

28. Hirata Y, Nomura K, Senga Y, et al. Hyperglycemia induces skeletal muscle atrophy via a WWP1/KLF15 axis. JCI Insight. 2019 Feb 21;4(4):e124952. doi: 10.1172/jci.insight.124952.

29. Gray S, Feinber MW, Hull S, et al. The Krüppel-like factor KLF15 regulates the insulin-sensitive glucose transporter GLUT4. J Biol Chem. 2002 Sep 13;277(37):34322-8. doi: 10.1074/jbc.M201304200. Epub 2002 Jul 3.

30. Odegaard JI and Chawla A. Pleiotropic actions of insulin resistance and inflammation in metabolic homeostasis. Science. 2013 Jan 11;339(6116):172-7. doi: 10.1126/science.1230721.

31. Escudero CA, Herlitz K, Troncoso F, et al. Pro-angiogenic Role of Insulin: From Physiology to Pathology. Front Physiol. 2017 Apr 5;8:204. doi: 10.3389/fphys.2017.00204. eCollection 2017.

32. Rask-Madsen C, Li Q, Freund B, et al. Loss of insulin signaling in vascular endothelial cells accelerates atherosclerosis in apolipoprotein E null mice. Cell Metab. 2010 May 5;11(5):379-89. doi: 10.1016/j.cmet.2010.03.013.

33. He Z, Opland DM, Way KJ, et al. Regulation of vascular endothelial growth factor expression and vascularization in the myocardium by insulin receptor and PI3K/Akt pathways in insulin resistance and ischemia. Arterioscler Thromb Vasc Biol. 2006 Apr;26(4):787-93. doi: 10.1161/01.ATV.0000209500.15801.4e. Epub 2006 Feb 9.

34. El-Hattab AW. Inborn errors of metabolism. Clin Perinatol. 2015 Jun;42(2):413-39, x. doi: 10.1016/j.clp.2015.02.010. Epub 2015 Apr 8.

35. Chou JY and Mansfield BC. Mutations in the glucose-6-phosphatase-alpha (G6PC) gene that cause type Ia glycogen storage disease. Hum Mutat. 2008 Jul;29(7):921-30. doi: 10.1002/humu.20772.

36. Zhu A, Lee D, and Shim H. Metabolic PET Imaging in Cancer Detection and Therapy Response. Semin Oncol. 2011 Feb; 38(1): 55–69. doi: 10.1053/j.seminoncol.2010.11.012.

37. Ancey PB, Contat C, and Meylan E. Glucose transporters in cancer – from tumor cells to the tumor microenvironment. FEBS J. 2018 Aug;285(16):2926-2943. doi: 10.1111/febs.14577.

38. Levine AJ and Puzio-Kuter AM. The control of the metabolic switch in cancers by oncogenes and tumor suppressor genes. Science. 2010 Dec 3;330(6009):1340-4. doi: 10.1126/science.1193494.

39. Reinfeld BI, Madden MZ, Wolf MW, et al. Cell-programmed nutrient partitioning in the tumour microenvironment. Nature. 2021 May;593(7858):282-288. doi: 10.1038/s41586-021-03442-1.

40. Hensley CT, Faubert B, Yuan Q, et al. Metabolic Heterogeneity in Human Lung Tumors. Cell. 2016 Feb 11;164(4):681-94. doi: 10.1016/j.cell.2015.12.034.

41. Mendez-Lucas A, Li X, Hu J, et al. Glucose Catabolism in Liver Tumors Induced by c-MYC Can Be Sustained by Various PKM1/PKM2 Ratios and Pyruvate Kinase Activities. Cancer Res. 2017 Aug 15;77(16):4355-4364. doi: 10.1158/0008-5472.CAN-17-0498.

42. Lunt SY and Vander Heiden MG. Aerobic glycolysis: meeting the metabolic requirements of cell proliferation. Annu Rev Cell Dev Biol. 2011;27:441-64. doi: 10.1146/annurev-cellbio-092910-154237.

43. Patra KC and Hay N. The pentose phosphate pathway and cancer. Trends Biochem Sci. 2014 Aug;39(8):347-54. doi: 10.1016/j.tibs.2014.06.005. Epub 2014 Jul 15.

44. Pate KT, Stringari C, Sprowl-Tanio S, et al. Wnt signaling directs a metabolic program of glycolysis and angiogenesis in colon cancer. EMBO J. 2014 Jul 1;33(13):1454-73. doi: 10.15252/embj.201488598. Epub 2014 May 13.

45. Shiraishi T, Verdone JE, Huang J, et al. Glycolysis is the primary bioenergetic pathway for cell motility and cytoskeletal remodeling in human prostate and breast cancer cells. Oncotarget. 2015 Jan 1;6(1):130-43. doi: 10.18632/oncotarget.2766.

46. Masin M, Vazquez J, Rossi S, et al. GLUT3 is induced during epithelial-mesenchymal transition and promotes tumor cell proliferation in non-small cell lung cancer. Cancer Metab. 2014 Jul 29;2:11. doi: 10.1186/2049-3002-2-11. eCollection 2014.

47. Kim NH, Cha YH, Lee J, et al. Snail reprograms glucose metabolism by repressing phosphofructokinase PFKP allowing cancer cell survival under metabolic stress. Nat Commun. 2017 Feb 8;8:14374. doi: 10.1038/ncomms14374.

48. Sasportas LS, Hori SS, Pratx G, et al. Detection and quantitation of circulating tumor cell dynamics by bioluminescence imaging in an orthotopic mammary carcinoma model. PLoS One. 2014 Sep 4;9(9):e105079. doi: 10.1371/journal.pone.0105079. eCollection 2014.

49. Li W, Xu M, Li Y, et al. Comprehensive analysis of the association between tumor glycolysis and immune/inflammation function in breast cancer. J Transl Med. 2020 Feb 18;18(1):92. doi: 10.1186/s12967-020-02267-2.

50. Kareva I and Hahnfeldt P. The emerging "hallmarks" of metabolic reprogramming and immune evasion: distinct or linked? Cancer Res. 2013 May 1;73(9):2737-42. doi: 10.1158/0008-5472.CAN-12-3696. Epub 2013 Feb 19.

51. Kogure A, Naito Y, Yamamoto Y, et al. Cancer cells with high-metastatic potential promote a glycolytic shift in activated fibroblasts. PLoS One. 2020 Jun 17;15(6):e0234613. doi: 10.1371/journal.pone.0234613. eCollection 2020.

52. Hamanaka RB and Chandel NS. Targeting glucose metabolism for cancer therapy. J Exp Med. 2012 Feb 13;209(2):211-5. doi: 10.1084/jem.20120162.

53. Akins NS, Nielson TC, and Le HV. Inhibition of Glycolysis and Glutaminolysis: An Emerging Drug Discovery Approach to Combat Cancer. Curr Top Med Chem. 2018;18(6):494-504. doi: 10.2174/1568026618666180523111351.

54. Pelicano H, Martin DS, Xu R-H, and Huang P. Glycolysis inhibition for anticancer treatment. Oncogene. 2006 Aug 7;25(34):4633-46. doi: 10.1038/sj.onc.1209597.

55. Ralser M, Wamelink MM, Struys ED, et al. A catabolic block does not sufficiently explain how 2-deoxy-D-glucose inhibits cell growth. Proc Natl Acad Sci U S A. 2008 Nov 18;105(46):17807-11. doi: 10.1073/pnas.0803090105.

56. Sahra IB, Laurent K, Giuliano S, et al. Targeting cancer cell metabolism: the combination of metformin and 2-deoxyglucose induces p53-dependent apoptosis in prostate cancer cells. Cancer Res. 2010 Mar 15;70(6):2465-75. doi: 10.1158/0008-5472.CAN-09-2782.

57. Liu H, Hu YP, Savaraj N, et al. Hypersensitization of tumor cells to glycolytic inhibitors. Biochemistry. 2001 May 8;40(18):5542-7. doi: 10.1021/bi002426w.

58. Maher JC, Wangpaichitr M, Savaraj N, et al. Hypoxia-inducible factor-1 confers resistance to the glycolytic inhibitor 2-deoxy-D-glucose. Mol Cancer Ther. 2007 Feb;6(2):732-41. doi: 10.1158/1535-7163.MCT-06-0407.

59. Oshima N, Ishida R, Kishimoto S, et al. Dynamic Imaging of LDH Inhibition in Tumors Reveals Rapid In Vivo Metabolic Rewiring and Vulnerability to Combination Therapy. Cell Rep. 2020 Feb 11;30(6):1798-1810.e4. doi: 10.1016/j.celrep.2020.01.039.

60. Gordon G, Mackow MC, and Levy HR. On the mechanism of interaction of steroids with human glucose 6-phosphate dehydrogenase. Arch Biochem Biophys. 1995 Apr 1;318(1):25-9. doi: 10.1006/abbi.1995.1199.

61. Fang Z, Jiang C, Feng Y, et al. Effects of G6PD activity inhibition on the viability, ROS generation and mechanical properties of cervical cancer cells. Biochim Biophys Acta. 2016 Sep;1863(9):2245-54. doi: 10.1016/j.bbamcr.2016.05.016. Epub 2016 May 20.

62. Morales AJ, Haubrich RH, Hwang JY, et al. The effect of six months treatment with a 100 mg daily dose of dehydroepiandrosterone (DHEA) on circulating sex steroids, body composition and muscle strength in age-advanced men and women. Clin Endocrinol (Oxf). 1998 Oct;49(4):421-32. doi: 10.1046/j.1365-2265.1998.00507.x.

63. Mele L, Paino F, Papaccio F, et al. A new inhibitor of glucose-6-phosphate dehydrogenase blocks pentose phosphate pathway and suppresses malignant proliferation and metastasis in vivo. Cell Death Dis. 2018 May 1;9(5):572. doi: 10.1038/s41419-018-0635-5.

64. Ghergurovich JM, Garcia-Canaveras JC, Wang J, et al. A small molecule G6PD inhibitor reveals immune dependence on pentose phosphate pathway. Nat Chem Biol. 2020 Jul;16(7):731-739. doi: 10.1038/s41589-020-0533-x. Epub 2020 May 11.

65. Yang C, Peng P, Li L, et al. High expression of GFAT1 predicts poor prognosis in patients with pancreatic cancer. Sci Rep. 2016 Dec 20;6:39044. doi: 10.1038/srep39044.

66. Sharma NS, Gupta VK, Garrido VT, et al. Targeting tumor-intrinsic hexosamine biosynthesis sensitizes pancreatic cancer to anti-PD1 therapy. J Clin Invest. 2020 Jan 2;130(1):451-465. doi: 10.1172/JCI127515.

67. Asthana A, Ramakrishnan P, Vicioso Y, et al. Hexosamine Biosynthetic Pathway Inhibition Leads to AML Cell Differentiation and Cell Death. Mol Cancer Ther. 2018 Oct;17(10):2226-2237. doi: 10.1158/1535-7163.MCT-18-0426. Epub 2018 Aug 6.

68. Wu X, Geng F, Cheng X, et al. Lipid Droplets Maintain Energy Homeostasis and Glioblastoma Growth via Autophagic Release of Stored Fatty Acids. iScience. 2020 Sep 17;23(10):101569. doi: 10.1016/j.isci.2020.101569. eCollection 2020 Oct 23.

69. Du W, Zhang L, Brett-Morris A, et al. HIF drives lipid deposition and cancer in ccRCC via repression of fatty acid metabolism. Nat Commun. 2017 Nov 24;8(1):1769. doi: 10.1038/s41467-017-01965-8.

70. Rozeveld CN, Johnson KM, Zhang L, and Razidlo GL. KRAS Controls Pancreatic Cancer Cell Lipid Metabolism and Invasive Potential through the Lipase HSL. Cancer Res. 2020 Nov 15;80(22):4932-4945. doi: 10.1158/0008-5472.CAN-20-1255. Epub 2020 Aug 19.

71. Cruz ALS, A Barreto Ed, Fazolini NPB, et al. Lipid droplets: platforms with multiple functions in cancer hallmarks. Cell Death Dis. 2020 Feb 6;11(2):105. doi: 10.1038/s41419-020-2297-3.

72. Li Y, Su X, Rohatgi N, et al. Hepatic lipids promote liver metastasis. JCI Insight. 2020 Sep 3;5(17):e136215. doi: 10.1172/jci.insight.136215.

73. Rusu P, Shao C, Neuerburg A, et al. GPD1 Specifically Marks Dormant Glioma Stem Cells with a Distinct Metabolic Profile. Cell Stem Cell. 2019 Aug 1;25(2):241-257.e8. doi: 10.1016/j.stem.2019.06.004. Epub 2019 Jul 11.

74. Xie J, Ye J, Cai Z, et al. GPD1 Enhances the Anticancer Effects of Metformin by Synergistically Increasing Total Cellular Glycerol-3-Phosphate. Cancer Res. 2020 Jun 1;80(11):2150-2162. doi: 10.1158/0008-5472.CAN-19-2852. Epub 2020 Mar 16.

75. Marchan R, Buttner B, Lambert J, et al. Glycerol-3-phosphate Acyltransferase 1 Promotes Tumor Cell Migration and Poor Survival in Ovarian Carcinoma. Cancer Res. 2017 Sep 1;77(17):4589-4601. doi: 10.1158/0008-5472.CAN-16-2065. Epub 2017 Jun 26.

76. Ellis JM, Paul DS, Depetrillo MA, et al. Mice deficient in glycerol-3-phosphate acyltransferase-1 have a reduced susceptibility to liver cancer. Toxicol Pathol. 2012 Apr;40(3):513-21. doi: 10.1177/0192623311432298. Epub 2012 Jan 3.

77. Kuhajda FP, Aja S, Tu Y, et al. Pharmacological glycerol-3-phosphate acyltransferase inhibition decreases food intake and adiposity and increases insulin

sensitivity in diet-induced obesity. Am J Physiol Regul Integr Comp Physiol. 2011 Jul;301(1):R116-30. doi: 10.1152/ajpregu.00147.2011. Epub 2011 Apr 13.

78. Maddocks ODK, Athineos D, Cheung EC, et al. Modulating the therapeutic response of tumours to dietary serine and glycine starvation. Nature. 2017 Apr 19;544(7650):372-376. doi: 10.1038/nature22056.

79. Sullivan MR, Mattaini KR, Dennstedt EA, et al. Increased Serine Synthesis Provides an Advantage for Tumors Arising in Tissues Where Serine Levels Are Limiting. Cell Metab. 2019 Jun 4;29(6):1410-1421.e4. doi: 10.1016/j.cmet.2019.02.015. Epub 2019 Mar 21.

80. Riscal R, Schrepfer E, Arena G, et al. Chromatin-Bound MDM2 Regulates Serine Metabolism and Redox Homeostasis Independently of p53. Mol Cell. 2016 Jun 16;62(6):890-902. doi: 10.1016/j.molcel.2016.04.033. Epub 2016 Jun 2.

81. McNamee MJ, Michod D, and Niklison-Chirou MV. Can small molecular inhibitors that stop de novo serine synthesis be used in cancer treatment? Cell Death Discov. 2021 Apr 30;7(1):87. doi: 10.1038/s41420-021-00474-4.

82. Madiraju AK, Erion DM, Rahimi Y, et al. Metformin suppresses gluconeogenesis by inhibiting mitochondrial glycerophosphate dehydrogenase. Nature. 2014 Jun 26;510(7506):542-6. doi: 10.1038/nature13270. Epub 2014 May 21.

83. Loubiere C, Clavel S, Gilleron J, et al. The energy disruptor metformin targets mitochondrial integrity via modification of calcium flux in cancer cells. Sci Rep. 2017 Jul 11;7(1):5040. doi: 10.1038/s41598-017-05052-2.

84. Wang Y, An H, Liu T, et al. Metformin Improves Mitochondrial Respiratory Activity through Activation of AMPK. Cell Rep. 2019 Nov 5;29(6):1511-1523.e5. doi: 10.1016/j.celrep.2019.09.070.

85. Cameron AR, Logie L, Patel K, et al. Metformin selectively targets redox control of complex I energy transduction. Redox Biol. 2018 Apr;14:187-197. doi: 10.1016/j.redox.2017.08.018. Epub 2017 Aug 26.

86. Molina JR, Sun Y, Protopopova M, et al. An inhibitor of oxidative phosphorylation exploits cancer vulnerability. Nat Med. 2018 Jul;24(7):1036-1046. doi: 10.1038/s41591-018-0052-4. Epub 2018 Jun 11.

87. Corbet C, Bastien E, Draoui N, et al. Interruption of lactate uptake by inhibiting mitochondrial pyruvate transport unravels direct antitumor and radiosensitizing effects. Nat Commun. 2018 Mar 23;9(1):1208. doi: 10.1038/s41467-018-03525-0.

88. Lee P, Malik D, Perkons N, et al. Targeting glutamine metabolism slows soft tissue sarcoma growth. Nat Commun. 2020 Jan 24;11(1):498. doi: 10.1038/s41467-020-14374-1.

89. Khan MW and Chakrabarti P. Gluconeogenesis combats cancer: opening new doors in cancer biology. Cell Death Dis. 2015 Sep; 6(9): e1872. doi: 10.1038/cddis.2015.245.

90. Khan T, Sullivan MA, Gunter JH, et al. Revisiting Glycogen in Cancer: A Conspicuous and Targetable Enabler of Malignant Transformation. Front Oncol. 2020 Oct 30;10:592455. doi: 10.3389/fonc.2020.592455. eCollection 2020.

91. Ahren B. Glucagon--Early breakthroughs and recent discoveries. Peptides. 2015. May;67:74-81. doi: 10.1016/j.peptides.2015.03.011.

92. Elliott AD, Ustione A, Piston DW. Somatostatin and insulin mediate glucose-inhibited glucagon secretion in pancreatic α-cell by lowering cAMP. Am J Physiol Endocrinol Metab. 2015. Jan 15;308(2):E130-43. doi: 10.1152/ajpendo.00344.2014.

93. Gerich JE, Langlois M, Noacco C, et al. Comparison of the suppressive effects of elevated plasma glucose and free fatty acid levels on glucagon secretion in normal and insulin-dependent diabetic subjects. Evidence for selective alpha-cell insensitivity to glucose in diabetes mellitus. J Clin Invest. 1976. Aug; 58(2): 320–325. doi: 10.1172/JCI108475.

94. Ramnanan CJ, Edgerton DS, Kraft G, and Cherrington AD. Physiologic action of glucagon on liver glucose metabolism. Diabetes Obes Metab. 2011. Oct;13 Suppl 1(Suppl 1):118-25. doi: 10.1111/j.1463-1326.2011.01454.x.

95. Habegger KM, Heppner KM, Geary N, et al. The metabolic actions of glucagon revisited. Nat Rev Endocrinol. 2010 Dec; 6(12): 689–697. doi: 10.1038/nrendo.2010.187.

96. Adeva-Andany MM, Funcasta-Calderon R, Fernandez-Fernandez C, et al. Metabolic effects of glucagon in humans. J Clin Transl Endocrinol. 2019. Mar; 15: 45–53. doi: 10.1016/j.jcte.2018.12.005.

97. Miller RA, Shi Y, Lu W, et al. Targeting hepatic glutaminase activity to ameliorate hyperglycemia. Nat Med. 2018 May;24(4):518-524. doi: 10.1038/nm.4514. Epub 2018 Mar 26.

98. Ellingsgaard H, Hauselmann I, Schuler B, et al. Interleukin-6 enhances insulin secretion by increasing glucagon-like peptide-1 secretion from L cells and alpha cells. Nat Med. 2011 Oct 30;17(11):1481-9. doi: 10.1038/nm.2513.

99. Shah M and Vella A. Effects of GLP-1 on appetite and weight. Rev Endocr Metab Disord. 2014 Sep;15(3):181-7. doi: 10.1007/s11154-014-9289-5.

100. Hayashi Y, Yamamoto M, Mizoguchi H, et al. Mice deficient for glucagon gene-derived peptides display normoglycemia and hyperplasia of islet {alpha}-cells but not of intestinal L-cell. Mol Endocrinol. 2009 Dec;23(12):1990-9. doi: 10.1210/me.2009-0296. Epub 2009 Oct 9.

101. Kedia N. Treatment of severe diabetic hypoglycemia with glucagon: an underutilized therapeutic approach. Diabetes Metab Syndr Obes. 2011;4:337-46. doi: 10.2147/DMSO.S20633. Epub 2011 Sep 6.

102. Qiao A, Han S, Li X, et al. Structural basis of G s and G i recognition by the human glucagon receptor. Science. 2020 Mar 20;367(6484):1346-1352. doi: 10.1126/science.aaz5346.

103.   Gelling RW, Du XQ, Dichmann DS, et al. Lower blood glucose, hyperglucagonemia, and pancreatic alpha cell hyperplasia in glucagon receptor knockout mice. Proc Natl Acad Sci U S A. 2003 Feb 4;100(3):1438-43. doi: 10.1073/pnas.0237106100. Epub 2003 Jan 24.

104.   Solloway MJ, Madjidi A, Gu C, et al. Glucagon Couples Hepatic Amino Acid Catabolism to mTOR-Dependent Regulation of α-Cell Mass. Cell Rep. 2015 Jul 21;12(3):495-510. doi: 10.1016/j.celrep.2015.06.034. Epub 2015 Jul 9.

105.   Smith DK, Kates L, Durinck S, et al. Elevated Serum Amino Acids Induce a Subpopulation of Alpha Cells to Initiate Pancreatic Neuroendocrine Tumor Formation. Cell Rep Med. 2020 Aug 25;1(5):100058. doi: 10.1016/j.xcrm.2020.100058.

106.   Hager J, Hansen L, Vaisse C, et al. A missense mutation in the glucagon receptor gene is associated with non-insulin-dependent diabetes mellitus. Nat Genet. 1995 Mar;9(3):299-304. doi: 10.1038/ng0395-299.

107.   Scheen AJ, Paquot N, and Lefebvre PJ. Investigational glucagon receptor antagonists in Phase I and II clinical trials for diabetes. Expert Opin Investig Drugs. 2017 Dec;26(12):1373-1389. doi: 10.1080/13543784.2017.1395020. Epub 2017 Oct 26.

108.   Morgan ES, Tai L-J, Pham NC, et al. Antisense Inhibition of Glucagon Receptor by IONIS-GCGR Rx Improves Type 2 Diabetes Without Increase in Hepatic Glycogen Content in Patients With Type 2 Diabetes on Stable Metformin Therapy. Diabetes Care. 2019 Apr;42(4):585-593. doi: 10.2337/dc18-1343. Epub 2019 Feb 14.

109.   Wang M-Y, Dean ED, Quittner-Strom E, et al. Glucagon blockade restores functional β-cell mass in type 1 diabetic mice and enhances function of human islets. Proc Natl Acad Sci U S A. 2021 Mar 2;118(9):e2022142118. doi: 10.1073/pnas.2022142118.

110.   Miller RA, Chu Q, Xie J, Foretz M, et al. Biguanides suppress hepatic glucagon signalling by decreasing production of cyclic AMP. Nature. 2013. Feb 14;494(7436):256-60. doi: 10.1038/nature11808.

111.   Smith FD, Esseltine JL, Nygren PJ, et al. Local protein kinase A action proceeds through intact holoenzymes. Science. 2017 Jun 23;356(6344):1288-1293. doi: 10.1126/science.aaj1669.

112.   Brushia RJ and Walsh DA. Phosphorylase kinase: the complexity of its regulation is reflected in the complexity of its structure. Front Biosci. 1999 Sep 15;4:D618-41. doi: 10.2741/brushia.

113.   Magnusson I, Rothman DL, Gerad DP, et al. Contribution of hepatic glycogenolysis to glucose production in humans in response to a physiological increase in plasma glucagon concentration. Diabetes. 1995 Feb;44(2):185-9. doi: 10.2337/diab.44.2.185.

114.   Djouder N, Tuerk RD, Suter M, et al. PKA phosphorylates and inactivates AMPKalpha to promote efficient lipolysis. EMBO J. 2010 Jan 20;29(2):469-81. doi: 10.1038/emboj.2009.339. Epub 2009 Nov 26.

115.   Duncan RE, Ahmadian M, Jaworski K, et al. Regulation of lipolysis in adipocytes. Annu Rev Nutr. 2007;27:79-101. doi: 10.1146/annurev.nutr.27.061406.093734.

116.   Peng I-C, Chen Z, Sun W, et al. Glucagon regulates ACC activity in adipocytes through the CAMKKβ/AMPK pathway. Am J Physiol Endocrinol Metab. 2012 Jun 15;302(12):E1560-8. doi: 10.1152/ajpendo.00504.2011. Epub 2012 Mar 27.

117.   Xu Y and Xie X. Glucagon receptor mediates calcium signaling by coupling to G alpha q/11 and G alpha i/o in HEK293 cells. J Recept Signal Transduct Res. 2009 Dec;29(6):318-25. doi: 10.3109/10799890903295150.

118.   Wang Y, Li G, Goode J, et al. Inositol-1,4,5-trisphosphate receptor regulates hepatic gluconeogenesis in fasting and diabetes. Nature. 2012 Apr 8;485(7396):128-32. doi: 10.1038/nature10988.

119.   Meyers JB, Zaegel V, Coultrap SJ, et al. The CaMKII holoenzyme structure in activation-competent conformations. Nat Commun. 2017 Jun 7;8:15742. doi: 10.1038/ncomms15742.

120.   Perry RJ, Zhang D, Guerra MT, et al. Glucagon stimulates gluconeogenesis by INSP3R1-mediated hepatic lipolysis. Nature. 2020 Mar;579(7798):279-283. doi: 10.1038/s41586-020-2074-6. Epub 2020 Mar 4.

121.   Herzig S, Long F, Jhala US, et al. CREB regulates hepatic gluconeogenesis through the coactivator PGC-1. Nature. 2001. Sep 13;413(6852):179-83. doi: 10.1038/35093131.

122.   Ozcan L, Wong CCL, Li G, et al. Calcium signaling through CaMKII regulates hepatic glucose production in fasting and obesity. Cell Metab. 2012. May 2;15(5):739-51. doi: 10.1016/j.cmet.2012.03.002.

123.   Longuet C, Sinclair EM, Maida A, et al. The glucagon receptor is required for the adaptive metabolic response to fasting. Cell Metab. 2008 Nov;8(5):359-71. doi: 10.1016/j.cmet.2008.09.008.

124.   Rui L. Energy metabolism in the liver. Compr Physiol. 2014. 2014 Jan;4(1):177-97. doi: 10.1002/cphy.c130024.

125.   Cappel DA, Deja S, Duarte JAG, et al. Pyruvate-Carboxylase-Mediated Anaplerosis Promotes Antioxidant Capacity by Sustaining TCA Cycle and Redox Metabolism in Liver. Cell Metab. 2019 Jun 4;29(6):1291-1305.e8. doi: 10.1016/j.cmet.2019.03.014. Epub 2019 Apr 18.

126.   Degerman E, Belfrage P, and Manganiello VC. Structure, localization, and regulation of cGMP-inhibited phosphodiesterase (PDE3). J Biol Chem. 1997 Mar 14;272(11):6823-6. doi: 10.1074/jbc.272.11.6823.

127.   Mika D, Richter W, and Conti M. A CaMKII/PDE4D negative feedback regulates cAMP signaling. Proc Natl Acad Sci U S A. 2015 Feb 17;112(7):2023-8. doi: 10.1073/pnas.1419992112. Epub 2015 Feb 2.

128. Kaur S, Chen Y, and Shenoy SK. Agonist-activated glucagon receptors are deubiquitinated at early endosomes by two distinct deubiquitinases to facilitate Rab4a-dependent recycling. J Biol Chem. 2020 Dec 4;295(49):16630-16642. doi: 10.1074/jbc.RA120.014532. Epub 2020 Sep 23.

129. Ji L, Wang Q, Liu M, et al. The 14-3-3 protein YWHAB inhibits glucagon-induced hepatic gluconeogenesis through interacting with the glucagon receptor and FOXO1. FEBS Lett. 2021 May;595(9):1275-1288. doi: 10.1002/1873-3468.14063. Epub 2021 Mar 21.

130. Halpern KB, Shenhav R, Matcovitch-Natan O, et al. Single-cell spatial reconstruction reveals global division of labour in the mammalian liver. Nature. 2017 Feb 16;542(7641):352-356. doi: 10.1038/nature21065. Epub 2017 Feb 6.

131. Cheng X, Kim SY, Okamoto H, et al. Glucagon contributes to liver zonation. Proc Natl Acad Sci U S A. 2018 Apr 24;115(17):E4111-E4119. doi: 10.1073/pnas.1721403115. Epub 2018 Mar 19.

132. Karim S, Adams DH, and Lalor PF. Hepatic expression and cellular distribution of the glucose transporter family. World J Gastroenterol. 2012 Dec 14;18(46):6771-81. doi: 10.3748/wjg.v18.i46.6771.

133. Wang Z and Dong C. Gluconeogenesis in Cancer: Function and Regulation of PEPCK, FBPase, and G6Pase. Trends Cancer. 2019. 2019 Jan;5(1):30-45. doi: 10.1016/j.trecan.2018.11.003.

134. Jin X, Pan Y, Wang L, et al. Fructose-1,6-bisphosphatase Inhibits ERK Activation and Bypasses Gemcitabine Resistance in Pancreatic Cancer by Blocking IQGAP1-MAPK Interaction. Cancer Res. 2017. Aug 15;77(16):4328-4341. doi: 10.1158/0008-5472.CAN-16-3143.

135. Lu C, Ren C, Yang T, et al. A Noncanonical Role of Fructose-1, 6-Bisphosphatase 1 Is Essential for Inhibition of Notch1 in Breast Cancer. Mol Cancer Res. 2020. May;18(5):787-796. doi: 10.1158/1541-7786.MCR-19-0842.

136. Li J, Wang Y, Li Q-G, et al. Downregulation of FBP1 Promotes Tumor Metastasis and Indicates Poor Prognosis in Gastric Cancer via Regulating Epithelial-Mesenchymal Transition. PLoS One. 2016. Dec 15;11(12):e0167857. doi: 10.1371/journal.pone.0167857.

137. Li B, Qiu B, Lee DSM, et al. Fructose-1,6-bisphosphatase opposes renal carcinoma progression. Nature. 2014. Sep 11;513(7517):251-5. doi: 10.1038/nature13557.

138. Li F, Huangyuang P, Burrows M, et al. FBP1 loss disrupts liver metabolism and promotes tumorigenesis through a hepatic stellate cell senescence secretome. Nat Cell Biol. 2020. 2020 Jun;22(6):728-739. doi: 10.1038/s41556-020-0511-2.

139. Montal ED, Dewi R, Bhalla K, et al. PEPCK Coordinates the Regulation of Central Carbon Metabolism to Promote Cancer Cell Growth. Mol Cell. 2015. Nov 19;60(4):571-83. doi: 10.1016/j.molcel.2015.09.025.

140.   Xiang J, Chen C, Liu R, et al. Gluconeogenic enzyme PCK1 deficiency promotes CHK2 O-GlcNAcylation and hepatocellular carcinoma growth upon glucose deprivation. J Clin Invest. 2021. Apr 15;131(8):144703. doi: 10.1172/JCI144703.

141.   Abbadi S, Rodarte JJ, Abutaleb A, et al. Glucose-6-phosphatase is a Key Metabolic Regulator of Glioblastoma Invasion. Mol Cancer Res. 2014. Nov; 12(11): 1547-1559. doi: 10.1158/1541-7786.MCR-14-0106-T.

142.   Lei KJ, Chen H, Pan CJ, et al. Glucose-6-phosphatase dependent substrate transport in the glycogen storage disease type-1a mouse. Nat Genet. 1996. Jun;13(2):203-9. doi: 10.1038/ng0696-203.

143.   Kishnani PS, Chuang T-P, Bali D, et al. Chromosomal and genetic alterations in human hepatocellular adenomas associated with type Ia glycogen storage disease. Hum Mol Genet. 2009. Dec 15;18(24):4781-90. doi: 10.1093/hmg/ddp441.

144.   Kim G-Y, Kwon JH, Cho J-H, et al. Downregulation of pathways implicated in liver inflammation and tumorigenesis of glycogen storage disease type Ia mice receiving gene therapy. Hum Mol Genet. 2017. May 15;26(10):1890-1899. doi: 10.1093/hmg/ddx097.

145.   Adeva-Andany MM, González-Lucán M, Donapetry-García C, Fernández-Fernández C, Ameneiros-Rodríguez E. Glycogen metabolism in humans. BBA Clin. 2016;5:85-100. doi:10.1016/J.BBACLI.2016.02.001.

146.   Calì C, Tauffenberger A, Magistretti P. The strategic location of glycogen and lactate: From body energy reserve to brain plasticity. Front Cell Neurosci. 2019;13(March):1-7. doi:10.3389/fncel.2019.00082.

147.   Gerich JE. Role of the kidney in normal glucose homeostasis and in the hyperglycaemia of diabetes mellitus: therapeutic implications. Diabet Med. 2010 Feb;27(2):136-42. doi: 10.1111/j.1464-5491.2009.02894.x.

148.   Stumvoll M, Meyer C, Mitrakou A, et al. Renal glucose production and utilization: new aspects in humans. Diabetologia. 1997 Jul;40(7):749-57. doi: 10.1007/s001250050745.

149.   Ma J, Wei K, Liu J, et al. Glycogen metabolism regulates macrophage-mediated acute inflammatory responses. Nat Commun. 2020 Apr 14;11(1):1769. doi: 10.1038/s41467-020-15636-8.

150.   Curtis M, Kenny HA, Ashcroft B, et al. Fibroblasts Mobilize Tumor Cell Glycogen to Promote Proliferation and Metastasis. Cell Metab. 2019 Jan 8;29(1):141-155.e9. doi: 10.1016/j.cmet.2018.08.007. Epub 2018 Aug 30.

151.   Rousset M, Zweibaum A, Fogh J. Presence of Glycogen and Growth-related Variations in 58 Cultured Human Tumor Cell Lines of Various Tissue Origins. Cancer Res. 1981;41(3):1165 LP - 1170. http://cancerres.aacrjournals.org/content/41/3/1165.abstract.

152.   Shen G-M, Zhang F-L, Liu X-L, and Zhang J-W. Hypoxia-inducible factor 1-mediated regulation of PPP1R3C promotes glycogen accumulation in human MCF-7 cells under hypoxia. FEBS Lett. 2010 Oct 22;584(20):4366-72. doi: 10.1016/j.febslet.2010.09.040. Epub 2010 Oct 1.

153.   Dauer P and Lengyel E. New Roles for Glycogen in Tumor Progression. Trends Cancer. 2019 Jul;5(7):396-399. doi: 10.1016/j.trecan.2019.05.003. Epub 2019 May 31.

154.   Chiu DKC, Tse APW, Law C-T, et al. Hypoxia regulates the mitochondrial activity of hepatocellular carcinoma cells through HIF/HEY1/PINK1 pathway. Cell Death Dis. 2019 Dec 9;10(12):934. doi: 10.1038/s41419-019-2155-3.

155.   Sharma AX, Quittner-Strom EB, Lee Y, et al. Glucagon Receptor Antagonism Improves Glucose Metabolism and Cardiac Function by Promoting AMP-Mediated Protein Kinase in Diabetic Mice. Cell Rep. 2018. Feb 13;22(7):1760-1773. doi: 10.1016/j.celrep.2018.01.065.

156.   Zhou C, Dhall D, Nissen NN, et al. A homozygous P86S mutation of the human glucagon receptor is associated with hyperglucagonemia, Œ± cell hyperplasia, and islet cell tumor. Pancreas. 2009. Nov; 38(8): 941-946. doi: 10.1097/MPA.0b013e3181b2bb03.

157.   Yu R, Dhall D, Nissen NN, et al. Pancreatic neuroendocrine tumors in glucagon receptor-deficient mice. PLoS One. 2011;6(8):e23397. doi: 10.1371/journal.pone.0023397.

158.   Yagi T, Kubota E, Koyama H, et al. Glucagon promotes colon cancer cell growth via regulating AMPK and MAPK pathways. Oncotarget. 2018. Feb 13; 9(12): 10650–10664. doi: 10.18632/oncotarget.24367.

159.   Villanueva A. Hepatocellular Carcinoma. N Engl J Med. 2019 Apr 11;380(15):1450-1462. doi: 10.1056/NEJMra1713263.

160.   Kim E and Viatour P. Hepatocellular carcinoma: old friends and new tricks. Exp Mol Med. 2020 Dec;52(12):1898-1907. doi: 10.1038/s12276-020-00527-1. Epub 2020 Dec 2.

161.   American Cancer Society. Cancer Facts & Figures 2018. Am Cancer Soc. 2018. doi:10.3322/caac.21442.

162.   Simonetti RG, Camma C, Fiorello F, et al. Hepatocellular carcinoma. A worldwide problem and the major risk factors. Dig Dis Sci. 1991 Jul;36(7):962-72. doi: 10.1007/BF01297149.

163.   Bedossa P and Paradis V. Hepatocellular Carcinoma. Pract Hepatic Pathol A Diagnostic Approach. 2011:489-501. doi:10.1016/B978-0-443-06803-4.00035-6.

164.   Wang Z, Sheng Y-Y, Gao X-M, et al. β-catenin mutation is correlated with a favorable prognosis in patients with hepatocellular carcinoma. Mol Clin Oncol. 2015 Jul;3(4):936-940. doi: 10.3892/mco.2015.569. Epub 2015 May 15.

165.   Kim SK, Takeda H, Takai A, et al. Comprehensive analysis of genetic aberrations linked to tumorigenesis in regenerative nodules of liver cirrhosis. J Gastroenterol. 2019 Jul;54(7):628-640. doi: 10.1007/s00535-019-01555-z. Epub 2019 Feb 12.

166.   Muller M, Bird TG, and Nault J-C. The landscape of gene mutations in cirrhosis and hepatocellular carcinoma. J Hepatol. 2020 May;72(5):990-1002. doi: 10.1016/j.jhep.2020.01.019. Epub 2020 Feb 8.

167.   Nault JC, Mallet M, Pilati C, et al. High frequency of telomerase reverse-transcriptase promoter somatic mutations in hepatocellular carcinoma and preneoplastic lesions. Nat Commun. 2013;4:2218. doi: 10.1038/ncomms3218.

168.   Villanueva A and Hoshida Y. Depicting the role of TP53 in hepatocellular carcinoma progression. J Hepatol. 2011 Sep;55(3):724-725. doi: 10.1016/j.jhep.2011.03.018. Epub 2011 May 14.

169.   Llovet JM, Ricci S, Mazzaferro V, et al. Sorafenib in advanced hepatocellular carcinoma. N Engl J Med. 2008;359(4):378-390. doi:10.1056/NEJMoa0708857.

170.   Bruix J, Takayama T, Mazzaferro V, et al. Adjuvant sorafenib for hepatocellular carcinoma after resection or ablation (STORM): A phase 3, randomised, double-blind, placebo-controlled trial. Lancet Oncol. 2015;16(13):1344-1354. doi:10.1016/S1470-2045(15)00198-9.

171.   Pinato DJ, Guerra N, Fessas P, et al. Immune-based therapies for hepatocellular carcinoma. Oncogene. 2020 Apr;39(18):3620-3637. doi: 10.1038/s41388-020-1249-9. Epub 2020 Mar 10.

172.   Finn RS, Qin S, Ikeda M, et al. Atezolizumab plus Bevacizumab in Unresectable Hepatocellular Carcinoma. N Engl J Med. 2020 May 14;382(20):1894-1905. doi: 10.1056/NEJMoa1915745.

173.   Jeng KS, Chang CF, Jeng WJ, et al. Heterogeneity of hepatocellular carcinoma contributes to cancer progression. Crit Rev Oncol Hematol. 2015;94(3):337-347. doi:10.1016/j.critrevonc.2015.01.009.

174.   Ally A, Balasundaram M, Carlsen R, et al. Comprehensive and Integrative Genomic Characterization of Hepatocellular Carcinoma. Cell. 2017;169(7):1327-1341.e23. doi:10.1016/j.cell.2017.05.046.

175.   NCI. SEER Cancer Sta Facts: Kidney and Renal Pelvis Cancer. 2018.

176.   Sanchez DJ, Simon MC. Genetic and metabolic hallmarks of clear cell renal cell carcinoma. Biochim Biophys Acta - Rev Cancer. 2018;1870(1):23-31. doi:10.1016/J.BBCAN.2018.06.003

177.   Gordan JD, Lal P, Dondeti VR, et al. HIF-α Effects on c-Myc Distinguish Two Subtypes of Sporadic VHL-Deficient Clear Cell Renal Carcinoma. Cancer Cell. 2008;14(6):435-446. doi:10.1016/J.CCR.2008.10.016

178.   Wallace EM, Rizzi JP, Han G, et al. A Small-Molecule Antagonist of HIF2α Is Efficacious in Preclinical Models of Renal Cell Carcinoma. Cancer Res. 2016;76(18):5491 LP - 5500. doi:10.1158/0008-5472.CAN-16-0473

179.   Courtney KD, Infante JR, Lam ET, et al. Phase I dose-escalation trial of PT2385, a first-in-class hypoxia-inducible factor-2a antagonist in patients with previously treated advanced clear cell renal cell carcinoma. J Clin Oncol. 2018;36(9):867-874. doi:10.1200/JCO.2017.74.2627

180.   Zhang Y, Udayakumar D, Cai L, et al. Addressing metabolic heterogeneity in clear cell renal cell carcinoma with quantitative Dixon MRI. JCI insight. 2017;2(15):1-14. doi:10.1172/jci.insight.94278

181.   Riscal R, Skuli N, and Simon MC. Even Cancer Cells Watch Their Cholesterol! Mol Cell. 2019. doi:10.1016/j.molcel.2019.09.008

182.   Qiu B, Ackerman D, Sanchez DJ, et al. HIF2α-Dependent Lipid Storage Promotes Endoplasmic Reticulum Homeostasis in Clear-Cell Renal Cell Carcinoma. Cancer Discov. 2015;5(6):652 LP - 667. doi:10.1158/2159-8290.CD-14-1507

183.   Ackerman D, Tumanov S, Qiu B, et al. Triglycerides Promote Lipid Homeostasis during Hypoxic Stress by Balancing Fatty Acid Saturation. Cell Rep. 2018;24(10):2596-2605.e5. doi:10.1016/j.celrep.2018.08.015

184.   Favaro E, Bensaad K, Chong MG, et al. Glucose Utilization via Glycogen Phosphorylase Sustains Proliferation and Prevents Premature Senescence in Cancer Cells. Cell Metab. 2012;16(6):751-764. doi:10.1016/J.CMET.2012.10.017

185.   Sun RC, Dukhande V V., Zhou Z, et al. Nuclear Glycogenolysis Modulates Histone Acetylation in Human Non-Small Cell Lung Cancers. Cell Metab. 2019;30(5):903-916.e7. doi:10.1016/J.CMET.2019.08.014

186.   Feoktistova M, Geserick P, and Leverkus M. Crystal Violet Assay for Determining Viability of Cultured Cells. Cold Spring Harb Protoc. 2016. Apr 1;2016(4):pdb.prot087379. doi: 10.1101/pdb.prot087379.

187.   Nagy A, Munkarcsy G, Gyorffy B. Pancancer survival analysis of cancer hallmark genes. Sci Rep. 2021. Mar 15;11(1):6047. doi: 10.1038/s41598-021-84787-5.

188.   Finan B, Clemmensen C, Zhu Z, et al. Chemical Hybridization of Glucagon and Thyroid Hormone Optimizes Therapeutic Impact for Metabolic Disease. Cell. 2016. Oct 20;167(3):843-857.e14. doi: 10.1016/j.cell.2016.09.014.

189.   Johannessen M, Delghandi MP, and Moens U. What turns CREB on? Cell Signal. 2004. Nov;16(11):1211-27. doi: 10.1016/j.cellsig.2004.05.001.

190.   Steven A, Leisz S, Sychra K, et al. Hypoxia-mediated alterations and their role in the HER-2/neu regulated CREB status and localization. Oncotarget. 2016. Aug 9;7(32):52061-52084. doi: 10.18632/oncotarget.10474.

191.   Karanth S, Adams JD, de Los Angeles Serrano M, et al. A Hepatocyte FOXN3-Œ± Cell Glucagon Axis Regulates Fasting Glucose. Cell Rep. 2018. Jul 10;24(2):312-319. doi: 10.1016/j.celrep.2018.06.039.

192.   Zhang Y, Chen W, Li R, et al. Insulin-regulated Srebp-1c and Pck1 mRNA expression in primary hepatocytes from zucker fatty but not lean rats is affected by feeding conditions. PLoS One. 2011;6(6):e21342. doi: 10.1371/journal.pone.0021342.

193.   Taddeo EP, Hargett SR, Lahiri S, et al. Lysophosphatidic acid counteracts glucagon-induced hepatocyte glucose production via STAT3. Sci Rep. 2017. Mar 9;7(1):127. doi: 10.1038/s41598-017-00210-y.

194.   Ribback S, Che Li, Pilo MG, et al. Oncogene-dependent addiction to carbohydrate-responsive element binding protein in hepatocellular carcinoma. Cell Cycle. 2018;17(12):1496-1512. doi: 10.1080/15384101.2018.1489182.

195.   Iizuka K, Tomita R, Takeda J, and Horikawa Y. Rat glucagon receptor mRNA is directly regulated by glucose through transactivation of the carbohydrate response element binding protein. Biochem Biophys Res Commun. 2012. Jan 27;417(4):1107-12. doi: 10.1016/j.bbrc.2011.12.042.

196.   Chen M, Zhang J, Li N, et al. Promoter hypermethylation mediated downregulation of FBP1 in human hepatocellular carcinoma and colon cancer. PLoS One. 2011;6(10):e25564. doi: 10.1371/journal.pone.0025564.

197.   Yang J, Jin X, Yan Y, et al. Inhibiting histone deacetylases suppresses glucose metabolism and hepatocellular carcinoma growth by restoring FBP1 expression. Sci Rep. 2017. Mar 6;7:43864. doi: 10.1038/srep43864.

198.   Liao K, Deng S, Xu L, et al. A Feedback Circuitry between Polycomb Signaling and Fructose-1, 6-Bisphosphatase Enables Hepatic and Renal Tumorigenesis. Cancer Res. 2020. Feb 15;80(4):675-688. doi: 10.1158/0008-5472.CAN-19-2060.

199.   McCabe MT, Ott HM, Ganji G, et al. EZH2 inhibition as a therapeutic strategy for lymphoma with EZH2-activating mutations. Nature. 2012. Dec 6;492(7427):108-12. doi: 10.1038/nature11606.

200.   Scuto A, Kirschbaum M, Kowolik C, et al. The novel histone deacetylase inhibitor, LBH589, induces expression of DNA damage response genes and apoptosis in Ph- acute lymphoblastic leukemia cells. Blood. 2008. May 15;111(10):5093-100. doi: 10.1182/blood-2007-10-117762.

201.   Ghoshal K, Datta J, Majumder S, et al. 5-Aza-deoxycytidine induces selective degradation of DNA methyltransferase 1 by a proteasomal pathway that requires the KEN box, bromo-adjacent homology domain, and nuclear localization signal. Mol Cell Biol. 2005. 2005 Jun;25(11):4727-41. doi: 10.1128/MCB.25.11.4727-4741.2005.

202.   Kato S, Weng QY, Insco ML, et al. Gain-of-Function Genetic Alterations of G9a Drive Oncogenesis. Cancer Discov. 2020 Jul;10(7):980-997. doi: 10.1158/2159-8290.CD-19-0532. Epub 2020 Apr 8.

203.   Han J, Zhang M, Froese S, et al. The Identification of Novel Protein-Protein Interactions in Liver that Affect Glucagon Receptor Activity. PLoS One. 2015. Jun 15;10(6):e0129226. doi: 10.1371/journal.pone.0129226.

204.   Xie F, Li BX, Kassenbrock A, et al. Identification of a Potent Inhibitor of CREB-Mediated Gene Transcription with Efficacious in Vivo Anticancer Activity. J Med Chem. 2015. Jun 25;58(12):5075-87. doi: 10.1021/acs.jmedchem.5b00468.

205.   Kang X, Lu Z, Cui C, et al. The ITIM-containing receptor LAIR1 is essential for acute myeloid leukaemia development. Nat Cell Biol. 2015. May;17(5):665-77. doi: 10.1038/ncb3158.

206.   Comit G, Ippolito L, Chiarugi P, and Cirri P. Nutritional Exchanges Within Tumor Microenvironment: Impact for Cancer Aggressiveness. Front Oncol. 2020. Mar 24;10:396. doi: 10.3389/fonc.2020.00396.

207.   Haedersdal S, Lund A, Knop FK, and Vilsboll T. The Role of Glucagon in the Pathophysiology and Treatment of Type 2 Diabetes. Mayo Clin Proc. 2018. 2018 Feb;93(2):217-239. doi: 10.1016/j.mayocp.2017.12.003.

208.   Kwok RP, Lundblad JR, Chrivia JC, et al. Nuclear protein CBP is a coactivator for the transcription factor CREB. Nature. 1994. Jul 21;370(6486):223-6. doi: 10.1038/370223a0.

209.   Puigserver P, Rhee J, Donovan J, et al. Insulin-regulated hepatic gluconeogenesis through FOXO1-PGC-1alpha interaction. Nature. 2003. May 29;423(6939):550-5. doi: 10.1038/nature01667.

210.   Rhee J, Inoue Y, Yoon JC, et al. Regulation of hepatic fasting response by PPARgamma coactivator-1alpha (PGC-1): requirement for hepatocyte nuclear factor 4alpha in gluconeogenesis. Proc Natl Acad Sci U S A. 2003. Apr 1;100(7):4012-7. doi: 10.1073/pnas.0730870100.

211.   Grontved L, John S, Baek S, et al. C/EBP maintains chromatin accessibility in liver and facilitates glucocorticoid receptor recruitment to steroid response elements. EMBO J. 2013. May 29;32(11):1568-83. doi: 10.1038/emboj.2013.106.

212.   Ericsson JL, Seljelid R OS. Comparative light and electron microscopic observations of the cytoplasmic matrix in renal carcinomas. Virchows Arch Pathol Anat Physiol Klin Med. 1966;341(3):204-223.

213.   Vinci M, Gowan S, Boxall F, et al. Advances in establishment and analysis of three-dimensional tumor spheroid-based functional assays for target validation and drug evaluation. BMC Biol. 2012;10(1):29. doi:10.1186/1741-7007-10-29.

214.   Ivanov DP, Parker TL, Walker DA, et al. Multiplexing spheroid volume, resazurin and acid phosphatase viability assays for high-throughput screening of tumour spheroids and stem cell neurospheres. PLoS One. 2014;9(8):1-14. doi:10.1371/journal.pone.0103817.

215.	Hakimi AA, Reznik E, Lee C-H, et al. An Integrated Metabolic Atlas of Clear Cell Renal Cell Carcinoma. Cancer Cell. 2016;29(1):104-116. doi:10.1016/J.CCELL.2015.12.004

216.	Zois CE, Harris AL. Glycogen metabolism has a key role in the cancer microenvironment and provides new targets for cancer therapy. J Mol Med. 2016;94(2):137-154. doi:10.1007/s00109-015-1377-9.

217.	Munro S, Ceulemans H, Bollen M, Diplexcito J, Cohen PTW. A novel glycogen-targeting subunit of protein phosphatase 1 that is regulated by insulin and shows differential tissue distribution in humans and rodents. FEBS J. 2005;272(6):1478-1489. doi:10.1111/j.1742-4658.2005.04585.x

218.	Shen GM, Zhang FL, Liu XL, Zhang JW. Hypoxia-inducible factor 1-mediated regulation of PPP1R3C promotes glycogen accumulation in human MCF-7 cells under hypoxia. FEBS Lett. 2010;584(20):4366-4372. doi:10.1016/j.febslet.2010.09.040

219.	Yang R, Zhang M, Gustafson AR, et al. Loss of protein targeting to glycogen sensitizes human hepatocellular carcinoma cells towards glucose deprivation mediated oxidative stress and cell death. Biosci Rep. 2015;35(3). doi:10.1042/BSR20150090

220.	Jurczak MJ, Danos AM, Rehrmann VR, Allison MB, Greenberg CC, Brady MJ. Transgenic overexpression of protein targeting to glycogen markedly increases adipocytic glycogen storage in mice. Am J Physiol - Endocrinol Metab. 2007;292(3):952-963. doi:10.1152/ajpendo.00559.2006

221.	Greenberg CC, Meredith KN, Yan L, Brady MJ. Protein targeting to glycogen overexpression results in the specific enhancement of glycogen storage in 3T3-L1 adipocytes. J Biol Chem. 2003;278(33):30835-30842. doi:10.1074/jbc.M303846200

222.	Bhanot H, Reddy MM, Nonami A, et al. Pathological glycogenesis through glycogen synthase 1 and suppression of excessive AMP kinase activity in myeloid leukemia cells. Leukemia. 2015;29(7):1555-1563. doi:10.1038/leu.2015.46

223.	Varnier M, Leese GP, Thompson J, Rennie MJ. Stimulatory effect of glutamine on glycogen accumulation in human skeletal muscle. Am J Physiol Metab. 1995;269(2):E309-E315. doi:10.1152/ajpendo.1995.269.2.E309

224.	Lundsgaard A-M, Fritzen AM, Kiens B. Molecular Regulation of Fatty Acid Oxidation in Skeletal Muscle during Aerobic Exercise. Trends Endocrinol Metab. 2018;29(1):18-30. doi:10.1016/J.TEM.2017.10.011

225.	Hardin CD, Roberts TM. Differential Regulation of Glucose and Glycogen Metabolism in Vascular Smooth Muscle by Exogenous Substrates. J Mol Cell Cardiol. 1997;29(4):1207-1216. doi:10.1006/JMCC.1996.0356

226.	O'Brien SG, Guilhot F, Larson RA, et al. Imatinib compared with interferon and low-dose cytarabine for newly diagnosed chronic-phase chronic myeloid leukemia. N Engl J Med. 2003 Mar 13;348(11):994-1004. doi: 10.1056/NEJMoa022457.

227.   Chapman PB, Hauschild A, Robert C, et al. Improved survival with vemurafenib in melanoma with BRAF V600E mutation. N Engl J Med. 2011 Jun 30;364(26):2507-16. doi: 10.1056/NEJMoa1103782. Epub 2011 Jun 5.

228.   Shaw AT, Kim D-W, Nakagawa K, et al. Crizotinib versus chemotherapy in advanced ALK-positive lung cancer. N Engl J Med. 2013 Jun 20;368(25):2385-94. doi: 10.1056/NEJMoa1214886. Epub 2013 Jun 1.

229.   Aldea M, Andre F, Marabelle A, et al. Overcoming Resistance to Tumor-Targeted and Immune-Targeted Therapies. Cancer Discov. 2021 Apr;11(4):874-899. doi: 10.1158/2159-8290.CD-20-1638.

230.   Dagogo-Jack I and Shaw AT. Tumour heterogeneity and resistance to cancer therapies. Nat Rev Clin Oncol. 2018 Feb;15(2):81-94. doi: 10.1038/nrclinonc.2017.166. Epub 2017 Nov 8.

231.   Goossens N, Nakagawa S, Sun X, and Hoshida Y. Cancer biomarker discovery and validation. Transl Cancer Res. 2015 Jun;4(3):256-269. doi: 10.3978/j.issn.2218-676X.2015.06.04.

232.   Birchmeier W. Orchestrating Wnt signalling for metabolic liver zonation. Nat Cell Biol. 2016 Apr 27;18(5):463-5. doi: 10.1038/ncb3349.

233.   Droin C, Kholtei JE, Halpern KB, et al. Space-time logic of liver gene expression at sub-lobular scale. Nat Metab. 2021 Jan;3(1):43-58. doi: 10.1038/s42255-020-00323-1. Epub 2021 Jan 11.

234.   Manco R and Itzkovitz S. Liver zonation. J Hepatol. 2021 Feb;74(2):466-468. doi: 10.1016/j.jhep.2020.09.003. Epub 2020 Dec 11.

235.   Kurosaki S, Nakagawa H, Hayata Y, et al. Cell fate analysis of zone 3 hepatocytes in liver injury and tumorigenesis. JHEP Reports. 2021 May. https://doi.org/10.1016/j.jhepr.2021.100315.

236.   Anstee QM, Reeves HL, Kotsiliti E, et al. From NASH to HCC: current concepts and future challenges. Nat Rev Gastroenterol Hepatol. 2019 Jul;16(7):411-428. doi: 10.1038/s41575-019-0145-7.

237.   Luo C, Liang J, Sharabi K, et al. Obesity/Type 2 Diabetes-Associated Liver Tumors Are Sensitive to Cyclin D1 Deficiency. Cancer Res. 2020 Aug 15;80(16):3215-3221. doi: 10.1158/0008-5472.CAN-20-0106. Epub 2020 Jun 30.

238.   Okamoto H, Cavino K, Na E, et al. Glucagon receptor inhibition normalizes blood glucose in severe insulin-resistant mice. Proc Natl Acad Sci U S A. 2017 Mar 7;114(10):2753-2758. doi: 10.1073/pnas.1621069114. Epub 2017 Jan 23.

239.   Kostic A, King TA, Yang F, et al. A first-in-human pharmacodynamic and pharmacokinetic study of a fully human anti-glucagon receptor monoclonal antibody in normal healthy volunteers. Diabetes Obes Metab. 2018 Feb;20(2):283-291. doi: 10.1111/dom.13075. Epub 2017 Sep 14.

240.   Landau DJ, Brooks ED, Perez-Pinera P, et al. In Vivo Zinc Finger Nuclease-mediated Targeted Integration of a Glucose-6-phosphatase Transgene Promotes Survival in Mice With Glycogen Storage Disease Type IA. Mol Ther. 2016 Apr;24(4):697-706. doi: 10.1038/mt.2016.35. Epub 2016 Feb 11.

241.   Hargreaves M and Spriet LL. Skeletal muscle energy metabolism during exercise. Nat Metab. 2020 Sep;2(9):817-828. doi: 10.1038/s42255-020-0251-4. Epub 2020 Aug 3.

242.   Chandel NS, Maltepe E, Goldwasser E, et al. Mitochondrial reactive oxygen species trigger hypoxia-induced transcription. Proc Natl Acad Sci U S A. 1998 Sep 29;95(20):11715-20. doi: 10.1073/pnas.95.20.11715.

243.   Ito M, Tanaka T, Ishii T, et al. Prolyl hydroxylase inhibition protects the kidneys from ischemia via upregulation of glycogen storage. Kidney Int. 2020 Apr;97(4):687-701. doi: 10.1016/j.kint.2019.10.020. Epub 2019 Nov 9.

244.   Raimondi V, Ciccarese F, and Ciminale V. Oncogenic pathways and the electron transport chain: a dangeROS liaison. Br J Cancer. 2020 Jan;122(2):168-181. doi: 10.1038/s41416-019-0651-y. Epub 2019 Dec 10.

245.   Bertout JA, Majmundar AJ, Gordan JD, et al. HIF2alpha inhibition promotes p53 pathway activity, tumor cell death, and radiation responses. Proc Natl Acad Sci U S A. 2009 Aug 25;106(34):14391-6. doi: 10.1073/pnas.0907357106. Epub 2009 Aug 12.

246.   Cid E, Cifuentes D, Baque S, et al. Determinants of the nucleocytoplasmic shuttling of muscle glycogen synthase. FEBS J. 2005 Jun;272(12):3197-213. doi: 10.1111/j.1742-4658.2005.04738.x.

247.   Diaz A, Martinez-Pons C, Fita I, et al. Processivity and subcellular localization of glycogen synthase depend on a non-catalytic high affinity glycogen-binding site. J Biol Chem. 2011 May 27;286(21):18505-14. doi: 10.1074/jbc.M111.236109. Epub 2011 Apr 4.

248.   Ma R, Ji T, Zhang H, et al. A Pck1-directed glycogen metabolic program regulates formation and maintenance of memory CD8 + T cells. Nat Cell Biol. 2018 Jan;20(1):21-27. doi: 10.1038/s41556-017-0002-2. Epub 2017 Dec 11.

249.   Thwe PM, Pelgrom LR, Cooper R, et al. Cell-Intrinsic Glycogen Metabolism Supports Early Glycolytic Reprogramming Required for Dendritic Cell Immune Responses. Cell Metab. 2017 Sep 5;26(3):558-567.e5. doi: 10.1016/j.cmet.2017.08.012.

250.   Sadiku P, Willson JA, Ryan EM, et al. Neutrophils Fuel Effective Immune Responses through Gluconeogenesis and Glycogenesis. Cell Metab. 2021 Feb 2;33(2):411-423.e4. doi: 10.1016/j.cmet.2020.11.016. Epub 2020 Dec 10.

251.   Motzer RJ, Banchereau R, Hamidi H, et al. Molecular Subsets in Renal Cancer Determine Outcome to Checkpoint and Angiogenesis Blockade. Cancer Cell. 2020 Dec 14;38(6):803-817.e4. doi: 10.1016/j.ccell.2020.10.011. Epub 2020 Nov 5.

252.   Braun DA, Street K, Burke KP, et al. Progressive immune dysfunction with advancing disease stage in renal cell carcinoma. Cancer Cell. 2021 May 10;39(5):632-648.e8. doi: 10.1016/j.ccell.2021.02.013. Epub 2021 Mar 11.